

STUDY OF NOVEL FEATURES IN LASER-PLASMA INTERACTIONS

By

ATUL KUMAR

PHYS06201304010

INSTITUTE FOR PLASMA RESEARCH, GANDHINAGAR

A thesis submitted to the
Board of Studies in Physical Sciences

In partial fulfillment of requirements

For the Degree of

DOCTOR OF PHILOSOPHY

of

HOMI BHABHA NATIONAL INSTITUTE

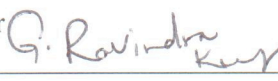


April, 2019

Homi Bhabha National Institute¹

Recommendations of the Viva Voce Committee

As members of the Viva Voce Committee, we certify that we have read the dissertation prepared by Atul Kumar entitled "Study of novel features in laser-plasma interactions" and recommend that it may be accepted as fulfilling the thesis requirement for the award of Degree of Doctor of Philosophy.

Chairman – Prof. Sudip Sengupta		Date: 22/04/2019
Guide / Convener – Prof. Amita Das		Date: 22/04/2019
Examiner - Prof. Arnab Rai Choudhuri		Date: 24/4/19
Member 1- Dr. Devendra Sharma		Date: 22/4/19
Member 2- Dr. Sarveshwar Sharma		Date: 22/04/19
Member 3- Prof. G. Ravindra Kumar		Date: 22/04/19

Final approval and acceptance of this thesis is contingent upon the candidate's submission of the final copies of the thesis to HBNI.

I/We hereby certify that I/we have read this thesis prepared under my/our direction and recommend that it may be accepted as fulfilling the thesis requirement.

Date: 22 April 2019

Place: Gandhinagar



Signature

(Prof. Amita Das)

Guide

¹ This page is to be included only for final submission after successful completion of viva voce.

STATEMENT BY AUTHOR

This dissertation has been submitted in partial fulfilment of requirements for an advanced degree at Homi Bhabha National Institute (HBNI) and is deposited in the Library to be made available to borrowers under rules of the HBNI.

Brief quotations from this dissertation are allowable without special permission, provided that accurate acknowledgement of source is made. Requests for permission for extended quotation from or reproduction of this manuscript in whole or in part may be granted by the Competent Authority of HBNI when in his or her judgement the proposed use of the material is in the interests of scholarship. In all other instances, however, permission must be obtained from the author.

Atul Kumar
ATUL KUMAR

DECLARATION

I, hereby declare that the investigation presented in the thesis has been carried out by me. The work is original and the work has not been submitted earlier as a whole or in part for a degree/diploma at this or any other Institution or University.

Atul Kumar
ATUL KUMAR

List of Publications arising from the thesis

Journal:

1. **"Energy principle for excitations in plasmas with counterstreaming electron flows"** , [Atul Kumar](#), Chandrasekhar Shukla, Amita Das, and Predhiman Kaw, AIP Advances, **2018**, 8, 055213.
2. **"Merger and reconnection of Weibel separated relativistic electron beam"**, Chandrasekhar Shukla, [Atul Kumar](#), Bhavesh Patel, and Amita Das, Physics of Plasmas, **2018**, 25, 022123.
3. **"A new finite beam instability for magnetic field generation"**, Amita Das, [Atul Kumar](#), Chandrasekhar Shukla, Ratan Kumar Bera, Deepa Verma, Devshree Mandal, Ayushi Vashishta, Bhavesh Patel, Y. Hayashi, K. A. Tanaka, G. Chatterjee, Amit D. Lad, G. R. Kumar, and Predhiman Kaw, arXiv: 1712.03099v1 [physics.plasm-ph], **2017**, 1-11.
4. **"Excitation of KdV magnetosonic solitons by a pulsed CO₂ laser in plasma in the presence of an external magnetic field"**, [Atul Kumar](#), Chandrasekhar Shukla, Deepa Verma, Amita Das, and Predhiman Kaw, in Press, Plasma Phys. Control. Fusion **2019**, <https://doi.org/10.1088/1361-6587/ab1408>

Other Publications

1. **"Observation of 1-D time dependent non-propagating laser plasma structures using Fluid and PIC codes"**, Deepa Verma, Ratan Kumar Bera, [Atul Kumar](#), Bhavesh Patel, and Amita Das, Physics of plasmas, **2017**, 24, 123111.
2. **"Fast ignition laser fusion using in-situ ion acceleration with pulsed CO₂ laser"**, [Atul Kumar](#), Chandrasekhar Shukla, Predhiman Kaw, and Amita Das, arXiv:1804.02200v2 [physics.plasm-ph], **2018**, 1-16.
3. **"Numerical study of bulk ion acceleration from laser-irradiated thin solid target in the presence of a strong axial magnetostatic field"** , Chandrasekhar Shukla, [Atul Kumar](#), and Amita Das, In preparation.

4. "MeV order of a superdense ($10^{29}m^{-3}$) helical electron bunch generation in laser interaction with carbon nanowire", Chandrasekhar Shukla, [Atul Kumar](#), and Amita Das, In preparation.
5. "Coupling of drift wave with dust acoustic wave in weakly and strongly coupled dusty plasma ", [Atul Kumar](#), Amita Das, and Predhiman Kaw, arXiv:1903.02211v1 [physics-plasm-ph], **2019**,1-17

Conferences:

International Participations

1. In-situ ion heating with pulsed CO_2 laser (Invited Talk), [Atul Kumar](#), Chandrasekhar Shukla, Predhiman Kaw, and Amita Das, 2^{nd} Asia-Pacific Conference on Plasma Physics (AAPPS-DPP2018),12-17 November 2018, Kanazawa, Japan.
2. Magnetic field generation in finite beam plasma system. (Poster), [Atul Kumar](#), Chandrasekhar Shukla, Bhavesh Patel , Amita Das and Predhiman Kaw, 59^{th} Annual meeting of APS-DPP, 23 - 27 October 2017, Wisconsin, USA.
3. Coupling of drift wave with dust acoustic wave (Poster), [Atul Kumar](#), Amita Das, and Predhiman Kaw, 10^{th} APFA, 14 - 18 December 2015, Gujarat, India.

National Participations

1. In-situ ion heating via a new absorption mechanism with pulsed CO_2 laser in presence of an external magnetic field (Oral Talk) , [Atul Kumar](#), Chandrasekhar Shukla, Deepa Verma, Amita Das and Predhiman Kaw, 33rd National Symposium on Plasma Science and Technology (Plasma-2018), University of Delhi, Delhi, 04-07 December 2018
2. Effect of finite beam width on current separation in beam plasma system. (Poster), [Atul Kumar](#), Amita Das, Chandrasekhar Shukla, Ratan K. Bera, Deepa

Verma, Bhavesh Patel, Devshree Mandal, Ayushi Vashishta, Y. Hayashi, K. A. Tanaka, Amit D. Lad, G. R. Kumar, Predhiman Kaw,
Conference on Plasma Simulation, IISc, Bengaluru, INDIA, 18-19 January 2018

3. Particle-in-Cell simulation of finite - beam width on space charge separation in beam-plasma system,
[Atul Kumar](#), Chandrasekhar Shukla and Amita Das,
29th National Symposium on Plasma Science and Technology (Plasma-2015), SINP Kolkata, West Bengal, 01-04 December 2015
4. Coupling of drift wave with dust acoustic wave,
[Atul Kumar](#), Amita Das, and Predhiman Kaw
29th National Symposium on Plasma Science and Technology and International Conference on Plasma and Nanotechnology (Plasma-2014), Kottayam, Kerala, 08-11 December 2014

Schools:

International Participations

1. International School on Ultra-Intense Lasers,
Moscow, Russia, 4- 9 October 2015.
2. Turbulence, magnetic fields and self organisations in laboratory and astrophysical plasmas,
Les-Houches, France, 23 March-03 April 2015

National Participation

1. Workshop on Laser Plasma accelerator,
ICTS, Bangalore, India, 06 - 17 March 2017
4. Hands-on-School on Nonlinear Dynamics (HSND-2015),
IPR, Gandhinagar-382428. India, 16-22 February 2015.


ATUL KUMAR

Dedicated to

My family and friends

ACKNOWLEDGEMENTS

First and foremost, I would like to express my sincere gratitude to my thesis supervisor Prof. Amita Das for giving me the opportunity to pursue my thesis research under her supervision. I will always remain indebted to her not only for her patience, advice, and immense knowledge over the course of my thesis research, but also for the hard questions which incited me to widen my research from various perspectives. Most importantly, for giving me enough freedom to make my own mistakes and to learn from them but at the same place to push me forward in the right direction. I feel myself privileged and grateful to work under the mentor-ship of Late. Prof. Predhiman Kaw during my entire Ph.D. tenure starting from my coursework itself to till his soul departed to the heavenly abode. He will always be a role model for me because of his ever inspiring enthusiasm and obsession towards learning physics. It is my privilege to thank, Dr. Sudip Sengupta and Prof. G. Ravindra Kumar for their useful suggestions which helped me to improve my thesis. I am highly thankful to Dr. Bhavesh Patel for his support and advice especially during my initial years of Ph.D. which helped me in learning the computational technique.

I am thankful to IPR library, IPR administration, IPR academic committee and computer center staff for their kind support during my thesis period. Mr. Avadhesh deserves special thanks for all official supports. Thanks to my seniors and juniors for providing me a homely atmosphere in the hostel and all the support whenever I needed. I am highly thankful to Dr. Chandrasekhar Shukla who constantly helped me in learning the computational technique and various stimulating physics discussions. I really feel grateful to my friends and colleagues Deepa, Ratan, Sandeep, Chaubeyji, Shivam, Sagar, Mendo, Alam for their love and support throughout Ph.D. tenure. My heartfelt thanks to my wife Meenu for her moral support and motivation, which drives me to give my best.

At the last but not the least, I would like to express the heartiest gratitude my parents, father, Shri Anil Kumar and mother, Smt. Kiran Sharma, for their encouragement, hearty and continual support in my life. A very special thanks to my elder brother, Dr. Alok Kumar and elder sister, Arpana Sharma who encouraged and advised me to pursue physics as my carrier and for always standing behind

me with their love and support.

Finally, I thank the Almighty GOD for giving me the strength and patience to complete my thesis work.

Contents

Synopsis	iv
List of Figures	xiv
1 Introduction	3
1.1 Introduction	4
1.2 Absorption of laser energy by the plasma medium	8
1.2.1 Collisional absorption process	9
1.2.2 Resonance absorption mechanism	10
1.2.3 Brunel/vacuum heating mechanism	11
1.2.4 $\mathbf{J} \times \mathbf{B}$ heating mechanism	12
1.2.5 Improving energy absorption efficiency	13
1.3 Propagation of relativistic electron beam in overdense plasma	13
1.3.1 Beam-plasma instabilities	14
1.3.2 Nonlinear regime of beam plasma instabilities	16
1.3.3 The role of instabilities and magnetic field generation on electron transport	17
1.3.4 Schemes for improved electron propagation	19
1.4 Thesis Layout	19
1.4.1 Chapter 1: Introduction	20
1.4.2 Chapter 2: Energy principle for beam-plasma system insta- bilities	20
1.4.3 Chapter 3: Nonlinear regime of beam plasma instability	21
1.4.4 Chapter 4: Effect of finite beam size and initial current	22
1.4.5 Chapter 5: Direct coupling of laser to ions	22
1.4.6 Chapter 6: Direct coupling of laser to ions: Magnetosonic excitations	23
1.4.7 Chapter 7: Conclusion	23
2 Energy principle for beam plasma instabilities	25
2.1 Introduction	25
2.2 Energy principle analysis of beam-plasma system	27
2.3 Inferences from Energy Principle	32
2.4 Simulation Setup	39

2.5	Simulation results and analysis	39
2.6	Summary	47
3	Nonlinear regime of beam-plasma instabilities	49
3.1	Introduction	50
3.2	Simulation Set-up	52
3.3	Linear stage of instability	53
3.4	Nonlinear stage of instability	55
	3.4.1 Current filaments	55
	3.4.2 Alfvén limited filaments	57
	3.4.3 Electron jet formation	59
3.5	Conclusions	60
4	Effect of finite beam size and initial current	61
4.1	Introduction	62
4.2	The new mechanism for long scale magnetic field generation	63
4.3	Existence of new finite beam instability	67
4.4	Simulation and experimental details	69
	4.4.1 Simulation details	69
	4.4.2 Experimental setup and methodology	70
4.5	Evidences of long scale magnetic field structures	70
	4.5.1 Simulation results	70
	4.5.2 Experimental results	73
4.6	Conclusion	76
5	Direct coupling of laser to ions	77
5.1	Introduction	78
5.2	System configuration	80
5.3	Results and Analysis	81
5.4	Conclusions	88
6	Direct coupling of laser to ions: Magnetosonic excitations	89
6.1	Introduction	90
6.2	Theory of magnetosonic soliton in a cold plasma	92
6.3	System configuration	96

6.4	Results and analysis	97
6.5	Conclusion	103
7	Conclusion and future scope	105
7.1	Main results of this thesis	105
7.1.1	Energy principle for beam plasma system instabilities	105
7.1.2	Nonlinear regime of beam plasma instability	106
7.1.3	Effect of finite beam size and initial current	107
7.1.4	Direct coupling of laser to ions	108
7.1.5	Direct coupling of laser to ions: Magnetosonic excitations	109
7.2	Future scope of these works	109
7.2.1	Theoretical and Numerical explorations	109
7.2.2	Experimental explorations	111

SYNOPSIS

There has been a tremendous progress in high-intensity, short pulse laser technologies in last few decades. As a result, lasers are now capable of delivering enormous energy density upto $10^{22}W/cm^2$ at very fast timescales in the range of femtoseconds/picoseconds. Moreover, many new facilities worldwide are poised to become operational (e.g ELI, XCELS, SULF, SEL etc.) in the near future where the intensity and pulse duration would be pushed to even higher limits namely that of intensities $\geq 10^{24}W/cm^2$ and attosecond scales respectively. Such lasers would open up newer regimes of physics exploration concerning fast ignition laser fusion,¹ generation of charged particle beams,^{2,3} bright source of X-rays⁴ and Gamma-ray flashes and generation of higher order harmonics,⁵ promising source of positron emitters for PET (positron emission tomography),⁶ cosmic accelerations (ultra-high energy cosmic rays),⁷ quantum gravity (Hawking radiation)⁸ etc.

When a laser of intensity ($> 10^{16}W/cm^2$) impinges over a solid target, the target gets immediately ionized to form a plasma. Electrons being a lighter species are the first to respond at rapid time scales of the laser frequency. These electrons absorb the laser energy by various well-known absorption mechanisms which have been studied extensively. These include anomalous skin effect, sheath inverse bremsstrahlung,⁹ sheath transit absorption,¹⁰ resonance absorption,¹¹ vacuum (Brunel) heating,¹² $\mathbf{J} \times \mathbf{B}$ acceleration,¹³ ponderomotive acceleration,^{14,15} stochastic heating,¹⁶ and absorption due to parametric decay instabilities.¹⁷ This leads to the generation of highly energetic and relativistic electron beam at an overdense plasma surface. In response to this, the background plasma induces a return shielding current. Such a system of spatially overlapping, forward and return current flows is fraught with several micro-instabilities, out of which the

electromagnetic Weibel mode is considered to be the dominant one. The Weibel instability¹⁸ creates a current separation at the length scale of an electron skin depth in the plasma. It is believed that the Weibel instability and its nonlinear evolution are responsible for the development of strong magnetic fields ($\sim \text{Mega} - \text{Gauss}$) in the beam plasma system. Thus the propagation of hot electrons generated in the target by laser absorption is another area of wide interest. Therefore, several attempts in past have been made towards curbing the beam-plasma instabilities which proves a major hindrance in beam propagation inside the plasma by destabilizing the system. Some technique involves the resistive collimation of fast electrons by generating guiding magnetic field on the boundary of two different material.^{19,20} Another experimental work by Chatterjee *et al.*²¹ involves using aligned carbon nano-wire arrays as the target. They have demonstrated experimentally efficient transportation of laser-generated mega- ampere electron currents over long distances compared to the flat solid target. A theoretical interpretation was provided by Mishra *et al.* which suggests that the beam Weibel instabilities get suppressed in such inhomogeneous targets.^{22,23} Moreover, the external static magnetic field can be used for suppression of these electron scale instabilities.²⁴ Recently it has been shown that the use strong axial magnetic field can also lead to better beam collimations.²⁵ Furthermore, laser-plasma lenses can also be utilized for relativistic electron beam collimation.²⁶

It is thus clear that the study of Weibel instability has attracted a lot of attention. The excitation of this mode, its nonlinear evolution, the possible ways by which the mode can be suppressed has continued to remain issues of research investigation. In this thesis we have investigated the Weibel mode from energetics angle. For this purpose energy cost associated with the perturbed equilibria is

evaluated to ascertain whether the growth of a particular mode is energetically favorable or not. This technique often provides an interesting physical insight and has been extensively employed in the context of plasma systems governed by Magnetohydrodynamics. Recently, it has been invoked for understanding the electrostatic two stream instability.²⁷ In contrast in the present thesis, it has been shown that even purely growing electromagnetic mode like Weibel instability for the electron beam plasma system is amenable to such a treatment. Such an analysis provides a succinct physical description of the energetics associated with this particular growing mode.²⁸

The strong magnetic field generated through the Weibel destabilization process influences the propagation of electron beam. During the nonlinear evolution of the Weibel instability, the current filaments coalesce to form larger structures. However, there are two distinct phases of the nonlinear evolution of the instability. During the first phase of the evolution, there is a growth of magnetic field energy at the expense of the kinetic energy of the beam. Furthermore, in the second phase of evolution, the magnetic energy shows decay and an increase in the kinetic energy in the system. The underlying physical understanding for the observed decay of magnetic field at later stages²⁹ has been explored in this thesis. The merger of current filaments leading to X point formation where reconnection happens has also been addressed in detail. The generation of the energetic electron jets at the magnetic field reconnecting X points have also been demonstrated.

It is observed that in theoretical analysis and computational studies for a beam-plasma system, the idealized condition of infinite cross section of the beam and/or covering the entire length of the periodic box has always been considered. This is an approximation as in reality the beam is always finite and is commensurate

with the transverse spot size of the laser falling on the plasma target. In such an approximate set-up, the experimental observation of long scale (laser focal spot size scale) magnetic field showing up right from the very beginning^{30,31} can never be accounted for. The Weibel instability in the periodic box appears at the electron skin depth and its nonlinear evolution wherein the current filaments coalesce are too slow to account for the experimental observations of long scale magnetic field spectra. In our studies, we have chosen the electron beam size to be of finite transverse extent. Our simulations provide a mechanism of the existence of long scale magnetic field spectra observed in laser plasma experiments. The mechanism may also have far-reaching consequences for the description of the all-pervading and often enigmatic presence of the long scale magnetic field structures in astrophysical plasmas which have aroused great curiosity and spawned many efforts towards its understanding.

There has been a great deal of interest towards possible mechanisms of enhancing laser energy absorption so as to increase the number and the energy of hot electrons in recent years. Most of these studies have emphasized the role of laser pulse duration, intensity, the role of pre-plasma formation on the front surface of the target etc. It is reported that the presence of pre-plasma on the front surface of the target increases the absorption of laser energy as well as the number of hot electrons.^{32,33} A novel technique using a structured target has shown significant absorption of laser energy as compared to the conventional approaches.³⁴⁻³⁸ The introduction of sub-wavelength nano-layer front has been shown to reduce the reflection and enhance the absorption of energy of the intense short pulse laser.³⁹ It has been demonstrated that the laser energy absorption can be enhanced manyfold using nano-structured targets²³ for both relativistic and non-relativistic high con-

trast, laser intensities. In fact, the structured target provides more surface area for Brunel's mechanism/vacuum heating process. These structured targets provide a geometry which can be used for laser energy absorption even in normal incidence where Brunel's mechanism does not seem to work. Recently, micro-scale fusion has been achieved using such nano-wire array plasmas.⁴⁰

The energetic electrons generated during laser-plasma interactions are then often employed to heat ions in applications such as fast ignition etc., for creating hot spot in the plasma for ignition. This is a secondary process to heat ions and consequently somewhat inefficient. The propagation of energetic electrons is marred by several instabilities which lead to their divergence and loss. Moreover, the Rutherford electron-ion collisional cross section to enable the transfer of energy reduces with increasing electron energy. It is thus desirable to have laser energy directly coupled to the heavier ion species. In addition, there are also many other applications where ion acceleration/heating is of importance, e.g. proton radiography, biomedical applications.⁴¹⁻⁴⁴

The advantages of direct in-situ ion heating/acceleration are many. For instance, there would be (1) Efficient coupling directly to fusion species, viz. background DT species ; (2) Ions being non relativistic and total current being much less than Alfvén critical current for ions, magnetic fluctuations are expected to play negligible role in beam transport and beam stopping; (3) Classical collisional stopping of few MeV ions in dense core will be adequate; (4) Return currents, if any, will excite electrostatic ion acoustic modes leading to anomalous heating of the background plasma. Therefore, there is a need to look for the possibility of new absorption mechanisms through which laser energy can directly be transferred to heavier species of plasma for efficient ion acceleration. This has been

another prime objective of this thesis. We have chosen to apply an external magnetic field of such a magnitude so as to selectively magnetize the electrons at the laser frequency. The heavier ions, however, remain unmagnetized. The electrons thus remain preferentially attached to the field lines whereas the ions can freely move in the electric field of laser. This helps in creating a charge imbalance. It is demonstrated that the ions in such simulations acquire more energy compared to electrons. We have also demonstrated the excitation of ion plasma oscillations and the formation of magnetosonic solitons.⁴⁵

This thesis thus focuses of the twin themes of (i) transport of electron beam through plasmas and (ii) the possibility of direct laser energy absorption by ions using new techniques by making the electrons preferentially magnetized by the choice of appropriate external magnetic field. The content of the thesis has been organized in seven chapters as outlined below:

- **Chapter - I:** In this chapter, a brief summary of the previous studies relevant to this thesis has been presented. It also contains a concise introduction on conventional laser energy absorption mechanisms, beam-plasma instabilities and its role in propagation on an electron beam inside a plasma, schemes to improve laser energy absorption and electron beam propagation in plasma etc.
- **Chapter - II:** In this chapter, an energy principle argument has been employed to study the energetics associated with the electromagnetic Weibel mode in the context of a beam-plasma system. It is clearly shown that there exist perturbations to equilibrium which have both positive and negative

energy contributions. Such perturbations can then grow to keep the total energy of the system conserved. In a typical beam-plasma system, the current filamentation instability leads to the growth of the electromagnetic field energy in the perturbed state at the expense of kinetic energy associated with the flows. Denoting, the beam and background plasma electrons by the suffix $\alpha = 1, 2$, it has been identified that $S_4 = \sum_{\alpha} \frac{n_{0\alpha} v_{0\alpha}^2}{n_0 \gamma_{0\alpha}}$ as the coefficient of the negative energy contributing term and is crucial for driving the instability. It has also been shown that a finite value of $S_3 = \sum_{\alpha} \frac{n_{0\alpha} v_{0\alpha}}{n_0 \gamma_{0\alpha}}$ is responsible for generating an electric field transverse to the flow and in fact, costs energy. Here, $v_{0\alpha}$, $n_{0\alpha}$ and $\gamma_{0\alpha}$ are the equilibrium velocity, electron density and the relativistic factor for the electron species ' α ' respectively and $n_0 = \sum_{\alpha} n_{0\alpha}$ is the total electron density. It is evident that S_3 is finite only for relativistic and asymmetric (beam and background plasma have different densities) flow profile. It is shown that filamentation modes are suppressed when the value of S_3 is finite by comparing the growth rates for various cases in this chapter. For instance, it has been shown that for a constant value of S_4 the growth rate is maximum for $|S_3| = 0$ and reduces monotonically with increasing value of $|S_3|$. We have also carried out 2-D Particle-in-Cell (PIC) simulations under OSIRIS-4.0^{46,47} framework to illustrate the difference between symmetric and asymmetric flow configurations. We have chosen two flow parameters for which S_4 is the same. The value of S_3 is zero for one case (symmetric flow configuration) and is finite for the asymmetric configurations. We have observed that even in the presence of 2-D perturbations (permitted by the 2-D PIC simulations carried out by us), the growth is higher for the symmetric case. Furthermore, the nonlinear saturation level

of the perturbed magnetic field is also found to be higher for the symmetric flow configuration.

- **Chapter - III:** The nonlinear regime of current filamentation/Weibel instability has been addressed in this chapter. The Weibel destabilization leads to the formation of current filaments which are typically of the size of electron skin depth during the linear stage of the instability. During their early nonlinear evolution, these filaments coalesce to form larger structures. With the help of 2-D PIC simulations using OSIRIS-4.0 in the plane perpendicular to the return electron beam (REB) propagation direction, it has been shown in this chapter that these mergers occur in two distinct nonlinear phases. During the first phase of evolution, the total magnetic energy increases in the system. Subsequently, however, during the second nonlinear phase, a reduction in magnetic energy . It has been shown that the transition from one nonlinear regime to another occurs when the typical current associated with individual filaments hits the Alfvén threshold. During the second nonlinear phase, therefore, the filaments can no longer permit any increase in current. Magnetic reconnection events then dissipate the excess current (and its associated magnetic energy) that would result from a merger process leading to the generation of energetic electrons jets in the perpendicular plane. At later times when only a few filaments are left, the individual reconnection events have been clearly identified. It has been observed that in between such events the magnetic energy remains constant and shows a sudden drop as and when the two filaments merge. The electron jets released in these reconnection events further leads to a transverse heating in the system which has also been mentioned in some previous studies⁴⁸

- **Chapter - IV** : The beam-plasma system as of now has been analysed and/or numerically simulated using infinite and/or periodic box conditions. For this case the transverse extent of the beam is chosen to be infinite and/or periodic. As illustrated in the previous chapters such a beam plasma is amenable to Weibel instability generating current filaments and consequently magnetic field structures of the size of electron skin depth scales. The non-linear evolution leads to the coalescence of these structures generating longer scale magnetic fields with time. This cannot account for laser plasma experiments conducted in laboratories which show that the magnetic field at the scale of beam width (longer than the electron skin depth) exists right from the very beginning.

In this chapter, we consider the realistic finite transverse profile of the electron beam. We demonstrate that for a small imbalance in the current (which is again natural in the electron beam system) not only does the long scale magnetic field persisted but also shows a rapid increase. This cannot be accounted for with the usual Kelvin Helmholtz and/or Weibel processes but is in agreement with experimentally observed spectra.^{30,31,49} A possible explanation has been provided analytically for this observation.

- **Chapter - V**: The possibility of ion heating directly with a laser has been another topic of interest. Some of the well-known mechanisms in this regard are the RPA (Radiation Pressure Acceleration)⁵⁰ and TNSA (Target Normal Sheath Acceleration).⁵¹ We have demonstrated another mechanism of ion heating by employing external magnetic fields. The external magnetic field is chosen so as to constrain the electron movement and have them tied to the magnetic field. The heavier ions remain unmagnetized and respond to the

laser electric field. The difference of electron and ion dynamics lead to charge separation and drives ion plasma oscillations, thereby transferring the laser energy to ions to a great extent directly. The proposed mechanism has been demonstrated by carrying out OSIRIS 4.0 simulations using parameters for a CO_2 laser for which the requirement of external magnetic field strength is smaller.

- **Chapter - VI:** We continue our studies on direct energy absorption of the laser by ions in this chapter and show that when the laser power is increased in addition to exciting ion plasma oscillations, the excitation of Korteweg - de Vries (KdV) magnetosonic solitons are also observed. Various diagnostics are employed to characterize these solitons. Interestingly we also observe that the solitons accelerate background electrons when the latter reflects off the front surface of the solitonic structures. The solitons, as expected, propagate stably for several hundreds of ion plasma periods. However, subsequently they are observed to develop transverse modulations which grow with time.
- **Chapter - VII:** We summarize the thesis in this chapter and recapitulate the salient points. We also provide an overview of the future research problems which can be carried out in continuation of the work described here.

List of Figures

1.1	Schematics (not to scale): Laser-matter interaction showing the generation of energetic electrons in the forward direction and shielding electron current induced by plasma in the backward direction	5
1.2	Schematics (not to scale): Resonance absorption of laser energy in plasma where cut-off (at critical density n_c) is followed by the resonance (with density n_r) where blue and orange spheres depicts hot electrons and ions respectively	10
2.1	Schematics (not to scale) of 2-D equilibrium geometry of the beam plasma system where the beam (red circles) and background plasma electrons (green circles) are flowing in positive and negative x direction respectively	28
2.2	The equilibrium condition of charge neutrality and zero current requires that only two parameters out of the four $n_{0\alpha}$ and $v_{0\alpha}$ can be chosen independently. For this figure n_{01} and v_{01} have been chosen independently to understand the variation of the growth rate with respect to them. The figure shows the plot of growth rate as a function of v_{01} . Each curve in the plot corresponds to a distinct value of n_{01} . It should be noted that the curve for $n_{01} = 0.5$ representing symmetric flow configuration, has the highest value of growth rate for all values of v_{01}	38
2.3	(a) Contours of S_4 in the plane of n_{01} and v_{01} : (b) zoomed section of contours of S_4 where astricks denote two points of symmetric and asymmetric flow configurations at the constant contour of $S_4 = 0.25$	38
2.4	The calculation of growth rate of instability by its slope on temporal evolution of magnetic field energy for the symmetric ($S_4 = 0.25$, $ S_3 = 0$) (solid red color curve) and asymmetric flow ($S_4 = 0.25$, $ S_3 = 0.1941$) (dotted blue curve) which match very well with the theoretical growth rate.	40

2.5 Evolution of magnetic field (left column) and electron charge density of the beam (right column) for symmetric flows (prepared by Vapor [J. Clyne *et. al.*, *New Journal of Physics*, 9, 8, (2007); J. Clyne and M. Rast, *Electronic Imaging*, 284-295, (2005)]): The formation of filamentary structures in magnetic field as well as in electron charge density at the order of an electron skin depth, d_e is shown just at the transition from linear to nonlinear stage ($t=15.24$). In the nonlinear stage of instability, the tilted structure of filaments in the magnetic field as well as in electron charge density which is a signature of oblique mode instability, can be seen. The magnetic field energy spectra in the linear regime peaking at d_e is shown within the top left corner of the figure. Further evolution of instability leads to the system in a turbulent regime which is caused by the deflection of charge particles due to a high amplitude magnetic field generated by the instability in the system. 42

2.6 Evolution of magnetic field (left column) and electron charge density (right column) of the beam for asymmetric flow (prepared by Vapor [J. Clyne *et. al.*, *New Journal of Physics*, 9, 8, (2007); J. Clyne and M. Rast, *Electronic Imaging*, 284-295, (2005)]): In the asymmetric flows, the term $|S_3| \neq 0$ stabilizes the system, therefore the growth rate of instability reduces as compared to symmetric flow. The nonlinear phase of the instability, therefore, has a slow onset. . . . 43

2.7 Beam and background particle dynamics for symmetric case in momentum space where isotropization of momentum of beam and background plasma particles can be clearly seen 45

2.8 Beam and background particle dynamics for asymmetric case in momentum space where isotropization of momentum of beam and background plasma particles can be clearly seen 46

3.1 Schematic (not to scale) of magnetic reconnection where the magnetic field lines reconnects and accelerates the plasma particles as a jet 52

3.2	The transverse magnetic field $B_{\perp} = \sqrt{B_x^2 + B_y^2}$ [in unit of $m_e c \omega_{pe} / e$] at $t \omega_{pe} = 51$: The size of magnetic field structure in linear regime is the order of c / ω_{pe}	54
3.3	Calculation of linear growth rate from PIC simulation	55
3.4	Evolution of energy (in unit of $n_0 m_e c^2$) with time: The solid blue curve shows the magnetic field energy $ B_{\perp} ^2 = B_x^2 + B_y^2 $ and the decay in magnetic field energy at later time can be clearly seen. The solid black curve is for transverse kinetic energy W_{beam}^{\perp} of beam and dotted red curve is for transverse kinetic energy W_{plasma}^{\perp} of plasma. In the plots, we observe the gain in the transverse kinetic energy of plasma as well as beam at the same time when magnetic reconnection phenomena occurs and magnetic field energy decay. The color plot of kinetic energy of plasma particle has been shown in the inset of figure which shows the jet like structure.	56
3.5	The merging of beam current filaments highlighted by white box	57
3.6	The time evolution of number of current filaments(solid red curve), average current per filament (solid blue curve) and Alfvén (solid green curve).	58
3.7	The formation of jet like structure during the magnetic reconnection process in background plasma charge density [highlighted by arrow]	59
4.1	Schematics (not to scale) of 2D- equilibrium geometry of the beam plasma system where beam has finite width '2a' in the transverse direction	64
4.2	Snapshots of magnetic field B [in the units of $(m c \omega_{pe} / e)$] and electron density evolution in time t [in the unit of ω_{pe}^{-1}] for asymmetric flow configuration (<i>i.e.</i> for a finite value of S_3) has been depicted (prepared by Vapor [J. Clyne <i>et. al.</i> , <i>New Journal of Physics</i> , 9, 8, (2007); J. Clyne and M. Rast, <i>Electronic Imaging</i> , 284-295, (2005)]). Case(a) and Case(b) depicts the spatio temporal evolution of magnetic field B_z and the electron density respectively. At time $t = 18.0$, development of only long scale structures (B_z field with the opposite polarity) can be seen, at $t = 30$ KH mode at the beam edge and a faint Weibel instability in the bulk appears.	71

4.3	Evolution of E_{1x} profile as a function of y showing the minimal variation inside the beam region in the beginning in conformity with generation of long scale magnetic field structures.	72
4.4	Snapshots of 3D PIC simulation with OSIRIS (prepared by Vapor [J. Clyne <i>et. al.</i> , <i>New Journal of Physics</i> , 9, 8, (2007); J. Clyne and M. Rast, <i>Electronic Imaging</i> , 284-295, (2005)]) at time $t = 78.6$ in the unit of ω_{pe}^{-1} . Subplots (a) and (b) depict 3D volume rendering of poloidal magnetic field and electron density respectively. In subplot (c) and (d) the cross sectional view in the $r - z$ plane have been shown for the magnetic field and the electron density respectively.	73
4.5	Evolution of Magnetic field spectra from PIC simulations with OSIRIS Case(a) Finite beam-plasma system was considered in simulation. The spectral maximum is at at the width of the beam right from the beginning; Case(b)-Periodic box simulations corresponding to infinite beam-plasma system where peak of the field spectra appears at the electron skin depth due to Weibel mode and the nonlinear cascade towards long scale can be seen to be very slow.	74
4.6	Power spectrum of magnetic field spatial profile measured at pump-probe delay of 0.4 picoseconds	75
5.1	Schematic [not to the scale] representing charge separation and laser energy absorption via $\vec{E} \times \vec{B}$ drift with pulsed CO_2 laser in presence of an external magnetic field B_{0z}	80
5.2	Laser energy evolution (red curve with square) and evolution of kinetic energy of plasma species viz. ions (blue solid curve with triangles) and electrons (blue solid line with red circles) via $\vec{E} \times \vec{B}$ drift with pulsed CO_2 laser in presence of an external magnetic field B_{0z}	82
5.3	Temporal evolution of electron and ions density fluctuations with respect to x and averaged over \hat{y} direction (a) without magnetic field and (b) with magnetic field . Charge separation between two species, electrons and ions are clearly evident in right two sub-plots in presence of a transverse external magnetic field, B_{0z}	84

5.4	Temporal evolution of transverse magnetic field B_z with respect to x and averaged over \hat{y} direction (a) without magnetic field and (b) with magnetic field. It is obvious from the left two sub-plots that laser gets totally reflected back in absence of an external magnetic field B_{0z}	85
5.5	Temporal evolution of particles (electrons and ions) distributions in momentum species (a) without a magnetic field and (b) with magnetic field. It is obvious from the left two sub-plots that laser energy does not get absorbed by ions when there is no any external magnetic field B_{0z} and a slight heating in electrons is observed. However, in presence of a transverse external magnetic field, laser energy gets coupled to heavier ion species in the plasma, leading to a significant heating in ion species.	86
5.6	Temporal evolution of electrons and ions count from the simulation showing that the ions are accelerated significantly whereas the electrons motion is restricted when there is an applied external magnetic field in the system	87
6.1	Schematic (not to the scale) which shows the system configuration for the excitation of magnetosonic KdV solitons with pulsed CO_2 laser in presence of an external magnetic field B_{0z}	96
6.2	Temporal evolution of plasma current with respect to x and averaged over \hat{y} direction (a) without magnetic field and (b) with magnetic field. it is clear from the left and right subplots that a significant amount of plasma current is generated when there is an external magnetic field and for higher intensities of CO_2 laser. Even when laser intensity is relativistic, the plasma current generated by $\vec{J} \times \vec{B}$ heating mechanism is negligible in absence of the external magnetic field	98
6.3	Temporal evolution of the ion density with respect to x and averaged over \hat{y} direction where three solitary structures A, B, and C are shown for higher intensities of pulsed CO_2 laser.	99

6.4	Temporal evolution of the perturbed electromagnetic fields B_z and E_y corresponding to the magnetosonic KdV solitons with respect to x and averaged over \hat{y} direction	100
6.5	Temporal evolution of the electron density n_e and electrostatic field E_x with respect to x and averaged over \hat{y} direction.	100
6.6	1D plot Ion density with respect to x and averaged over \hat{y} direction. It is evident from this plot that magnetosonic solitons do get excited with different mass ratios.	102
6.7	Surface plot of the ion charge density. Transverse filamentation of each peak of the ion charge density of the magnetosonic KdV soliton is quite evident from this figure. It has been shown that at $t = 1696.8fs$, transverse filamentation starts and it continues to grow with time	103

1

Introduction

This thesis makes important forays in two directions, namely (i) electron beam propagation through plasmas and (ii) the possibility of direct laser energy absorption by ions using a new technique based on CO_2 laser along with a strong external applied magnetic field.

In the first theme of electron beam propagation, several issues has been addressed. An energy principle have been obtained for the Weibel instability which provides a clear physical understanding of the instability. Furthermore, PIC (Particle - In - Cell) simulations have been carried out to understand the nonlinear regime of instability. It has been demonstrated that as the Weibel generated electron current filaments coalesce, magnetic field lines reconnect and energetic electron jets are produced in the transverse plane. This process illustrates a rapid mechanism of isotropization of electron distribution in momentum phase space. Another important contribution of the thesis is the discovery of a new mechanism, distinct from Weibel and Kelvin Helmholtz (KH) mode, which is operative when an electron beam propagates through a plasma medium. Unlike Weibel and KH modes, where the magnetic field forms at the electron skin depth scale preferentially, it has been shown that in practical situations magnetic fields at long scales commensurate with the transverse width of the electron beam gets generated. Theoretical analysis and PIC simulations have been carried out to illustrate these phenomena.

It is well known that an intense laser transfers its energy preferentially to the lighter electron species in the plasma. To heat ions in the plasma one relies on its coupling with electrons which becomes inefficient with increasing electron energy. A new mechanism of direct coupling of laser energy to heavier ion species has been

proposed. It utilizes pulsed CO_2 long wavelength laser along with an external applied magnetic field of the order of tens of kilo Tesla to keep the electrons tied to the field lines. With the recent advancement of magnetic field of the order of several tens of Kilo-Tesla in the laboratory⁵²⁻⁵⁴ these requirements appear to be within technological reach in near future.

1.1 Introduction

There has been a tremendous progress in high-intensity, short pulse laser technologies in last few decades. At present lasers are capable of delivering enormous energy density upto $10^{22}W/cm^2$ at very fast time scales in the range of femtoseconds/picoseconds. In the near future many new facilities worldwide are poised to become operational (e.g ELI, XCELS, SULF, SEL etc.^{6,55-57}) where the intensity and timescale limit would be pushed to even higher limits namely that of intensities $\geq 10^{24}W/cm^2$ and attosecond scales respectively. Such laser would open up newer regimes of exploration in terms of physics in fast ignition laser fusion,¹ generation of charge particle beams,^{2,3,58} bright source of X-rays^{4,59} and Gamma-ray flashes and generation of higher order harmonics,⁵ promising source of positron emitters for PET (positron emission tomography),⁶ cosmic accelerations (ultra-high energy cosmic rays),⁷ quantum gravity (Hawking radiation)^{8,60} etc.

When a laser of intensities ($> 10^{16}W/cm^2$) interacts with a solid target, the target gets ionized to form a plasma instantaneously. Fig. (1.1) shows the schematics of such a laser and its pre-pulse interacting with a solid density target. The time scale of the laser being rapid, the lighter electron species in the plasma are the first to respond and absorb its energy by various well known mechanisms namely anomalous skin effect, sheath inverse bremsstrahlung,⁹ sheath transit absorption,¹⁰ resonance absorption,¹¹ vacuum (Brunel) heating,¹² $\mathbf{J} \times \mathbf{B}$ acceleration,¹³ ponderomotive acceleration,^{14,15} stochastic heating,¹⁶ and absorption due to parametric decay instabilities.¹⁷ This leads to the generation of a relativistic electron beam at an overdense plasma surface. When these energetic electrons created by the laser field move in the preformed plasma, the plasma provides for return shielding currents. The combination of forward and return currents is susceptible to many instabilities. Weibel being one of the dominant one. The Weibel instability

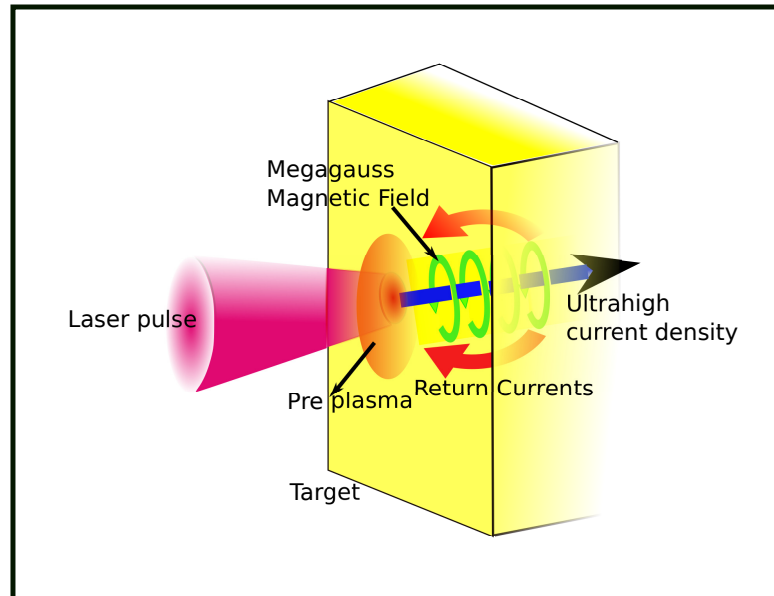


Figure 1.1: Schematics (not to scale): Laser-matter interaction showing the generation of energetic electrons in the forward direction and shielding electron current induced by plasma in the backward direction

creates a current separation at the length scale of an electron skin depth in the plasma, which leads to a generation of a strong magnetic field ($\sim MGauss$).³⁰ It is believed that the Weibel instability and its nonlinear evolution are largely responsible for the development of strong magnetic fields in astrophysical contexts like the relativistic shock formation in Gamma-ray bursts (GRBs),⁶¹ the high energy cosmic rays,^{62,63} active galactic nuclei (AGN)⁶⁴ etc. In laser driven laboratory experiments also, Huntington *et. al.*⁶⁵ have observed the ion-Weibel instability in interpenetrating plasma flows. However, the experimental observation of magnetic field generation by the Weibel instability at electron dynamics scale still remains a challenge. In a typical beam-plasma system, a fraction of the kinetic energy (δK) associated with the flows get converted into the electromagnetic excitations. Such disturbances feed upon themselves leading to the development of Weibel/current filamentation instabilities.

The energy principle often provides a succinct physical description for analysing the stability of hydrodynamic fluids in a conservative system.⁶⁶⁻⁷¹ In plasmas also, the ideal Magnetohydrodynamic (MHD) excitations have often been interpreted using energy principle⁷²⁻⁷⁶ for both equilibria with and without flows in a variety

of contexts, e.g. magnetic fusion,^{77,78} astrophysics, solar and space physics^{79,80} etc. Very recently, Lashmore-Davis²⁷ has carried out energy principle analysis for the electrostatic perturbation in a beam-plasma system leading to the two-stream instability. In this thesis, an energy principle analysis has been enunciated to understand the energy exchange from the kinetic energy of the particle to electromagnetic energy during the linear evolution of Weibel instability in a homogeneous beam-plasma system.

The growth of magnetic field through the Weibel destabilization process influences the propagation of electron current filaments. In the nonlinear stage, current filaments are observed to coalesce and form larger structures. There are indications from previous studies⁸¹ that at the early nonlinear stage of evolution there is a growth of magnetic field energy. Subsequently, however, the magnetic energy shows decay. The physical mechanism for the observed decay of magnetic field at later stages has been the focus of our studies. There are suggestions that the merging process of super Alfvénic currents carrying filaments leads to the decay of the magnetic energy.⁸¹ On the other hand, the mechanism of magnetic reconnection which rearranges the magnetic topology in plasma converts the magnetic energy to kinetic energy of the particles. This can result in thermal particles or the particles may even get accelerated^{82,83} by the reconnection process. The merger of current filaments leading to X point formation where reconnection happens has also been addressed in this thesis.

The all-pervading and often enigmatic presence of the magnetic field in many natural phenomena has aroused great curiosity and spawned many efforts to understand the generation mechanisms. The conventional existing theories on beam-plasma systems consider Weibel/current filamentation instability responsible for the mega-gauss order of magnetic field generation in a beam-plasma system. However, many laboratory experiments^{30,31} on laser-solid interactions have reported the generation of magnetic field at the scale lengths much longer (comparable to the transverse beam dimension) than the conventional Weibel and Kelvin Helmholtz modes typically associated with the beam plasma system. The long-standing puzzle of long scale magnetic field generation laser-plasma experiments has been addressed in this thesis.

Often, one is interested in the transport of electron beam which gets generated from the laser when incident on the solid target. The crucial aspects of transport

and dynamics of these particles especially in the context of fast ignition scheme of laser fusion can be understood from the following discussion. Fast ignition is an alternative concept of laser fusion in which the task of compressing the fusion pellet to super solid densities ($\sim 1000gm/cc$) or more is accomplished by conventional high energy nanosecond glass lasers and the task of igniting the compressed pellet is given to a separate high intensity, moderate energy pico second energy source which can set pellet ablaze (with DT fusion reactions) by creating an adequate size hot spot with ignition temperatures $\sim 5KeV$ in it. The use of very high intensity 1 micron laser picosecond pulses have not proven to be efficacious because the laser energy ends up in a relativistic electron beam at overdense compressed surface, which creates massive forward and return currents, current instabilities and filamentations of the beam on a rapid electron time scale.^{18,28,86-94} These instabilities lead to a divergence of the incident electron beam away from the central compressed target, thus preventing the formation of a hot spot in the interior. Few attempts have been made in past to curb the electron scale instabilities and beam collimation for instance by using axial magnetic field.⁹⁵ Other schemes considered, include mitigation of instabilities leading to turbulent magnetic fields with externally produced guiding magnetic fields (in the range of $1 - 10Kilo - Tesla$),⁹⁶⁻¹⁰¹ initiation using shock waves, using externally produced ion beams etc., but none so far have shown significantly improved results. It is thus clear from the above discussion that the success of fast ignition crucially hinges upon efficient absorption of laser energy and also the subsequent propagation and dynamics of the energetic charge particles like electrons and ions through the plasma. One point of departure from the past experience can be a mechanism for the efficient coupling of laser energy preferentially to ions and restricting the motion of electrons by applying an external magnetic field to mitigate electron scale instabilities. The CO_2 lasers can be most suitable lasers available in the market and immediately come to mind in this regard because of their low frequency and their recent availability for short pulse applications.¹⁰² But how do we utilize the CO_2 laser for giving its energy directly to ions? If we consider ion heating for fast ignition of a fusion pellet, the requirements may be put as ion energy $\sim 10MeV$, beam current $250MAmps$, beam period $10psec$ which is a $25KJ$ beam pulse. An efficient conversion of CO_2 laser energy into ion beam energy can thus give the required source of energy for fast ignition laser fusion. Therefore, there is a need to look for the possibilities of

new absorption mechanisms by which energy of laser can be preferentially coupled to ions in plasma and restricting the electron motion to avoid the electron scale instabilities. We have carried out theoretical analyses for new laser absorption mechanisms for ion accelerations/heating in this thesis which is further aided by PIC simulations also.

It is now clear that the absorption of laser energy is one of the crucial aspects of laser-plasma interactions. One would like such a process to be efficient. Most mechanisms of laser energy absorption result in the creation of energetic electrons which are employed for several applications. These applications often rely on the propagation and energy dissipation of these energetic electron beams through the plasma, which is another important issue. In the subsequent sections, we discuss the present understanding of these two issues. We discuss the various known mechanism of laser energy absorption by the plasma medium. We also provide the present status of the physics understanding of energetic electron beam propagation in plasmas. New possibilities and issues that need to be looked into with new perspective in these areas are highlighted. Thereafter, we provide a summary of the contribution that has been made in this thesis in these areas.

1.2 Absorption of laser energy by the plasma medium

An intense light/laser interaction with a solid target leads to many exotic physical phenomena. However, efficient absorption mechanisms of light energy to the highly dense plasma is still a challenging task. High intensity laser pulses have a pre-pulse and pedestal features with an intensity of at least 10^{-8} of the main pulse intensity. Thus the pre-pulse of a laser has sufficient energy to ionize the solid target to the plasma state. Afterwards, the main laser pulse is absorbed inside this plasma by various absorption mechanisms like collisional absorption process,^{103,104} $\mathbf{J} \times \mathbf{B}$ heating,¹⁰⁵ vacuum heating,¹⁰⁶ resonance heating¹⁰⁷ etc. The absorption, reflection or propagation of laser in plasma depends on characteristic features of the laser as well as the plasma. The intensity of the laser, its pulse duration, the shape of the pulse, laser wavelength, polarization, the angle of the incident etc., are the main effective parameters of laser which influence the absorption process. The plasma density profile and the scale length of its inhomogeneity are the plasma re-

lated important determining factors for the absorption process. The conventional methods of laser energy absorption into the plasma is briefly described in the next few subsections.

1.2.1 Collisional absorption process

At lower intensities ($< 10^{15} \text{W/cm}^2$) and longer pulse durations ($\sim ns$) of lasers, collisional absorption process is the dominant mechanism of laser energy absorption in plasma. In this process, plasma electrons acquire the energy from the laser. These electrons transfer a fraction of energy to ion species through coulombic interaction. This ultimately leads to plasma heating. The electron-ion Coulomb collision frequency in critical surface of plasma¹⁰⁸ is given by:

$$\nu_{ei} = \frac{4\sqrt{2\pi}}{3} \frac{n_e Z_i e^4 \ln \Lambda}{m_e^{1/2} (k_B T_e)^{3/2}} \quad (1.1)$$

where n_e , T_e and m_e are the plasma density profile, electron temperature, and electron mass respectively. Z_i is the ion charge, $\ln \Lambda$ is the Coulomb logarithm and k_B is the Boltzmann constant. The electron-ion collisional frequency is much smaller than the laser frequency in an overdense plasma *i.e* $\nu_{ei} \ll \omega_L$ and $\omega_L^2 - \omega_{pe}^2 \gg \frac{\nu_{ei}}{\omega_L} \omega_{pe}^2$ where, ω_L and ω_{pe} are the laser and electron plasma frequencies. As the laser propagates through the plasma, laser energy dissipates to heat the plasma through electron-ion collision mainly via inverse bremsstrahlung^{109,110} and normal skin effect.¹¹¹ As it is evident from the Eq.(1.1) that the collisional frequency is inversely proportional to the electron temperature, the collisional absorption mechanism becomes less effective at higher intensities. For laser intensities $I > 10^{15} \text{W/cm}^2$, the collisionless absorption mechanisms start to play dominant role. The main collisionless absorption mechanisms are anomalous skin effect, sheath inverse bremsstrahlung,⁹ sheath transit absorption,¹⁰ resonance absorption,¹¹ vacuum (Brunel) heating,¹² $\mathbf{J} \times \mathbf{B}$ acceleration,¹³ ponderomotive acceleration,^{14,15} stochastic heating,¹⁶ and absorption due to parametric decay instabilities.¹⁷ While vacuum heating, resonance absorption, $\mathbf{J} \times \mathbf{B}$ acceleration and ponderomotive acceleration are for overdense plasmas while stochastic and parametric decay instabilities aid the absorption processes in underdense plasmas.

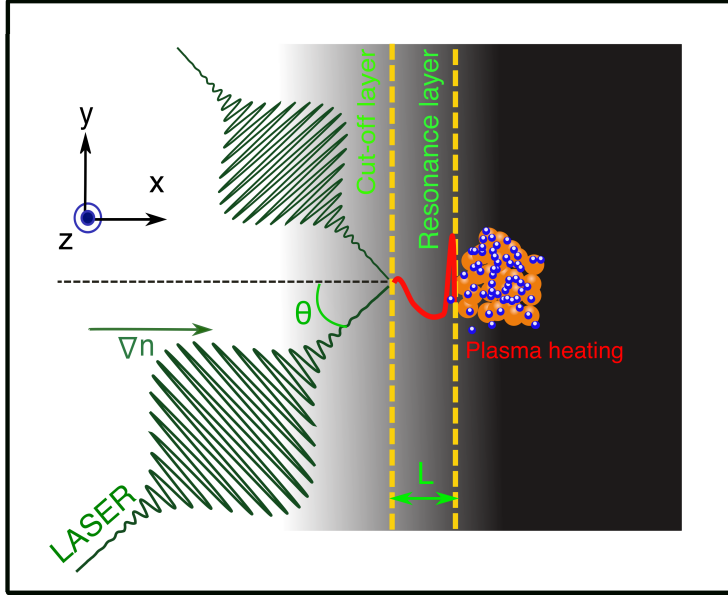


Figure 1.2: Schematics (not to scale): Resonance absorption of laser energy in plasma where cut-off (at critical density n_c) is followed by the resonance (with density n_r) where blue and orange spheres depicts hot electrons and ions respectively

1.2.2 Resonance absorption mechanism

In an inhomogeneous density profile such that a cutoff is followed by the resonance, a laser incident obliquely can be absorbed via resonance absorption process which leads to plasma heating. Fig. (1.2) shows the schematics of resonance absorption of laser energy into plasma. However, it has been shown by Budden¹¹² and others^{113–115} that when an electromagnetic (EM) wave is incident from the region with cut off followed by resonance, the sum of the reflection and transmission coefficients does not add up to unity. This puzzle was solved by Budden¹¹² when he showed by mathematical analyses that the difference of energy is absorbed because of the coupling to electrostatic waves in the resonance region. When the cut off and the resonance are sufficiently close to each other, the evanescent electric field which gets tunnelled from the cut-off region, sets up a nonlinear plasma electron oscillations parallel to density gradient direction through mode conversion to electrostatic wave from the electromagnetic wave which is further resonantly enhanced by plasma. This high amplitude nonlinear plasma oscillations ultimately suffer wave breaking leading to the generation of a sufficiently large number of

energetic electrons. The wave breaking of plasma wave further used to heat the plasma species. This process is called resonance absorption and dominates over all the other processes when the condition

$$\omega_L L/c \sim \sin\theta, \quad (1.2)$$

is satisfied. Here L is the plasma density scale length and ω_L is the laser frequency. However, this mechanism fails to work when the laser falls on the steep density gradient plasma surface. The resonance absorption mechanism breaks when the amplitude of the plasma oscillation is greater than the gradient scale length *i.e.* $L < v_{osc}/\omega_L$ where v_{osc} is the electron quiver velocity.

1.2.3 Brunel/vacuum heating mechanism

Brunel¹² gave another absorption mechanism named after him as Brunel mechanism or vacuum heating process for a p-polarized laser incident obliquely to a plasma surface with sharp interface. This process is based on ‘capacitor approximation’ in which magnetic field of the wave is ignored (*i.e.* $\vec{v} \times \vec{B}$ term can be neglected when electron quiver velocity is very less than the speed of light c). Now the obliquely incident laser has an electric field component normal to the sharp interface plasma surface. This electric field component pulls out electrons in the vacuum from the plasma with the steep density profile in first half cycle of laser and sends them back in the plasma with electron quiver velocity in the other half cycle of the laser. This process increases the kinetic energy of the electrons and the laser energy in this way gets converted to kinetic energy of the electrons efficiently. This mechanism is highly efficient when the following conditions are satisfied

$$L < v_{osc}/\omega_L; \quad v_{osc} > v_t$$

where v_{osc} and v_t are the quiver and the thermal velocity of the electron respectively. However, this mechanism does not work when a p-polarized laser incident normal to the sharp interface plasma surface as a normal component of electric field is absent in this case.

1.2.4 $\mathbf{J} \times \mathbf{B}$ heating mechanism

The intensity at which the quiver velocity of electrons become comparable to the speed of light c is known as relativistic intensity. A normalized vector potential a_0 is defined as

$$a_0 = \frac{eA}{m_e c^2}. \quad (1.3)$$

For highly intense lasers ($\sim I > 10^{18} \text{W/cm}^2$) which corresponds to $a_0 \geq 1$, relativistic effects becomes important. At such intensities, for a p-polarized, intense laser incident normal to a sharp vacuum plasma interface, dominant absorption mechanism at such high intensities is the $\mathbf{J} \times \mathbf{B}$ heating.¹⁰⁵ At such intensities, the quiver velocity of electrons becomes comparable to the speed of light c . Therefore, the $\vec{v} \times \vec{B}$ term cannot be neglected now. This term becomes the driving term in this case which oscillates at twice the laser frequency. A linearly polarized wave $E = E_0(x) \sin \omega_L t$ provides to a longitudinal force term

$$F_x = -\frac{m}{4} \frac{\partial v_{osc}^2}{\partial x} (1 - \cos 2\omega t) \quad (1.4)$$

The first term in right-hand side of Eq.(1.4) is the DC ponderomotive force which pushes the electron inwards and the second term leads to pull the electrons in vacuum and send it back to plasma in a fashion analogous to the Brunel mechanism. Thus $\vec{J} \times \vec{B}$ term couples the laser energy to the plasma electron. Therefore, this absorption process is known as $\mathbf{J} \times \mathbf{B}$ heating mechanism. It works for any polarization of laser apart from the circular and is the most efficient mechanism of laser absorption for a normal incident laser when electron quiver velocity is relativistic.

In all these conventional schemes the laser energy is dumped into the lighter electron species. If one wishes to heat the plasma then one has to rely on the transfer of electron energy to the heavier ion species. This process can sometimes be pretty inefficient with increasing electron energy as Rutherford's collisional cross section decreases at higher electron energy. In this thesis, we provide a mechanism whereby the laser energy can be directly transferred to ions without invoking the intermediary role of electrons.

1.2.5 Improving energy absorption efficiency

There has been a great deal of interest towards possible mechanisms of enhancing laser energy absorption so as to increase the number and the energy of hot electrons¹¹⁶⁻¹²² in recent years. Most of these studies have emphasized the role of laser pulse duration, intensity, the role of pre-plasma formation on the front surface of the target etc. It is reported that the presence of pre-plasma on the front surface of the target increases the absorption of laser energy as well as the number of hot electrons.^{32,33,118} Recently, a novel technique of structured target has been used which shows significant absorption of laser energy as compared to the conventional approaches. Both experimental and simulation works have been carried out towards observing and understanding increased production of hot electrons by designed target.³⁴⁻³⁸ The introduction of sub-wavelength nano-layer front has been shown to reduce the reflection and enhance the absorption of energy of the intense short pulse laser.³⁹ It has been demonstrated that the laser energy absorption can be enhanced manifold using nano-structured targets²³ for both relativistic and non-relativistic high contrast laser intensities. In fact, the structured target provides more surface area for Brunel's mechanism/vacuum heating process. These structured targets also provide a geometry which can be used for laser energy absorption even in normal incidence where Brunel's mechanism does not seem to work without any structured target. Recently, micro-scale fusion has been achieved using such nano-wire array plasmas.⁴⁰

1.3 Propagation of relativistic electron beam in over-dense plasma

The energetic electrons which are created by the lasers are often utilized for various applications. These involve table top radiation sources, fast ignition scheme of laser fusion etc. In the fast ignition scheme, one wishes to create the ignition spark in an already compressed fusion pellet using the energetic electrons created by lasers at the critical density surface. There are number of ways to approach this scheme. One such scheme is known as "Re-entrant cone guided fast ignition".^{1,84,85} In this scheme a small gold cone is embedded into the side of the spherical fuel capsule,

providing a clear pathway to the central region where the compressed fuel globule is formed. The ultra-intense laser that ignites the fuel is fired into the cone. Where it interacts with the cone tip, an enormous number of extremely energetic electrons are generated. These electrons fly out into the fuel, heating to the temperatures required for fusion. This, therefore, requires that the energetic electrons should propagate through the plasma from the critical density to the compressed core and then dump its energy to create a hot spot for ignition. In such an application, therefore, the physics of electron beam transport through the plasma medium has a crucial role. Furthermore, the propagation of electron beam through plasma itself is interesting in its own right. It throws light on the possible mechanisms of magnetic field generation, its nonlinear evolution, turbulent excitations etc., the understanding of which is relevant in astrophysical scenarios also.

The highly energetic and relativistic electrons generated during the laser-solid interaction carries a massive electron current ($\sim MAmps$). In the vacuum, the electron trajectories carrying this current would turn due to the self generated magnetic field. In fact, the maximum current that an electron beam can carry in the vacuum is provided by the Alfvén current limit, which is $17\beta\gamma$ kAmps, where $\beta = v_e/c$ and γ is the Lorentz factor. In plasma, propagation of fast electrons with the current exceeding the Alfvén limit is permissible. Plasma induces a return current in response to the forward electron current generated during the interaction of laser with a solid target. If the electron beam spot size is less the electron skin depth c/ω_{pe} , then the return current flows from outside of the beam in the backward direction to shield the electron current generated in the forward direction. When the beam width is few times electron skin depth, the return current and the beam current spatially overlap making it a current neutral system. The width of the electron beam is typically commensurate with the laser spot size and is in general greater than the electron skin depth.

1.3.1 Beam-plasma instabilities

The spatially overlapping forward and return electron current flows are susceptible to several microinstabilities. For instance two stream instability,^{90,123} current filamentation instability,^{124,125} oblique instability⁹¹ Weibel instability,^{18,28} Buneman instability⁸⁸ are the few such instabilities which are generated due to forward and

return current flow in the system. These instabilities severely affect the transport of the energy and momentum of the electron beam inside the plasma. While the two-stream and the Buneman instability are of electrostatic character, the other instabilities are primarily of electromagnetic nature.

The configuration of counterstreaming forward and return current leads to a charge separation in the system. It was Langmuir¹²⁶ in year 1925 who suggested the existence of oscillations in a beam-plasma system. Pierce in the year 1948 demonstrated that these oscillations can go unstable in nonlinear regime.¹²⁷ Bohm and Gross then explained using kinetic theory on the unstable perturbation propagating along the beam direction.¹²⁸ This unstable perturbation in the beam-plasma system is popularly known as ‘two stream instability’. It leads to creation of a charge separation along the beam propagation direction in the system and is of purely electrostatic nature. Later, it has been shown by Fried¹²⁹ that a beam-plasma system is also unstable to electromagnetic perturbations which grow transverse to the beam flow direction. This class of instability is known as ‘current filamentation instability’.

Weibel¹⁸ in 1959 showed that a temperature anisotropy in a counterstreaming current flows can also lead to a space charge separation in the system and it is known as ‘Weibel instability’. The Weibel instability is driven by an anisotropy in the velocity distribution of the plasma particles, where the velocity spread in one direction is larger than another, that is both electromagnetic, and electrostatic (as the current filaments also contain static charge). The wavenumber is always directed perpendicular to the "hot" direction where the velocity spread is greater. In the case where there are two plasma populations, at the same location moving in opposite directions, the velocity spread is greater in the direction of the flow, and in this case, the Weibel instability is referred to as the current filamentation instability. The Weibel instability was originally derived in the non-relativistic limit. In the relativistic limit, the exact distribution of velocities becomes important, and distinguishing the current filamentation instability becomes more relevant. Although the current filamentation instability is driven by the velocity spread of the two counter-propagating plasmas, the two-stream instability also occurs which is driven by the two peaked velocity distribution with a wavenumber parallel to the flow direction. There exists a hybrid of these two instabilities known as the ‘oblique instability’, which grows fastest with a wavenumber somewhere between the cur-

rent filamentation and two-stream modes. The tilted current filament structure in beam-plasma system are the signature of this instability.^{130,131}

It should be noted that in the analytical as well as numerical studies of these beam-plasma instabilities have always been carried out under the assumption of the infinite and/or periodic system. The real electron beam generated from the laser has a finite transverse as well as longitudinal extent. Furthermore, the background plasma current would not instantaneously neutralize the beam current entirely everywhere. The course of evolution with these realistic considerations need to be understood.

Furthermore, it is important to note that the electromagnetic instabilities discussed above have growth rates which dominate at the scale length of the electron skin depth and hence they are responsible for the generation of magnetic field at such scales. These magnetic fields, in turn, react on the flow of the beam and background plasma electrons and play a very important role in their propagation. A better understanding of this can be gleaned only from nonlinear studies for which one has to rely on numerical simulations.

1.3.2 Nonlinear regime of beam plasma instabilities

The nonlinear fate of the electrostatic two-stream instabilities has been studied in detail by Goldman¹³² and Wharton *et. al.*¹³³ In the nonlinear regime of two-stream instability, a periodic chain of electron phase space holes are formed upon saturation leading to the increase of electrostatic field energy at the expense of kinetic energies of the flows in the system. These coherent structuring of phase space have been first observed experimentally in Ref.⁽⁹⁰⁾. In the post-saturation phase of nonlinear two-stream instability, these phase space holes coalesce due to coalescence instability until they form single coherent structure. These structures are unstable to transverse instability¹³⁴ in multidimensional space which is different than the coalescence instability. Any charge modulation transverse to the electron phase space holes is amplified by the self focusing until it get disrupted. The guided magnetic field can be used to minimize the self-focusing and lifespan of these structures.¹³⁵ However, these structures are stable enough to be observed in space¹³⁶ and in laboratory experiments.¹³⁷

The space charge separation created by the current filamentation/Weibel in-

stability in their nonlinear evolution passes through two distinct phases. Similar to electrostatic two stream case, in the first phase of nonlinear evolution, the magnetic energy of the current filaments continues to grow at the expense of kinetic energies of the electron flows in the system. This is because of the coalescence of the current filaments.²⁸ In the later phase of the nonlinear regime of the instability, there is an increase in the kinetic energy of particles and decrease in the magnetic energy of the system because of magnetic reconnection process between two filaments. Magnetic reconnection events then dissipate the excess current (and its associated magnetic energy) that would result from a merger process leading to the generation of energetic electrons jets in the perpendicular plane. These energetic electrons causes a transverse heating and an increase in the kinetic energy of the system. The current filaments produced by the Weibel instability are subject to violent kink-type deformations which are associated with a resonance between drift velocity of the current carrying ions and a longitudinal drift kink mode.¹³⁸ This dominates the slows down of the electrons flows and leads to isotropization of the magnetic field in the system. Furthermore, magnetic turbulence leading to the turbulent fragmentations and filamentations of the electron beam in laser-plasma experiments has also been observed in recent experiments.³¹

1.3.3 The role of instabilities and magnetic field generation on electron transport

Laser energy is preferentially absorbed by the lighter electron species of the plasmas as they respond at the fast laser frequency. This leads to the generation of the energetic electron beam which propagates inside the plasma. However, the electron beam thus produced are severely affected the induction of return shielding current in the plasma leading to several streaming instabilities mentioned earlier in the system. A huge amount of Mega-Gauss magnetic field is generated due to these instabilities. The electron beam rapidly diverges due to this large magnetic field in the system. Thus the transport of momenta and energy associated with the electron beam to larger distances can be realized in practical situations.

The energetic electrons thus generated are then often employed to heat ions in applications such as fast ignition etc., for creating hot spot in the plasma for ignition.¹ This is a secondary process to heat ions and consequently somewhat

inefficient. The propagation of energetic electrons is marred by several instabilities mentioned above which lead to their divergence and loss. Moreover, the Rutherford electron-ion collisional cross-section to enable the transfer of energy reduces with increasing electron energy. It is thus desirable to have laser energy directly coupled to the heavier ion species. In addition, there are also many other applications where ion acceleration/heating is of importance, e.g. proton radiography, biomedical applications.⁴¹⁻⁴⁴

The advantages of direct in-situ ion heating/acceleration are many. For instance, there would be (1) Efficient coupling directly to fusion species, viz. background DT species ; (2) Ions being non relativistic and total current being much less than Alfvén critical current for ions, magnetic fluctuations are expected to play negligible role in beam transport and beam stopping; (3) Classical collisional stopping of few MeV ions in dense core will be adequate; (4) Return currents, if any, will excite electrostatic ion acoustic modes leading to anomalous heating of the background plasma. Therefore, there is a need to look for the possibility of new absorption mechanisms through which laser energy can directly be transferred to heavier species of plasma for efficient ion acceleration. This is the prime focus of our study here.

It is shown in later part of this thesis that the use of a several Kilo Tesla of external magnetic field transverse to a plasma would bind the electrons preventing their motion. The long wavelength, high power pulsed CO_2 laser is then shown to get coupled to a heavier ion species in the plasma

The technological requirements for such an experiment also seem to be within the reach. The CO_2 lasers are today well known as efficient industrial laser available in the market for long pulse and continuous wave applications. However, the high power short pulse CO_2 lasers are also now recently available¹⁰² and hence short pulse applications such as the one discussed here can now be easily explored. Furthermore, kilo-Tesla order of magnetic fields have already been prepared in laboratory⁵²⁻⁵⁴. Therefore, it is merely a matter of time now when several tens of Kilo Tesla of magnetic fields can be generated, thereby paving the way for conducting experiments for direct ion accelerations via laser-plasma interactions.

1.3.4 Schemes for improved electron propagation

The propagation of hot electrons which get generated in the target by laser energy absorption is another area of wide interest. The techniques for possible guiding and reduction in divergence of beam propagation through plasma medium are being explored. It is well known that the beam propagation in the plasma is fraught with various instabilities which are responsible for the deterioration in the beam transport. The attempt has been, therefore, towards curbing the growth of such instabilities.

Some other technique involves the resistive collimation of fast electrons by generating a guiding magnetic field on the boundary of two different material. This has been proposed in Ref.¹⁹ The experimental investigations, based on this scheme, have been carried out by S. Kar *et al.*²⁰ and show the similar results which were predicted in Ref.¹⁹ Another experimental work by Chatterjee *et al.*²¹ involves using aligned carbon nano-wire arrays as the target. The irradiation of such a target generates inhomogeneous plasma. They have demonstrated experimentally efficient transportation of laser-generated mega- ampere electron currents over long distances compared to flat solid target. This is based on the fact that the structured target suppresses Weibel instabilities which allows the unhindered propagation of energetic electrons in the plasma over longer distances. A theoretical interpretation was provided by Mishra *et al.* which suggests that the beam Weibel instabilities get suppressed in such inhomogeneous targets.^{22,23} Moreover, the external static magnetic field can be used for suppression of these electron scale instabilities.²⁴ Recently it has been shown that the use strong axial magnetic field can also lead to better beam collimation.²⁵ Furthermore, laser-plasma lenses can also be utilized for relativistic electron beam collimation.²⁶

1.4 Thesis Layout

As mentioned earlier important issues pertaining to the energetic electron beam propagation in plasma and the possibility of direct energy absorption by ions from laser has been explored in this thesis. The thesis has been divided into seven chapters including this introduction.

1.4.1 Chapter 1: Introduction

In this chapter, a brief summary of the previous studies relevant to this thesis has been presented. It also contains a concise introduction on conventional laser energy absorption mechanisms, beam-plasma instabilities and its role in propagation on an electron beam inside a plasma, schemes to improve laser energy absorption and electron beam propagation in plasma etc.

1.4.2 Chapter 2: Energy principle for beam-plasma system instabilities

As mentioned earlier, a relativistic electron beam propagating through plasma induces a return electron current in the system. Such a system of interpenetrating forward and return electron current is susceptible to a host of instabilities.^{18,28,88,90,91,123–125} The physics of such instabilities underlies the conversion of the flow kinetic energy to the electromagnetic field energy. Keeping this in view, an energy principle analysis has been enunciated in this chapter. The energy principle often provides a succinct physical description of the excitations prevalent in any system. It has been regularly adopted for studying the stability of hydrodynamic fluids in a conservative system.^{66–71} In plasmas also, the ideal Magnetohydrodynamic (MHD) excitations have often been interpreted using energy principle^{72–76} for both equilibria with and without flows. The stability theory with energy principle for ideal magnetohydrodynamics has been employed to study problems in a variety of contexts, e.g. magnetic fusion,^{77,78} astrophysics, solar and space physics^{79,80} etc. For fast electron time scale phenomena (e.g. the case of beam plasma system) Lashmore-Davis²⁷ has shown the applicability of energy principle for the electrostatic excitations leading to the two-stream instability. In chapter 2, a succinct physical description of Weibel/current filamentation instability using the energetics has been provided. It has been shown that the for identical values of $S_4 = \sum_{\alpha} n_{0\alpha} v_{0\alpha}^2 / n_0 \gamma_{0\alpha}$, the growth rate is higher when the counterstreaming beams are symmetric (i.e. $S_3 = \sum_{\alpha} n_{0\alpha} v_{0\alpha} / n_0 \gamma_{0\alpha} = 0$) compared to the case when the two beams are asymmetric (i.e. when S_3 is finite). Here, $v_{0\alpha}$, $n_{0\alpha}$ and $\gamma_{0\alpha}$ are the equilibrium velocity, electron density and the relativistic factor for the electron species ‘ α ’ respectively and $n_0 = \sum_{\alpha} n_{0\alpha}$ is the total electron density. These beam

plasma instabilities arise as a result of the conversion of the kinetic energy of beam and background electron flows to electric and magnetic fields. In the case when the two flows are asymmetric, i.e. S_3 is finite in addition to electromagnetic field perturbations, the electrostatic field also gets excited. This costs energy, thereby reducing the growth rate of the instability.

Particle - In - Cell simulations under OSIRIS 4.0 framework have been employed to show that the saturated amplitude of the field energy is also higher in the symmetric case.

1.4.3 Chapter 3: Nonlinear regime of beam plasma instability

As mentioned in previous subsection, the relativistic electron beam (REB) propagation in a plasma is fraught with beam-plasma instabilities. The prominent amongst them is the collisionless Weibel destabilization which spatially separates the forward propagating REB and the return shielding currents. This results in the formation of REB current filaments which are typically of the size of electron skin depth during the linear stage of the instability. It has been observed that in the nonlinear stage the filaments size increases as they merge with each other. With the help of 2-D PIC simulations in the plane perpendicular to the REB propagation, it is shown in this chapter that these mergers occur in two distinct nonlinear phases. In the first phase, the total magnetic energy increases. Subsequently, however, during the second phase, one observes a reduction in magnetic energy. It is shown that the transition from one nonlinear regime to another occurs when the typical current associated with individual filaments hits the Alfvén threshold. In the second nonlinear regime, therefore, the filaments can no longer permit any increase in current. Magnetic reconnection events then dissipate the excess current (and its associated magnetic energy) that would result from a merger process leading to the generation of energetic electrons jets in the perpendicular plane. At later times when there are only a few filaments left the individual reconnection events can be clearly identified. It is observed that in between such events the magnetic energy remains constant and shows a sudden drop as and when two filaments merge. The electron jets released in these reconnection events are thus responsible for the transverse heating which has been mentioned in some previous

studies⁴⁸

1.4.4 Chapter 4: Effect of finite beam size and initial current

The beam-plasma system as of now has been analysed and/or numerically simulated using infinite and/or periodic box conditions. For this case the transverse extent of the beam is chosen to be infinite and/or periodic. As illustrated in the previous chapters such a beam plasma is amenable to Weibel instability generating current filaments and consequently magnetic field structures of the size of electron skin depth scales. The nonlinear evolution leads to the coalescence of these structures generating longer scale magnetic fields with time. This cannot account for laser plasma experiments conducted in laboratories which show that the magnetic field at the scale of beam width (longer than the electron skin depth) exists right from the very beginning.

In this chapter, we consider the realistic finite transverse profile of the electron beam. We demonstrate that for a small imbalance in the current (which is again natural in the electron beam system) not only does the long scale magnetic field persist but also shows a rapid increase. This cannot be accounted for with the usual Kelvin Helmholtz and/or Weibel processes but is in agreement with experimentally observed spectra.^{30,31,49} A possible explanation has been provided analytically for this observation.

1.4.5 Chapter 5: Direct coupling of laser to ions

The possibility of ion heating directly with a laser has been another topic of interest. Some of the well-known mechanisms in this regard are the RPA (Radiation Pressure Acceleration)⁵⁰ and TNSA (Target Normal Sheath Acceleration).⁵¹ We have demonstrated another mechanism of ion heating by employing external magnetic fields. The external magnetic field is chosen so as to constrain the electron movement and have them tied to the magnetic field. The heavier ions remain unmagnetized and respond to the laser electric field. The difference of electron and ion dynamics lead to charge separation and drives ion plasma oscillations, thereby transferring the laser energy to ions to a great extent directly. The proposed mechanism has been demonstrated by carrying out OSIRIS 4.0 simulations

using parameters for a CO_2 laser for which the requirement of external magnetic field strength is smaller.

1.4.6 Chapter 6: Direct coupling of laser to ions: Magnetosonic excitations

We continue our studies on direct energy absorption of the laser by ions in this chapter and show that when the laser power is increased in addition to exciting ion plasma oscillations, the excitation of Korteweg - de Vries (KdV) magnetosonic solitons are also observed. Various diagnostics are employed to characterize these solitons. The solitons, as expected, propagate stably for several hundreds of ion plasma periods. However, subsequently they are observed to develop transverse modulations which grow with time.

1.4.7 Chapter 7: Conclusion

We summarize the thesis in this chapter and recapitulate the salient points. We also provide an overview of the future research problems which can be carried out in continuation of the work described here.

2

Energy principle for beam plasma instabilities

As mentioned in chapter 1, a relativistic electron beam propagating through plasma induces a return electron current in the system. Such a system of interpenetrating forward and return electron current is susceptible to a host of instabilities. The physics of such instabilities underlies the conversion of the flow kinetic energy to the electromagnetic field energy. Keeping this in view, an energy principle analysis has been enunciated in this chapter^{*}. It has been shown that even purely growing mode like Weibel/current filamentation instability for the electron beam plasma system is indeed amenable to such a treatment. The treatment provides an understanding of the energetics associated with the growing mode. Particle - In - Cell simulations have been employed to validate our findings from the energy principle treatment for Weibel/current filamentation instability in linear regime.

2.1 Introduction

An intense laser interacting with an overdense solid target generates highly energetic, relativistic electrons carrying a massive electron current ($\sim MAmps$) in the forward direction.¹³⁹⁻¹⁴¹ In response to this, the background plasma supplies a return shielding electron current. Depending on the width of the beam being greater or lesser than the electron skin depth ($d_e = c/\omega_{pe}$), the return current flows

^{*} **Atul Kumar**, Chandrasekhar Shukla, Amita Das, and Predhiman Kaw, *AIP Advances* 8, 055213 (2018)

inside or outside of the beam respectively to neutralize the system. The spatially overlapping forward and return electron current flows are susceptible to several micro-instabilities.^{18, 88–91, 93, 94, 123} The current filamentation instability,^{92, 125, 142, 143} which is often referred to as the Weibel instability,¹⁸ creates a current separation at the length scale of an electron skin depth in the plasma, which leads to a generation of strong magnetic field ($\sim MGauss$).³⁰ It is believed that the Weibel instability and its nonlinear evolution are largely responsible for the development of strong magnetic fields in astrophysical contexts like the relativistic shock formation in Gamma ray bursts (GRBs),⁶¹ the high energy cosmic rays,^{62, 63} active galactic nuclei (AGN)⁶⁴ etc. In laser driven laboratory experiments also, Huntington *et. al.*⁶⁵ have observed the ion-Weibel instability in interpenetrating plasma flows. However, the experimental observation of magnetic field generation by the Weibel instability at electron dynamics scale still remains a challenge. In a typical beam plasma system, a fraction of the kinetic energy (δK) associated with the flows get converted into the electromagnetic excitations. Such disturbances feed upon themselves leading to the development of Weibel/current filamentation instabilities.

The energy principle often provides a succinct physical description of the excitations prevalent in any system. It has been regularly adopted for studying the stability of hydrodynamic fluids in a conservative system.^{66–71} In plasmas also, the ideal Magnetohydrodynamic (MHD) excitations have often been interpreted using energy principle^{72–76} for both equilibria with and without flows. The stability theory with energy principle for ideal magnetohydrodynamics has been employed to study problems in a variety of contexts, e.g. magnetic fusion,^{77, 78} astrophysics, solar and space physics^{79, 80} etc. For fast electron time scale phenomena (e.g. the case of beam plasma system) Lashmore-Davis²⁷ has shown the applicability of energy principle for the electrostatic excitations leading to the two stream instability. Weibel mode is an instability having mixed electrostatic and electromagnetic character. As the wavenumber gets more aligned transverse to the flow direction, electromagnetic character predominates. When it is directed totally orthogonal to the direction of flow, it is also referred to as the current filamentation instability. In this case, the mode has a purely growing character. We have employed the energy principle for this particular configuration. The origin of the positive and negative contributions to the total energy has been clearly identified. The term

providing a negative contribution to the energy is responsible for the growth of the mode. The energy conservation, however, should ensure a balance between the positive and negative energy contributions. This condition provides the expression for the growth rate, which is found to be in good agreement with earlier derivations. We have discussed the flow configurations which are more susceptible to the excitation of this mode. It is inferred that a symmetric flow configuration (i.e. when both the beam and the background plasma electrons have identical densities with equal and opposite flow velocities) has the optimal/fastest growth. This is in agreement with results obtained from the linear stability analysis carried out in earlier studies.^{124,125}

2.2 Energy principle analysis of beam-plasma system

We have considered an equilibrium configuration for a collection of the beam and background plasma electrons flowing in opposite direction to each other against a background of stationary ions. The charge neutrality and the current balance are ensured initially. The charge of the beam and the plasma electron densities are neutralized by the background plasma ions. Thus we have $\sum_{\alpha} n_{0\alpha} = n_{0i}$, where α is a dummy index which is 1 and 2 representing the beam and plasma electrons respectively. Here, $n_{0\alpha}$ represents the density of the two electron species and n_{0i} is the background density of ions. We will restrict to the 2-D geometry of $x - y$ plane shown in Fig.(2.1) for our analysis. The beam (depicted by red circles) and background plasma electrons (green circles) are chosen to flow in the $\pm x$ direction respectively. The equilibrium current balance is ensured by choosing $\sum_{\alpha} n_{0\alpha} \vec{v}_{0\alpha} = 0$, where $\vec{v}_{0\alpha}$ is the equilibrium flow velocity for species ' α '. The system is considered to be of infinite extent in both x and y directions. Such a system in the collisionless limit is in equilibrium with no forces acting on the particles. The total energy of this system is in the form of electron kinetic energy in the beam and the background electrons. Any electromagnetic instability in such a system would develop only if the energy requirement for the growth of electromagnetic fields is compensated by the reduction in the kinetic energy of the electrons.

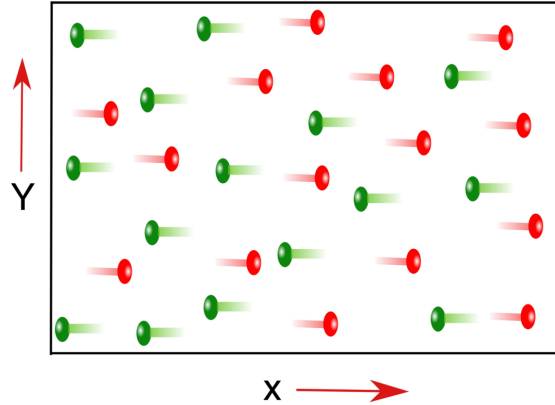


Figure 2.1: Schematics (not to scale) of 2-D equilibrium geometry of the beam plasma system where the beam (red circles) and background plasma electrons (green circles) are flowing in positive and negative x direction respectively

The dynamical evolution of the system about this equilibrium is clearly governed by the coupled set of Maxwell's and electron fluid equations. The ions in this treatment are assumed to be heavy and their response is considered to be negligible. The Maxwell's equations lead to the following equation for the evolution of field energy in the presence of plasma:

$$\frac{\partial}{\partial t} \left(\frac{E^2 + B^2}{8\pi} \right) + \frac{c}{4\pi} \vec{\nabla} \cdot (\vec{E} \times \vec{B}) + \vec{J} \cdot \vec{E} = 0 \quad (2.1)$$

This is the well known Poynting flux theorem for the electromagnetic energy in the plasma. In the vacuum, $\vec{J} \cdot \vec{E}$ term is absent and the rate of change of electromagnetic energy is determined simply by the Poynting flux. In plasma or any conducting media, the flow of currents leads to a finite value of $\vec{J} \cdot \vec{E}$. This term represents the possibility of energy transfer from the kinetic energy of the particles to the field energy and vice versa. For the infinite system considered by us, the Poynting flux would not contribute to the electromagnetic field energy evolution. We would only have the $\vec{J} \cdot \vec{E}$ term responsible for any rearrangement between field and the kinetic energies. Integrating Eq.(2.1) over space we obtain:

$$\frac{\partial}{\partial t} \int \left(\frac{E^2 + B^2}{8\pi} \right) dx dy + \int (\vec{J} \cdot \vec{E}) dx dy = 0 \quad (2.2)$$

We now evaluate Eq.(2.1) for fluctuations excited about the homogeneous equilib-

rium. Thus, a disturbance in any field is represented by the collection of Fourier modes having the form:

$$f(\vec{r}, t) \sim f_k \exp(i\vec{k} \cdot \vec{r} - i\omega_k t) + c.c \quad (2.3)$$

where *c.c* indicates complex conjugate of the expression to preserve the reality of the left hand side. We consider filamentation instability for which the wavenumber \vec{k} is directed along \hat{y} . We represent this component simply by k . Here, $\omega_k = \omega_{rk} + i\Gamma_k$ with ω_{rk} and Γ_k corresponding to the real and imaginary part of ω_k respectively. For the purely growing mode, $\omega_k = i\Gamma_k$ where Γ_k represents the growth rate. For the perturbed current flow confined in 2-D $x - y$ plane, the associated magnetic field is directed along the \hat{z} direction and is denoted by B_{1z} . The perturbed electric field \vec{E}_1 lies in the x-y plane. The variations being along \hat{y} , E_{1y} is the electrostatic component of the field and E_{1x} , B_{1z} correspond to electromagnetic excitation. These field perturbations are generated as a result of the conversion of the kinetic energy associated with the beam and return electron currents of the system into the electric and magnetic field energies. For the small amplitude linear disturbances, only up to quadratic terms (associated with the perturbed fields) in the energy expression have to be retained. We thus have:

$$\frac{\partial}{\partial t} \left(\frac{E^2 + B^2}{8\pi} \right) = \frac{\partial}{\partial t} \left[\frac{1}{8\pi} (E_{1x}^2 + E_{1y}^2 + B_{1z}^2) \right] \quad (2.4)$$

$$\vec{J} \cdot \vec{E} = - \sum_{\alpha} \left[en_{0\alpha} v_{1\alpha x} E_{1x} + en_{0\alpha} v_{1\alpha y} E_{1y} + en_{1\alpha} v_{0\alpha} E_{1x} \right] \quad (2.5)$$

he linearized continuity equation for the species α can be written as:

$$\frac{\partial n_{1\alpha}}{\partial t} + \frac{\partial}{\partial y} (n_{0\alpha} v_{1\alpha y}) = 0 \quad (2.6)$$

Similarly, linearizing the x and y components of momentum equation for the species α we have:

$$\frac{\partial}{\partial t} (m\gamma_{0\alpha}^3 v_{1\alpha x}) = -eE_{1x} \quad (2.7)$$

$$\frac{\partial}{\partial t} (m\gamma_{0\alpha} v_{1\alpha y}) = -eE_{1y} + ev_{0\alpha} B_{1z}/c; \quad (2.8)$$

where ‘e’ is the magnitude of the electronic charge and ‘m’ is the rest mass of an electron. Employing the Fourier representation of Eq.(2.3) for the linearised fields (density, velocity, electric and magnetic field), we can cast the Eqs.(2.6, 2.7, 2.8) respectively to obtain:

$$n_{1\alpha k} = \frac{k}{\omega_k} n_{0\alpha} v_{1\alpha y k} \quad (2.9)$$

$$v_{1\alpha x k} = -\frac{\iota e}{m\gamma_{0\alpha}^3 \omega_k} E_{1x k} \quad (2.10)$$

$$v_{1\alpha y k} = -\frac{\iota e}{m\gamma_{0\alpha} \omega_k} E_{1y k} - \frac{\iota e}{mc\gamma_{0\alpha} \omega_k^2} k v_{0\alpha} E_{1x k} \quad (2.11)$$

The Faraday’s law gives the following relationship between the \hat{z} component of magnetic field and the \hat{x} component of electric field:

$$B_{1z k} = -\frac{k}{\omega_k} E_{1x k} \quad (2.12)$$

In addition, we have used the following definitions:

$$S_1 = \sum_{\alpha} \frac{n_{0\alpha}}{n_0 \gamma_{0\alpha}}; \quad S_2 = \sum_{\alpha} \frac{n_{0\alpha}}{n_0 \gamma_{0\alpha}^3} \quad (2.13)$$

$$S_3 = \sum_{\alpha} \frac{n_{0\alpha} v_{0\alpha}}{n_0 \gamma_{0\alpha}}; \quad S_4 = \sum_{\alpha} \frac{n_{0\alpha} v_{0\alpha}^2}{n_0 \gamma_{0\alpha}} \quad (2.14)$$

The Poisson’s equation can be written as:

$$\frac{\partial E_{1y}}{\partial y} = -\sum_{\alpha} 4\pi e n_{1\alpha} \quad (2.15)$$

Using Eqs.(2.9, 2.10, 2.11), we can express the Poisson equation as:

$$\iota k E_{1y k} = -\sum_{\alpha} 4\pi e \frac{k}{\omega_k} n_{0\alpha} \left[-\frac{\iota e}{m\gamma_{0\alpha} \omega_k} E_{1y k} - \frac{\iota e}{mc\gamma_{0\alpha} \omega_k^2} k v_{0\alpha} E_{1x k} \right] \quad (2.16)$$

Rearranging terms in Eq.(2.16) along with the definition of S_1 and S_3 provided in Eqs.(2.13, 2.14), we can cast E_{1y} in terms of E_{1x} as:

$$E_{1y k} = \frac{\omega_{pe}^2 S_3}{\left(1 - \frac{\omega_{pe}^2}{\omega_k^2} S_1\right) \omega_k^3} E_{1x k} \quad (2.17)$$

It should be noted that when $S_3 = 0$, we have $E_{1yk} = 0$. Thus a symmetric flow configuration for which S_3 vanishes does not generate any electrostatic field and hence, the energy cost in this case for the development of Weibel mode is less. We eliminate all the other fields in terms of E_{1x} and use the normalized variables, i.e. $\omega_k/\omega_{pe} \rightarrow \omega_k$ and $kc/\omega_{pe} \rightarrow k$ to obtain:

$$\begin{aligned}
 \vec{J} \cdot \vec{E} &= \frac{\iota}{8\pi} \left[S_2 \left\{ \frac{1}{\omega_k} - \frac{1}{\omega_{k*}} \right\} + S_4 k^2 \left\{ \frac{1}{\omega_k^3} - \frac{1}{\omega_{k*}^3} \right\} \right] |E_{1xk}|^2 \\
 &+ \frac{\iota}{8\pi} \left[\frac{S_3^2 S_1 k^2}{|\omega_k|^6 (1 - \frac{1}{\omega_k^2} S_1) (1 - \frac{1}{\omega_{k*}^2} S_1)} \left\{ \frac{1}{\omega_k} - \frac{1}{\omega_{k*}} \right\} \right] |E_{1xk}|^2 \\
 &+ \frac{\iota}{8\pi} \left[\frac{S_3^2 k^2}{|\omega_k|^4} \left\{ \frac{1}{\omega_{k*}} \left(1 - \frac{1}{\omega_{k*}^2} S_1 \right) - \frac{1}{\omega_k \left(1 - \frac{1}{\omega_k^2} S_1 \right)} \right\} \right] |E_{1xk}|^2 \\
 &+ \frac{\iota}{8\pi} \left[S_3^2 k^2 \left\{ \frac{1}{\omega_k^5 \left(1 - \frac{1}{\omega_k^2} S_1 \right)} - \frac{1}{\omega_{k*}^5 \left(1 - \frac{1}{\omega_{k*}^2} S_1 \right)} \right\} \right] |E_{1xk}|^2
 \end{aligned} \tag{2.18}$$

where ω_{k*} is the *c.c* of ω_k . The above expression can be simplified to write:

$$\begin{aligned}
 \vec{J} \cdot \vec{E} &= \frac{2\Gamma_k}{8\pi} \left[\frac{S_2}{\Gamma_k^2} + \frac{S_1 S_3^2 k^2}{\Gamma_k^4 (\Gamma_k^4 + 2S_1 \Gamma_k^2 + S_1^2)} - \frac{S_4}{\Gamma_k^4} \right] |E_{1xk}|^2 \\
 &= \frac{1}{8\pi} \frac{\partial}{\partial t} \left[\frac{S_2}{\Gamma_k^2} + \frac{S_1 S_3^2 k^2}{\Gamma_k^4 (\Gamma_k^4 + 2S_1 \Gamma_k^2 + S_1^2)} - \frac{S_4}{\Gamma_k^4} \right] |E_{1xk}|^2
 \end{aligned} \tag{2.19}$$

It should be noted that we have replaced $2\Gamma_k$ by $\partial/\partial t$ because $E_{1x} = E_{1xk} \exp(iky - i\omega_k t)$. Thus $|E_{1xk}|^2 \sim \exp(2\Gamma_k t)$. Here, Γ_k is the imaginary part of the frequency ω_k . Similarly, we have:

$$\begin{aligned}
 \frac{\partial}{\partial t} \left(\frac{E^2 + B^2}{8\pi} \right) &= \frac{1}{8\pi} \frac{\partial}{\partial t} \left[\left\{ 1 + \frac{k^2 S_3^2}{|\omega_k|^6 (1 - \frac{1}{\omega_k^2} S_1) (1 - \frac{1}{\omega_{k*}^2} S_1)} + \frac{k^2}{|\omega_k|^2} \right\} \right] |E_{1x}|^2 \\
 &= \frac{1}{8\pi} \frac{\partial}{\partial t} \left[\left\{ 1 + \frac{S_3^2 k^2}{\Gamma_k^2 (\Gamma_k^4 + 2S_1 \Gamma_k^2 + S_1^2)} + \frac{k^2}{\Gamma_k^2} \right\} \right] |E_{1x}|^2
 \end{aligned} \tag{2.20}$$

Since the Poynting flux for the homogeneous infinite periodic system is zero, we can express Eq.(2.1) by summing Eq.(2.19) and Eq.(2.20), to obtain Eq.(2.21).

We have chosen to normalize time with the inverse of electron plasma frequency, $\omega_{pe} = \sqrt{\frac{4\pi n_0 e^2}{m}}$ and length with the electron skin depth, $d_e = c/\omega_{pe}$ (i.e. , $t \cdot \omega_{pe}^{-1} \rightarrow t$

and $y \cdot d_e \rightarrow y$) to obtain the following expression:

$$\frac{1}{8\pi} \frac{\partial}{\partial t} \left[\left(1 + \frac{S_2}{\Gamma_k^2}\right) |E_{1xk}|^2 + \left(1 + \frac{S_1}{\Gamma_k^2}\right) \frac{S_3^2 k^2}{\Gamma_k^2 (\Gamma_k^4 + 2S_1 \Gamma_k^2 + S_1^2)} |E_{1xk}|^2 + \frac{k^2}{\Gamma_k^2} |E_{1xk}|^2 - \frac{S_4}{\Gamma_k^4} k^2 |E_{1xk}|^2 \right] = \frac{\partial}{\partial t} [\chi_k] = 0 \quad (2.21)$$

The parameters S_1 , S_2 and S_4 are always positive. It should be noted that though the parameter S_3 can be either positive or negative, it appears only as S_3^2 in Eq.(2.21). Hence, the sign of S_3 does not matter but its magnitude $|S_3|$ is important. Furthermore, Eq.(2.21) shows that χ_k (the energy in the k th mode) should remain conserved. This is because in the linear regime the modes do not interact. The system is in a state of equilibrium initially with infinitesimal perturbations around it. Therefore, $\chi_k \approx 0$ for all k initially and from Eq.(2.21), χ_k would continue to remain zero while the linear approximation remains valid. We thus have:

$$\chi = \frac{1}{8\pi} \left[\left(1 + \frac{S_2}{\Gamma^2}\right) |E_{1x}|^2 + \left(1 + \frac{S_1}{\Gamma^2}\right) \frac{S_3^2 k^2}{\Gamma^2 (\Gamma^4 + 2S_1 \Gamma^2 + S_1^2)} |E_{1x}|^2 + \frac{k^2}{\Gamma^2} |E_{1x}|^2 - \frac{S_4}{\Gamma^4} k^2 |E_{1x}|^2 \right] = 0 \quad (2.22)$$

In writing Eq.(2.22), we have dropped the suffix k .

2.3 Inferences from Energy Principle

The expression for χ in Eq.(2.22) has both positive and negative terms contributing to it which is essential for the existence of any instability in the system. When the positive terms balance with the negative terms to have $\chi = 0$ at a finite value of Γ , the corresponding mode is unstable. The growth rate is thus a function of S_1, S_2, S_3 and S_4 , which in turn, are functions of the density and flow parameters of the equilibrium configuration of the beam as well as the background plasma electrons. The first three terms of the expression for χ are positive definite (S_1 and S_2 are positive and S_3 which could be negative, appears as a square). The

positive terms require additional energy. The fourth term with a negative sign (S_4 and other factors being positive definite in this term) corresponds to a reduction in energy of the perturbed configuration. The presence of this fourth term is thus energetically favorable and is crucial for instability.

It should be noted here that $\vec{J} \cdot \vec{E} = \sum_{\alpha} n_{\alpha} \vec{v}_{\alpha} \cdot (-e\vec{E})$. Here $-e\vec{E}$ is the force due to the electric field experienced by the electrons. Thus, the positive/negative terms in $\vec{J} \cdot \vec{E}$ represent the gain/loss rate in the kinetic energy of electrons respectively. The negative terms are responsible for the growth of Weibel instability at the expense of the kinetic energy of electrons. We now identify the terms in the expression of $\vec{J} \cdot \vec{E}$ in Eq.(2.5) which provide a negative contribution to the total energy of the system.

Let us first consider the case of symmetric flow for which S_3 is zero. For this case, it is evident from Eq.(2.17) that $E_{1y} = 0$. Thus, only the first and third term of Eq.(2.5) are finite for this particular case. Let us now identify their contributions in Eq.(2.22). The first term of Eq.(2.22) with the coefficient $(1 + S_2/\Gamma^2)$ of $|E_{1x}|^2$ arises as follows. The coefficient unity clearly comes from $\partial|E_{1x}^2|/\partial t$ of Eq.(2.4). The term with the factor S_2/Γ^2 is the plasma dressing contribution arising from $(-\sum_{\alpha} en_{0\alpha} v_{1\alpha x} E_{1x})$ (viz. the first term of Eq.2.5). This can be obtained by expressing E_{1x} in terms of $v_{1\alpha x}$ from Eq.(2.10) which leads to $(-\sum_{\alpha} en_{0\alpha} v_{1\alpha x} E_{1x}) = \sum_{\alpha} n_{0\alpha} m \gamma_{0\alpha}^3 |v_{1\alpha x}|^2 \Gamma$. Clearly, this is a positive definite and represents the rate of kinetic energy acquired by the electrons due to the perturbed velocity along the \hat{x} direction (i.e. along the equilibrium flow direction). Let us now look at the last term of Eq.(2.5) by substituting $n_{1\alpha}$ and E_{1x} in terms of the velocities. It is evident from Eq.(2.9) that the density perturbations are related to $v_{1\alpha y}$ by the continuity equation. Since E_{1y} is absent for the symmetric flow configuration, $v_{1\alpha y}$ gets generated by the $\vec{v} \times \vec{B}$ force in the momentum equation (Eqs.(2.7, 2.8)). It should be noted that since the equilibrium flow is oppositely directed for the two electron fluids, this force acts in the opposite directions for the two species and is responsible for the separation of the two beams transverse to the equilibrium flow direction (i.e. along \hat{y}). This causes the spatial separation of the forward and return currents leading to magnetic field generation causing the system to be destabilized by Weibel instability. We substitute for $n_{1\alpha}$ and E_{1x} in terms of $v_{1\alpha}$ to write the last term of Eq.(2.5) as $-\sum_{\alpha} k^2 v_{0\alpha}^2 m \gamma_{0\alpha}^3 |v_{1\alpha x}|^2 / \Gamma$ which is negative and hence, it represents the loss rate of electron kinetic energy. In

Eq.(2.22), it can be traced as the term with $-S_4 k^2/\Gamma^4$ coefficient.

For asymmetric flows with non zero values of S_3 , E_{1y} is finite. A finite value of E_{1y} contributes to $\vec{J} \cdot \vec{E}$ through the second term in Eq.(2.5) and also through the dependence of $n_{1\alpha}$ on $v_{1\alpha y}$ (Eq. (2.9), which in turn is influenced by the force $-eE_{1y}$ through the momentum equation (Eq.(2.9,2.8)). It should be noted that the force due to E_{1y} acts on the two fluids along the same direction and hence does not lead to any current separation required for the Weibel destabilization process. The sum of both these terms can be seen to be positive definite and they are responsible for the gain in electron kinetic energy acquired by the perturbed \hat{y} component of the velocity v_{1y} . The term with the coefficient S_1/Γ^2 in Eq.(2.22) represents the sum of both these contributions. The unity in the bracket containing S_1/Γ^2 arises from $\partial|E_{1y}|^2/\partial t$ of Eq.(2.4). Furthermore, the term $k^2|E_{1x}|^2/\Gamma^2$ corresponds to the last term of Eq.(2.4). It also represents the rate of change of the magnetic field energy, $\partial|B_{1z}|^2/\partial t$.

It is, therefore, clear that the negative term arises from the correlation between $n_{1\alpha}$ and E_{1x} , which is the last term appearing in the expression of $\vec{J} \cdot \vec{E}$ (Eq.(2.5)). This can also be simply viewed as a crucial term reducing the overall spatially averaged perturbed kinetic energy of the electrons as demonstrated below.

$$\left\langle \delta K \right\rangle = \frac{1}{2} \left\langle \sum_{\alpha} \left[(n_{0\alpha} + n_{1\alpha})(\vec{v}_{0\alpha} + \vec{v}_{1\alpha})^2 - n_{0\alpha} v_{0\alpha}^2 \right] \right\rangle \quad (2.23)$$

$$= \frac{1}{2} \left\langle \sum_{\alpha} \left[n_{0\alpha} \vec{v}_{1\alpha}^2 + 2n_{1\alpha} \vec{v}_{0\alpha} \cdot \vec{v}_{1\alpha} \right] \right\rangle \quad (2.24)$$

$$= \frac{1}{2} \left\langle \sum_{\alpha} \left[n_{0\alpha} |v_{1\alpha x}|^2 + n_{0\alpha} |v_{1\alpha y}|^2 + 2n_{1\alpha} \vec{v}_{0\alpha} \cdot \vec{v}_{1\alpha} \right] \right\rangle \quad (2.25)$$

It should be noted that the terms linear in perturbation average out to zero and thus have been dropped. The terms with third order in perturbation have been ignored. The first and second terms in Eq.(2.25) are positive definite. However, the sign of the third term depends on the correlation between $n_{1\alpha}$ and $v_{1\alpha x}$. Using Eq.(2.10) and the fact that $\omega = i\Gamma$, we end up with the same correlation term as in the expression for $\vec{J} \cdot \vec{E}$ which is responsible for decreasing the kinetic energy.

Now, we derive the expression for the growth rate of the unstable mode. Equating the coefficient of $|E_{1x}|^2$ in Eq.(2.21) to zero, we obtain the following 6th order

polynomial equation as the dispersion relation from which the growth rate can be obtained.

$$(\Gamma^2 + S_1)[\Gamma^4 + (S_2 + k^2)\Gamma^2 - S_4k^2] = -S_3^2k^2 \quad (2.26)$$

Equation(2.26) is in agreement with earlier derivation.¹²⁴ For $S_3 = 0$, the analytical expression for the growth rate can be obtained as:

$$\Gamma = \frac{1}{\sqrt{2}} \left[\sqrt{(S_2 + k^2)^2 + 4S_4k^2} - (S_2 + k^2) \right]^{1/2} \quad (2.27)$$

The other root of $\Gamma^2 = -S_1$ is the electron plasma oscillations. The analytical expression for the growth rate can also be obtained in the asymptotic limit of small beam density, i.e. $n_{01} \ll n_{02}$, $v_{01} \gg v_{02}$ and the beam velocity approaches the speed of light, i.e $|v_{01}| \approx 1$. This implies that $\gamma_{01} = \gamma_0 \gg 1$ and $\gamma_{02} \sim 1$. We can then expand the parameters S_1, S_2, S_3 and S_4 of Eq. (2.26) in powers of n_{01} . Retaining terms of n_{01} upto first order in the expression we obtain: $S_1 \approx S_2 \approx 1$, $S_3 \approx n_{01}v_{01}$, $S_4 \approx n_{01}v_{01}(v_{01}/\gamma_0 - v_{02})$. The expression for growth rate under this approximation is then given by

$$\Gamma = \left[\frac{k^2 n_{01} v_{01}^2}{(1 + k^2) \gamma_0} \right]^{1/2} \quad (2.28)$$

In the limit $k \ll 1$ the growth rate becomes,

$$\Gamma_1 = (n_{01} v_{01}^2 / \gamma_0)^{1/2} k \quad (2.29)$$

In the other asymptotic limit $k \gg 1$,

$$\Gamma_2 = (n_{01} v_{01}^2 / \gamma_0)^{1/2} \quad (2.30)$$

This is a highly asymmetric flow configuration in which the beam density is much lower than the background plasma density but it has relativistic speeds. The value of $|S_3|$ for such configurations would be very high. On the other hand, $|S_3| = 0$ corresponds to a symmetric flow configuration. This can be understood as follows. Using the condition of charge neutrality $\sum_{\alpha} n_{0\alpha} = n_0 = 1$ and zero current $\sum_{\alpha} n_{0\alpha} v_{0\alpha} = 0$ for an equilibrium, we have $n_{01} = 1 - n_{02}$ and $v_{02} = -n_{01}v_{01}/(1 - n_{01})$. All the parameters S_1, S_2, S_3 and S_4 , on which the growth rate

depends, can then be cast entirely in terms of the beam density and its equilibrium velocity. The parameter S_3 takes the form:

$$S_3 = n_{01}v_{01} \left(\frac{1}{\gamma_{01}} - \frac{1}{\gamma_{02}} \right) \quad (2.31)$$

Thus, S_3 has a negligible role in non relativistic cases. In the relativistic case, it is zero only when the flow configuration is symmetric. This corresponds to $v_{01} = -v_{02}$, which is possible only when $n_{01} = n_{02} = 0.5$. We will refer to the case of $n_{01} = 0.5$ (corresponding to $|S_3| = 0$) as the ‘symmetric’ flow configuration and for any other value of n_{01} for which $|S_3|$ is finite the flow configuration is termed as ‘asymmetric’ henceforth. It is interesting to note from Eq.(2.17) that the electrostatic field $E_{1y} = 0$ when $|S_3| = 0$. Thus, for the symmetric flow configuration, no electrostatic field gets generated and hence, it is favorable from the energetics point of view to excite the instability for this particular configuration. In the expression for χ provided in Eq(2.22) also, it can be seen that the second positive term vanishes entirely when $|S_3| = 0$. We have carried out a detailed investigation of the growth rate evaluated from the dispersion relation of Eq.(2.26) in the parameter domain of n_{01} vs. v_{01} to show that this inference drawn from the energy principle is indeed correct.

In Fig.(2.3a,b), we have shown the constant contours of S_4 in the $n_{01} - v_{01}$ plane. When the growth rate using the values of n_{01} and v_{01} on the points of any constant S_4 contour is evaluated, we observe that the growth rate is always highest for the symmetric case. We have employed Eq.(2.26) to evaluate the growth rate numerically and used $k = 1$ where the growth rate maximizes.¹²⁴ In TABLE I, we have evaluated the growth rate for the constant contours of $S_4 = 0.25$ for various values of n_{01} and v_{01} . We observe that the growth rate is highest for $|S_3| = 0$, as expected. In fact, the growth rate decreases monotonically with increasing value of $|S_3|$.

We have also shown the plot of growth rate for various values of n_{01} as a function of v_{01} in Fig.(2.2) and observe that the growth rate maximizes when $n_{01} = 0.5$, i.e. for the symmetric flow configuration.

TABLE I

The maximum growth rate of current filamentation instability evaluated analytically on a contour of $S_4 = 0.25$

n_{01}	v_{01}	$ S_3 $	$\Gamma(\text{max.})$
0.343	0.898	0.1365	0.3748
0.346	0.923	0.1558	0.3722
0.360	0.960	0.1941	0.3636
0.367	0.970	0.2078	0.3581
0.383	0.983	0.2291	0.3475
0.400	0.991	0.2445	0.3336
0.429	0.996	0.2453	0.3258
0.466	0.994	0.1798	0.3857
0.487	0.982	0.0827	0.4392
0.5	0.963	0	0.4519

It is thus clear that the symmetric flow configuration has the maximum growth rate. It would be interesting to know how the two flow configurations behave in the nonlinear regime. In the next section, we have explored this by carrying out 2-D PIC simulations through OSIRIS for the symmetric and asymmetric flow configurations corresponding to the two points depicted by asterisks in Fig.(2.3b). For these two points, both S_4 and v_{01} are identical. Here, Case(A) is for the symmetric flow with $n_{01} = 0.5$, whereas Case (B) is for asymmetric configuration with $n_{01} = 0.36$.

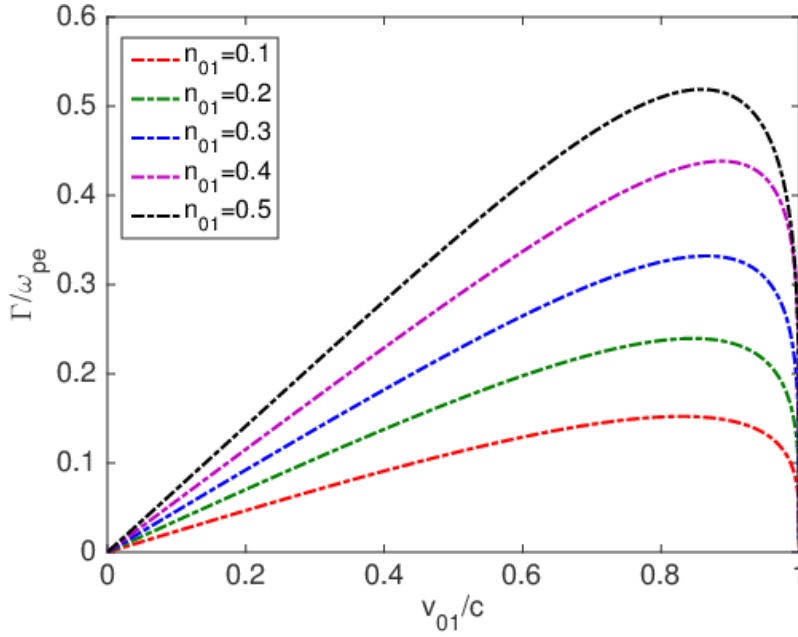


Figure 2.2: The equilibrium condition of charge neutrality and zero current requires that only two parameters out of the four $n_{0\alpha}$ and $v_{0\alpha}$ can be chosen independently. For this figure n_{01} and v_{01} have been chosen independently to understand the variation of the growth rate with respect to them. The figure shows the plot of growth rate as a function of v_{01} . Each curve in the plot corresponds to a distinct value of n_{01} . It should be noted that the curve for $n_{01} = 0.5$ representing symmetric flow configuration, has the highest value of growth rate for all values of v_{01} .

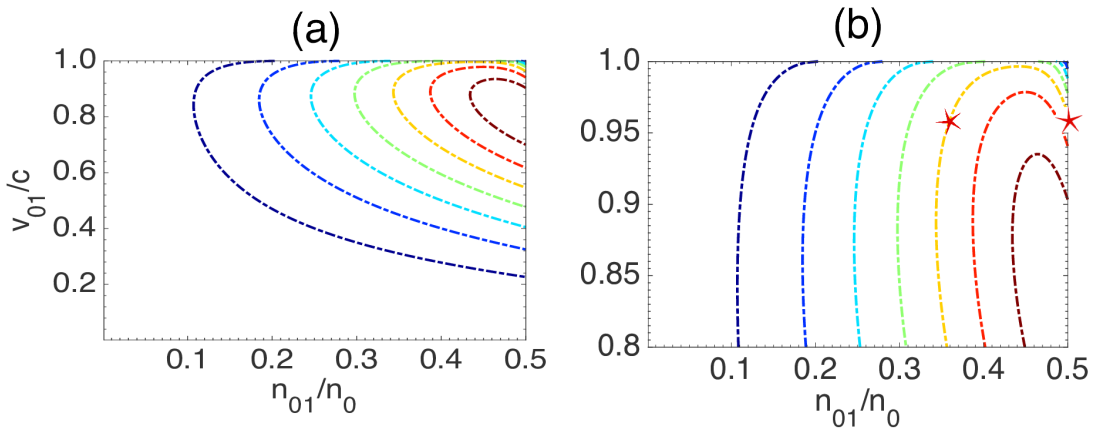


Figure 2.3: (a) Contours of S_4 in the plane of n_{01} and v_{01} : (b) zoomed section of contours of S_4 where astricks denote two points of symmetric and asymmetric flow configurations at the constant contour of $S_4 = 0.25$

2.4 Simulation Setup

PIC simulations using OSIRIS^{46,47} have been carried out for a system of the forward electron beam and a compensating return current by the background plasma. The equilibrium configuration in Fig.(2.1) has been initialized in a 2-D simulation box. The simulation box size was chosen to be $25c/\omega_{pe} \times 25c/\omega_{pe}$. The spatial resolution is taken to be 50 cells per c/ω_{pe} with 64 particles per cell which corresponds to a grid size of $\Delta x = 0.02c/\omega_{pe}$ and time step $\Delta t = 0.012\omega_{pe}^{-1}$. A small noise in terms of initial thermal velocity of $v_{th} = 0.0001397c$ in each of the two electron species has been introduced initially. In typical beam plasma experiments, one envisages the forward beam current to have high velocities and low density. On the other hand, the background plasma electrons have high density and move with slower speed. Thus the two flows would, in general, be highly asymmetric. We investigate here both the cases of symmetric and asymmetric flows. For a proper comparison, we have ensured in the choice of the equilibrium flow parameters to have identical values of S_4 as well as the beam velocity v_{01} for both the cases. For the symmetric flow (**Case (A)**), a forward moving beam of density $0.50n_0$ moving with the velocity of $0.963c$ and a compensating return electron beam with same density and speed moving in opposite direction has been chosen. For asymmetric flow (**Case (B)**), a beam electron density of $0.36n_0$ moving along \hat{x} with a velocity of $0.960c$ in the forward direction and a shielding current of background electrons along $-\hat{x}$ with density $0.64n_0$ moving with a velocity of $0.540c$ has been considered. We have tracked the spatio - temporal evolution of magnetic field and particle density along with the evolution of total magnetic field energy in the system defined by $\frac{1}{8\pi} \int B^2(x, y) dx dy$.

2.5 Simulation results and analysis

We have shown in Fig.(2.4), the evolution of the normalized magnetic field energy in the system for Case (A) and (B) respectively. It can be observed from the semilog plot of Fig.(2.4) that the magnetic field energy grows linearly in the beginning. However, the symmetric flow *i.e.*, Case (A) shows a higher growth rate than that of Case (B), as expected. The field energy in Case (A) also saturates at a higher

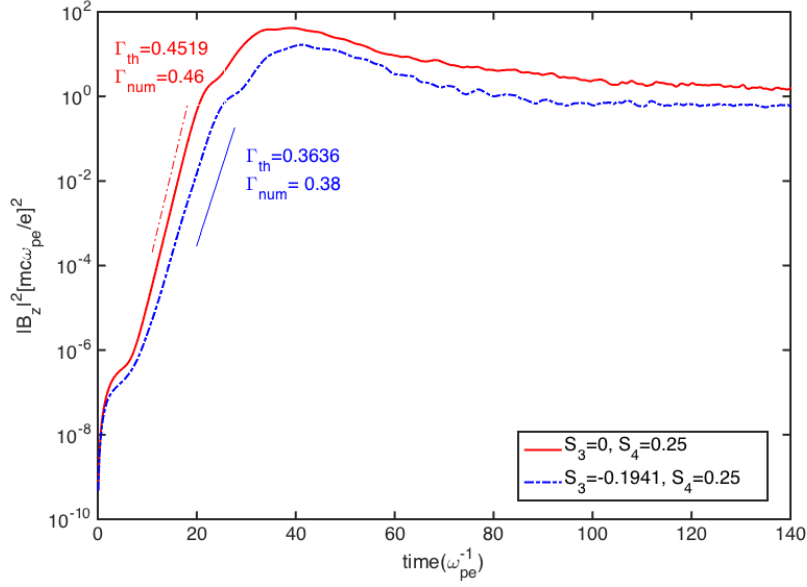


Figure 2.4: The calculation of growth rate of instability by its slope on temporal evolution of magnetic field energy for the symmetric ($S_4 = 0.25$, $|S_3| = 0$) (solid red color curve) and asymmetric flow ($S_4 = 0.25$, $|S_3| = 0.1941$) (dotted blue curve) which match very well with the theoretical growth rate.

value. The 2-D color plots for the z component of the magnetic field (left column) and the charge density (right column) for Case (A) and Case (B) have been shown in Fig.(2.5) and Fig.(2.6) respectively. The first subplot in both the figures [Fig.(2.5) and Fig.(2.6)] corresponds to the linear regime. After this, the system shows the onset of nonlinear effects. This can be clearly observed from the plots in Fig.(2.4) where the lines start to curve. This happens for Case (A) and Case (B) at $t = 15.24$ and $t = 18.0$ respectively. At the linear stage of instability ($t = 15.24$ in Fig.(2.5) and $t = 18.0$ in Fig.(2.6)), the formation of filaments in the magnetic field as well as in the electron charge density are observed. The scale length of these filaments are of the order of electron skin depth d_e . However, the magnitude of the perturbed magnetic field in the asymmetric case is comparatively much weaker. It is evident from Eq. (2.21) that finite value of $|S_3|$ (which is the case for asymmetric plasma flows) can stabilize the growth of Weibel instability as compared to the system of symmetric plasma flows ($|S_3| = 0$). The slope corresponding to the numerically evaluated growth rate has been indicated by the short straight lines alongside the two respective cases. They show a good match in the linear regime of

numerical simulation. The quantitative value of the growth rate calculated by PIC simulation is $\Gamma_{num} = 0.46$ which is in good agreement with theoretical growth rate [Eq. (2.27)] $\Gamma_{th} = 0.4519$ (red solid color in Fig.(2.4)). In the case of asymmetric flow ($|S_3| = 0.1941$), the growth rate obtained from simulation is $\Gamma_{num} = 0.38$ which also matches with the theoretical result [Eq. (2.26)] $\Gamma_{th} = 0.3636$ (dotted blue color line) and confirms the theoretical prediction that non-zero value of $|S_3|$ reduces the growth rate of Weibel instability. It should, however, be noted that analytical derivation corresponds to the filamentation configuration with perturbation wave vector directed transverse to the flow direction. However, the simulation shows variations along the flow direction as well, for both the cases. The slight difference between analytical and simulation growth rate is reasonable as the oblique modes are the ones which supposedly dominate the beam plasma instability. However, since the variations along the flow direction are of much longer scales, they do not seem to influence the growth rate much. This is the reason for a good agreement between the analytically evaluated growth rate and that obtained from simulation.

It has also been found in our simulations that the nonlinear onset of Weibel instability occurs sooner (just after $t = 15.24$) in Case (A) than in Case (B) ($t = 18.0$). The nonlinear saturation level in Case(A) is also typically higher as compared to Case (B).

In the nonlinear regime, the perturbed magnetic field first keeps increasing at a slower rate (phase 1). The magnetic field structures during this time coalesce and form longer scale structures. Thus, a cascade of power towards longer scales is distinctly observed. The energy evolution plots of Fig.(2.4), also show a subsequent later regime (phase 2) in which the magnetic energy shows a steady decrease. The color subplots of Fig.(2.5) at $t = 27.24$ and $t = 39.24$ for Case (A) correspond to these two distinct nonlinear phases. For Fig.(2.6) the subplot at $t = 30.0$ and $t = 42.0$ depicts the two nonlinear phases for Case (B). During the first phase of the nonlinear regime, the filamentary nature of the structures continues to exist as can be seen from Fig.(2.5) and Fig.(2.6). Thus, variations along the propagation direction continue to remain at longer spatial scales. In this regime, the coalescence of magnetic filaments increases the transverse scale length. In the second phase of the nonlinear regime, the magnetic structures start to isotropize as can be observed from the last two subplots of Fig.(2.5) and Fig.(2.6).

We have also shown the phase space plot of the beam and background electrons

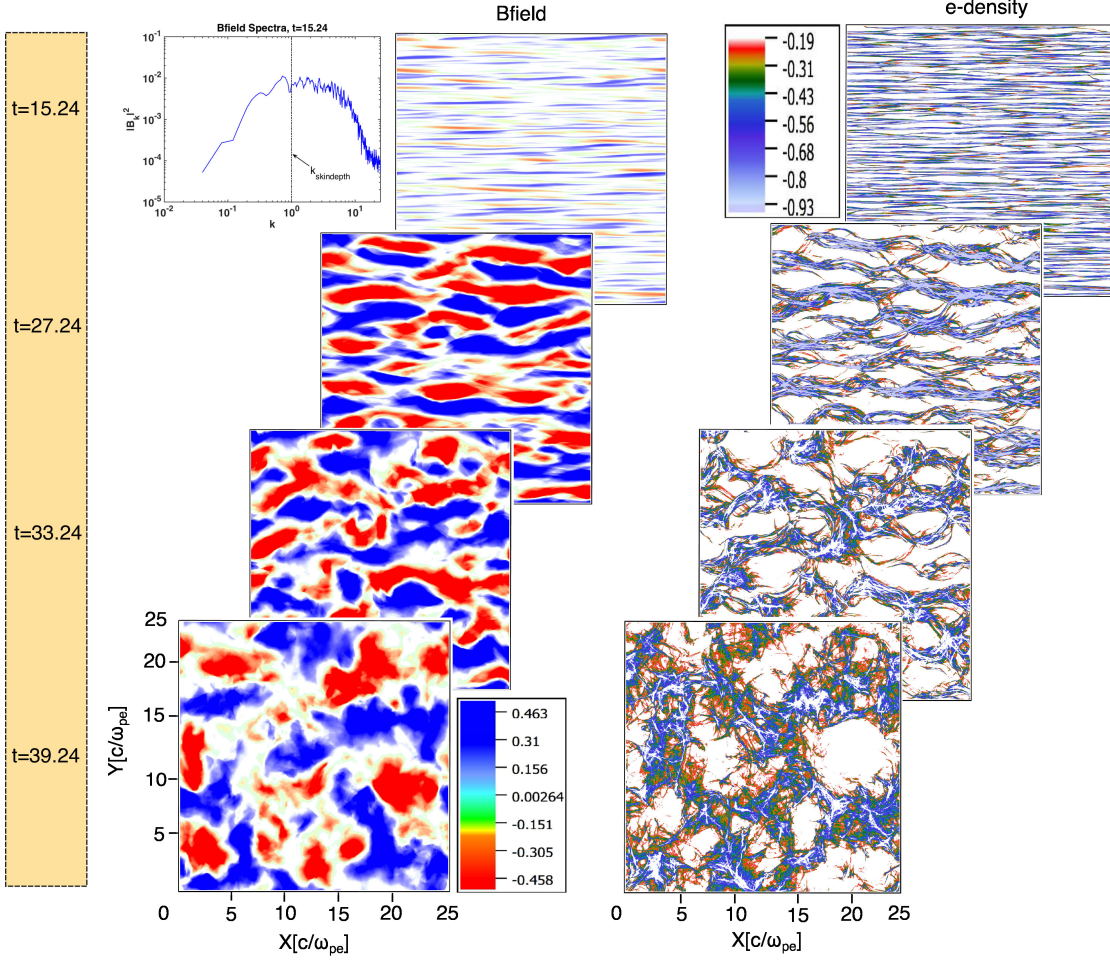


Figure 2.5: Evolution of magnetic field (left column) and electron charge density of the beam (right column) for symmetric flows (prepared by Vapor [J. Clyne *et. al.*, *New Journal of Physics*, 9, 8, (2007); J. Clyne and M. Rast, *Electronic Imaging*, 284-295, (2005)]): The formation of filamentary structures in magnetic field as well as in electron charge density at the order of an electron skin depth, d_e is shown just at the transition from linear to nonlinear stage ($t=15.24$). In the nonlinear stage of instability, the tilted structure of filaments in the magnetic field as well as in electron charge density which is a signature of oblique mode instability, can be seen. The magnetic field energy spectra in the linear regime peaking at d_e is shown within the top left corner of the figure. Further evolution of instability leads to the system in a turbulent regime which is caused by the deflection of charge particles due to a high amplitude magnetic field generated by the instability in the system.

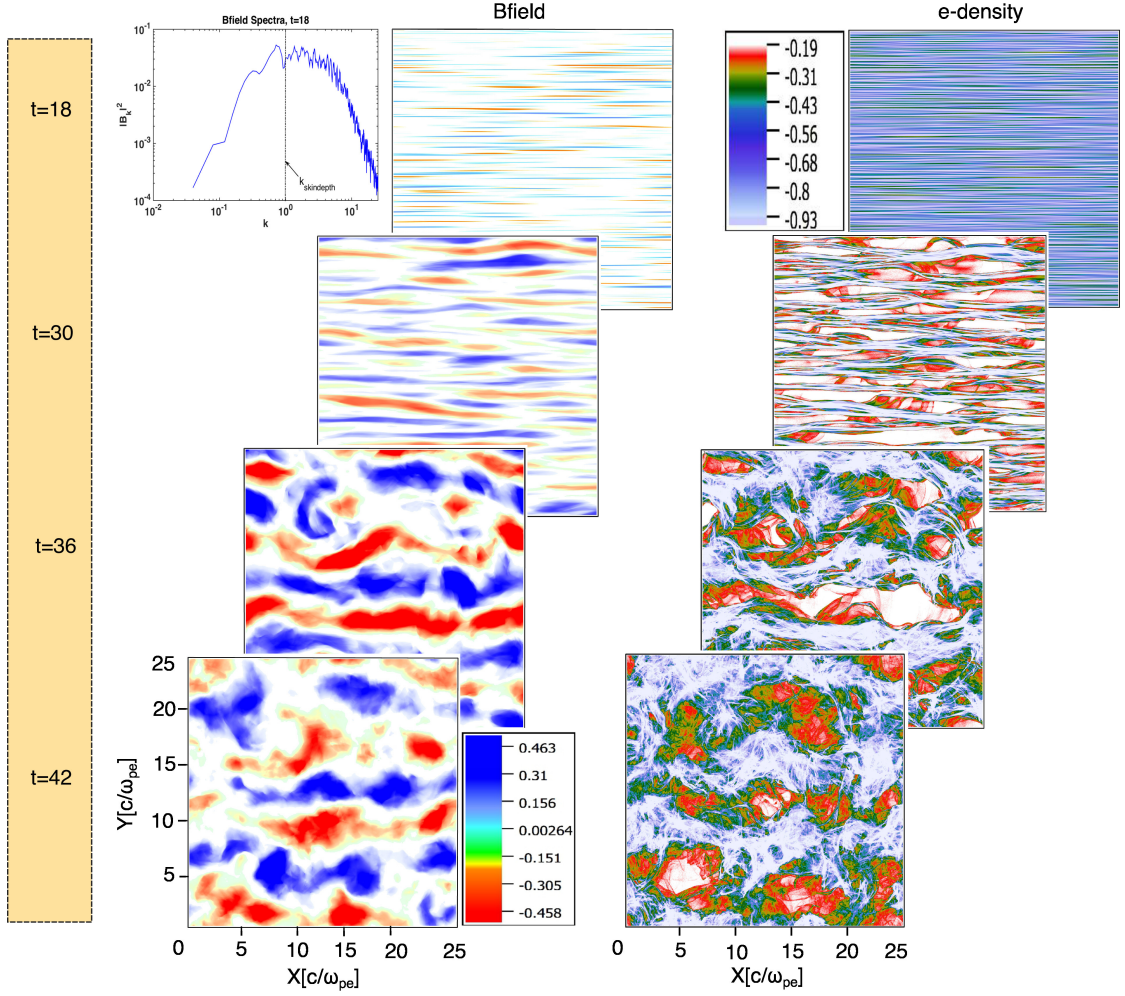


Figure 2.6: Evolution of magnetic field (left column) and electron charge density (right column) of the beam for asymmetric flow (prepared by Vapor [J. Clyne *et al.*, *New Journal of Physics*, 9, 8, (2007); J. Clyne and M. Rast, *Electronic Imaging*, 284-295, (2005)]): In the asymmetric flows, the term $|S_3| \neq 0$ stabilizes the system, therefore the growth rate of instability reduces as compared to symmetric flow. The nonlinear phase of the instability, therefore, has a slow onset.

at various times. For the symmetric case(A) the beam and background electrons have the same density and speed, as shown in Fig. 2.7. The color scale represents the particle numbers on the logarithmic scale. It can be observed from the plot that the phase space plots show considerable evolution with time. In the linear regime $t = 36$, there is an increase in the thermal spread in momentum space. However, subsequently in nonlinear regime the shape of the phase space shows considerable evolution. In the nonlinear regime the phase space acquires a crescent structure. The particles with transverse temperature close to zero acquire a faster velocity, whereas the particles with higher transverse temperature show signs of slowing down. This creates a particle hole at the trailing end (see $t = 36$) subsequently this hole gets filled up and an isotropic momentum distribution is achieved. Thus during a nonlinear phase and the particle momentum essentially tries to isotropize. It is observed that the isotropization occurs faster in the case of symmetric flows.

For the asymmetric case also the stages in development seem to be similar (See Fig. 2.8) qualitatively. The central particles with weak transverse temperature get accelerated and the ones which have higher transverse temperature slow down. It is observed that the system isotropization time is longer when flow configurations are asymmetric as compared to the case when flow configuration is symmetric. In symmetric case, the phase space structures acquire a triangular and/or a tear drop form with the elongated edge being along the propagation direction.

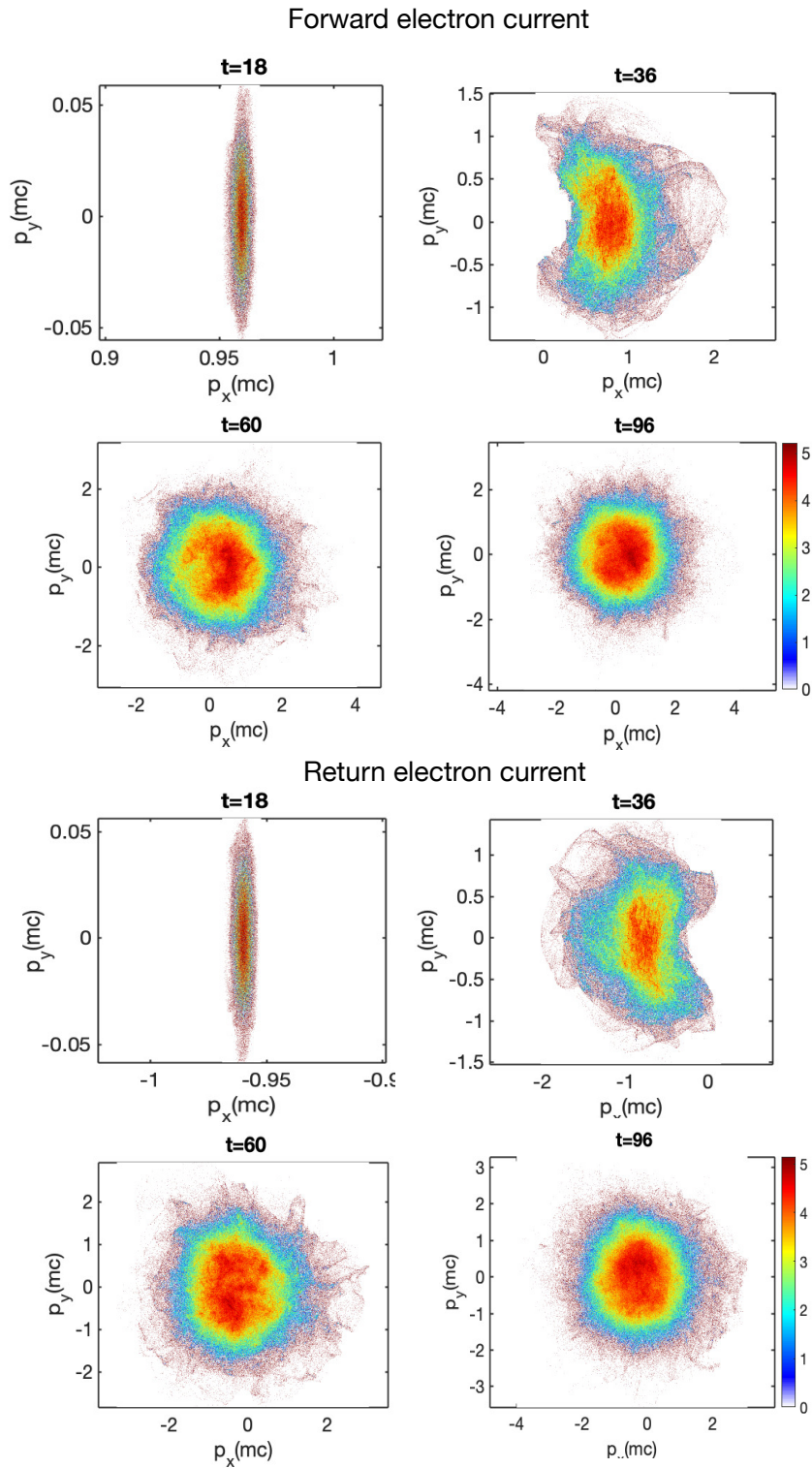


Figure 2.7: Beam and background particle dynamics for symmetric case in momentum space where isotropization of momentum of beam and background plasma particles can be clearly seen

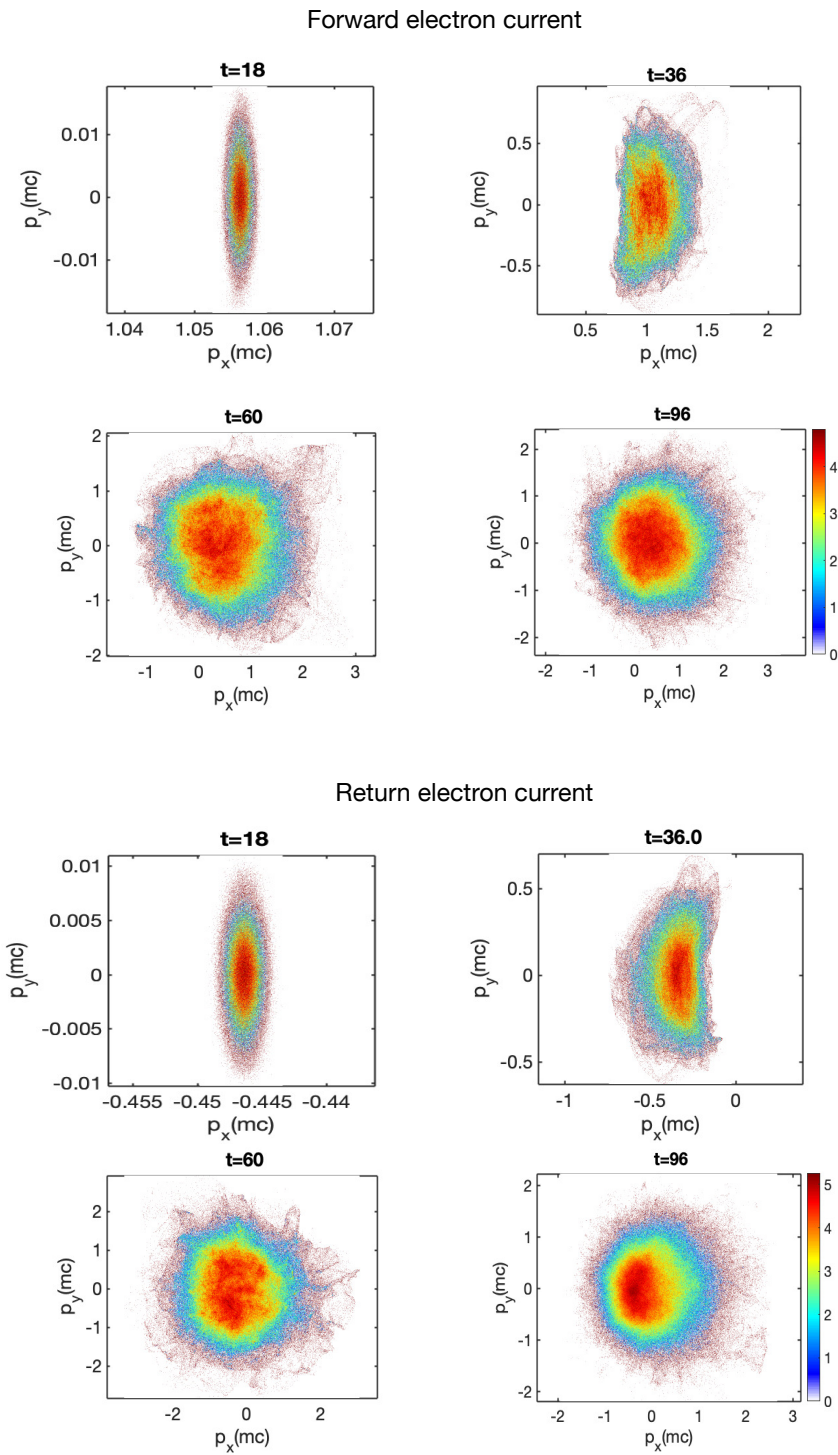


Figure 2.8: Beam and background particle dynamics for asymmetric case in momentum space where isotropization of momentum of beam and background plasma particles can be clearly seen

2.6 Summary

The energy principle utilizes the energy cost associated with the perturbed equilibria to ascertain whether the growth of a particular mode is energetically favorable or not. This technique often provides an interesting physical insight and has been extensively employed in the context of plasma systems governed by Magnetohydrodynamics. Recently, it has been invoked for understanding the electrostatic two stream instability.

In this study, we have shown that an energy principle argument can be put forth for the electromagnetic Weibel mode in the context of beam plasma system. The perturbations in linear regime provide both positive and negative energy contributions in the system. This is essential for the instability, as for conservative system the total energy of the system is constant. The system should allow the possibility of the growth of perturbations without any additional cost of energy. This can happen only when the perturbations merely transfer energy from one form to another. Thus causing one form of energy to grow at the cost of another. For the beam filamentation instability, the electromagnetic field energy in the perturbed state grows at the cost of kinetic energy of the equilibrium flow. We have identified $S_4 = \sum_{\alpha} \frac{n_{0\alpha} v_{0\alpha}^2}{n_0 \gamma_{0\alpha}}$ as the coefficient of the negative energy contributing term and is crucial for the instability. We have also shown that a finite value of $S_3 = \sum_{\alpha} \frac{n_{0\alpha} v_{0\alpha}}{n_0 \gamma_{0\alpha}}$ is responsible for generating the electric field transverse to the flow profile and in fact, costs energy. It is clear that S_3 is finite only in the relativistic case and for the case when the flow profile is asymmetric (beam and background plasma have different densities). The finite value of S_3 suppresses the filamentation mode. This has been verified by comparing the growth rates for various cases in this manuscript. For instance, it has been shown that for a constant value of S_4 the growth rate is maximum for $|S_3| = 0$ and reduces monotonically with increasing value of $|S_3|$. We have also carried out 2-D PIC simulations to illustrate the difference between symmetric and asymmetric flow configurations. We have chosen two flow parameters for which S_4 is same. The value of S_3 is zero for one case and is finite for the other case corresponding to symmetric and asymmetric configurations respectively. We have observed that even in the presence of 2-D perturbations (permitted by the 2-D PIC simulations carried out by us) the symmetric case has higher growth rate. Furthermore, the nonlinear saturation level of

the perturbed magnetic field is also observed to be higher for the symmetric flow configuration. There are two distinct phases of nonlinear evolution. In the first phase, the magnetic energy continues to grow and is the result of the coalescence of current filaments. In the second phase, the magnetic energy shows a steady decrease. This happens as a result of particles acquiring kinetic energy. However, we have shown that the momenta of the particles in this nonlinear regime tries to isotropize the flow. Now when the two current filaments merge, the topology of magnetic field structures also changes because of magnetic reconnection. Furthermore, the isotropization occurs faster in the case of symmetric flow configuration as compared to the case when flows are asymmetric in nature.

The increase of the kinetic energy of particles at the expense of magnetic field energy in the system during later phase of nonlinear evolution of Weibel instability can be associated with the magnetic reconnection in the merging of two current/magnetic filaments. The magnetic field energy decreases during the process of magnetic reconnection and particles are accelerated in the transverse plane. These results are explained in Ch. 3.

It is well known that the Poynting flux in homogeneous beam-plasma system where spatial extensions of beam and plasma electron flows are infinite, will be zero. However, when the beam is of finite extent, there exists a possibility that Poynting flux will not be zero and thus leads to radiative leakage from the finite edges. Detailed explanations of radiative leakage and other features of finite beam-plasma system where beam has finite transverse extent is provided in Ch. 4

3

Nonlinear regime of beam-plasma instabilities

A detailed study on linear regime of current filamentation/ Weibel instability has been discussed in Chapter (2). The nonlinear evolution of current filamentation/Weibel instability has been presented in detail in this chapter ^{*}. The growth of magnetic field in linear regime of the instability saturates due to the magnetic trapping of charged particles. However there exists two distinct nonlinear phases of evolution of Weibel instability. In the first phase of the nonlinear evolution, the current filaments, flowing in the same direction, attract each other and thus merge together to form long scale structures. In this first phase, the total magnetic energy increases. Subsequently, however, during the second phase, one observes a reduction in magnetic energy. It is shown that the transition from one nonlinear regime to another occurs when the typical current associated with individual filaments hits the Alfvén threshold. In the second nonlinear regime, therefore, the filaments can no longer permit any increase in current. Magnetic reconnection events then dissipate the excess current (and its associated magnetic energy) that would result from a merger process leading to the generation of energetic electrons jets in the perpendicular plane. At later times when there are only few filaments left the individual reconnection events can be clearly identified. It is observed that in between such events the magnetic energy remains constant and shows a sudden drop as and when two filaments merge. The electron jets released in these

^{*} Chandrasekhar Shukla, **Atul Kumar**, Amita Das and Bhavesh G. Patel, *Physics of Plasmas* 25, 022123 (2018)

reconnection events are thus responsible for the transverse heating which has been mentioned in previous studies⁴⁸

3.1 Introduction

The existence and impact of the magnetic field in astrophysical events have continued to excite researchers, posing interesting issues pertaining to plasma physics. With the advent of high intensity lasers, it has been possible to make interesting observations on the dynamical evolution of magnetic field in laboratory experiments on laser matter interaction.^{30,31,52,144} The intense lasers ionize the matter into plasma state and dump their energy into the lighter electron species, generating relativistic electron beam (REB)^{15,139,145} in the medium. Though the propagation of relativistic electron beam with current more than Alfvén current limit i.e. $I = (m_e c^3 / e) \gamma_b = 17 \beta \gamma_b k A$, where $\beta = v_b / c$, v_b is velocity of beam and $\gamma_b = (1 - v_b^2 / c^2)^{-1/2}$ is relativistic Lorentz factor, is not permitted in the vacuum (as the associated magnetic fields are large enough to totally curve back the trajectories of the electrons). In plasma medium, this is achieved as the current due to REBs are compensated by the return shielding current in the opposite direction provided by the electrons of the background plasma medium. The two currents initially overlap spatially, resulting in zero net currents and so no magnetic field is present initially. The combination of forward and reverse shielding current is, however, susceptible to several micro-instabilities. A leading instability in the relativistic regime is the filamentation instability.¹²⁹ It is often also termed as the Weibel instability.¹⁸ The filamentation/ Weibel instability creates spatial separation of the forward and reverse shielding currents. The current separation leads to the generation of the magnetic field at the expense of the kinetic energy of the beam and plasma particles. The typical scale length at which the Weibel separation has the maximum growth rate is at the electron skin depth scale c / ω_{pe} . The Weibel separation, thus, leads to the formation of REB current filaments of the size of electron skin depth scale and is responsible for the growth of the magnetic energy in the system. The dynamics, long term evolution and energetics associated with the Weibel instability of current filaments are of central importance in many contexts. For instance, in fast ignition concept of fusion, the energetic REB is ex-

pected to create an ignition spark at the compressed core of the target for which it has to traverse the lower density plasma corona^{48,146-149} and dump its energy at the central dense core of the target. This requires a complete understanding of REB propagation in the plasma medium. In astrophysical scenario, the generation of cosmological magnetic field and relativistic collisionless shock formation in gamma ray bursts have often been attributed to the collisionless Weibel instability.¹⁵⁰⁻¹⁵⁴ The formation of collisionless shock and its behavior depends on long term evolution and dynamics of the magnetic field generated through Weibel destabilization process.

The growth of magnetic field through the Weibel destabilization process influences the propagation of REB filaments. In this nonlinear stage, the current filaments are observed to coalesce and form the larger structure. There are indications from previous studies⁸¹ that at the early nonlinear stage of evolution there is a growth of magnetic field energy. Subsequently, however, the magnetic energy shows decay. The physical mechanism for the observed decay of magnetic field at later stages is the focus of the present studies. There are suggestions that the merging process of super Alfvénic currents carrying filaments leads to the decay of magnetic energy.⁸¹ On the other hand, the mechanism of magnetic reconnection which rearranges the magnetic topology in plasma is also invoked which converts the magnetic energy to kinetic energy of the particles. This can result in thermal particles or the particles may even get accelerated^{82,83} by the reconnection process. The merger of current filaments leading to X point formation where reconnection happens has been shown in the schematic diagram Fig.(3.1).

In this chapter, the linear and non-linear stage of Weibel instability in detail with the help of 2-D Particle - In- Cell (PIC) simulation has been studied. The 2-D plane of simulation is perpendicular to the current flow direction. The initial condition is chosen as two overlapping oppositely propagating electron currents. The development of the instability, the characteristic features during nonlinear phase etc., are studied in detail.

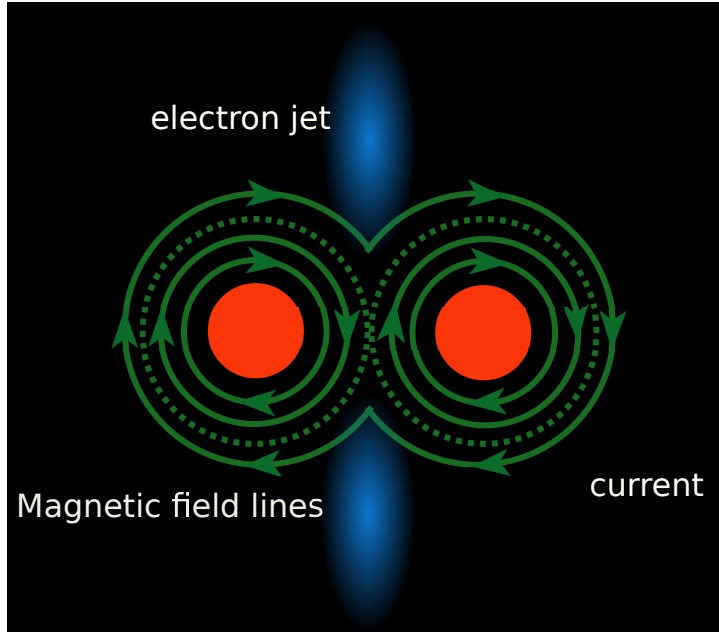


Figure 3.1: Schematic (not to scale) of magnetic reconnection where the magnetic field lines reconnects and accelerates the plasma particles as a jet

3.2 Simulation Set-up

We employ OSIRIS^{46,47} Particle - In - Cell (PIC) code to study the evolution of the two counterstreaming electron current flows in a 2-D $x_1 - x_2$ plane perpendicular to the current flow direction of $\pm\hat{z}$. We have considered the ion response to be negligible and treated them as merely providing a stationary neutralizing background. Thus the dynamics is governed by electron species alone. However, this would not be applicable at longer times where ion response may become important and introduce new features.

The boundary conditions are chosen to be periodic for both the electromagnetic field and the charged particles in all direction. We choose the area of the simulation box R as $64 \times 64 (c/\omega_{pe})^2$ corresponding to 640×640 cells. The time step is chosen to be $7.07 \times 10^{-2}/\omega_{pe}$ where $\omega_{pe} = \sqrt{4\pi n_{0e}e^2/m_e}$ and $n_{0e} = n_{0b} + n_{0p}$ is the total electron density which is the sum of beam and the plasma electrons denoted by suffix b and p respectively. The total number of electrons and ions per cell in the simulations are chosen to be 500 each. The quasi neutrality is maintained in the system by choosing equal number of electrons and ions. The

velocity of beam electrons and the cold plasma electrons are chosen to satisfy current neutrality condition. The uniform plasma density n_{0e} is taken as $1.1 \times 10^{22} \text{cm}^{-3}$ and the ratio of electron beam density to background electron density has been taken as ($n_{0b}/n_{0p} = 1/9$) is the simulations presented here. The fields are normalized by $m_e c \omega_{pe} / e$. The evolution of field energy normalized by $m_e c^2 n_{0e}$ is averaged over the simulation box. We have carried simulations for the choice of cold as well as finite temperature beams. Several choices of beam temperature were considered.

3.3 Linear stage of instability

The charge neutrality and the current balance condition, chosen initially ensures that there are no electric and magnetic fields associated with the system and equilibrium conditions are satisfied. We observe a development of magnetic field structures of the typical size of electron skin depth with time. This can be seen in Fig.(3.2) where the contours of the transverse magnetic field have been shown in the 2D $x_1 - x_2$ plane. The development of this magnetic field can be understood as arising due to the spatial separation of forward and return currents through Weibel destabilization process. The growth of transverse magnetic field energy with time has been shown in Fig.(3.3) for the two cases with following parameters: (I) $v_{0b} = 0.9c$ and (II) $v_{0b} = 0.9c$, $T_{0b} = 1 \text{keV}$, $T_{0p} = 0.1 \text{keV}$. The initial linear phase of growth is depicted by the straight line region in the log linear plot. A comparison with the analytically estimated maximum growth rate for the two cases has been provided by the dashed line drawn alongside.

The growth rate for case (I) with $v_{0b} = 0.9c$ the growth rate obtained from the simulation by measuring the half of the slope of the magnetic energy evolution in Fig.(3.3) is 0.18 and it compares well with the analytical value of 0.1879 ($\delta_{max}^{cold} \sim \left(\frac{v_{0b}}{c}\right) \sqrt{\frac{n_{0b}/n_{0p}}{\gamma_{0b}}} \omega_p$ ¹⁵⁵). Similarly for case (II) when the beam temperature is finite the growth rate of 0.023 from simulation agrees well with the analytical estimate obtained from kinetic calculations for these parameters of 0.025 ($\delta_{max}^{hot} \sim \frac{2\sqrt{6}}{9\sqrt{\pi}} \frac{[\omega_b^2 v_{0b}^2 m_e / T_b + \omega_b^2 (\gamma_{0b} - 1 / \gamma_{0b}^3)]^{3/2}}{\omega_p^2 (v_{0p}^2 + T_p / m_e) c} (T_p / m_e)^{3/2}$ ⁴²). It should be noted that this is consistent with the well known characteristic feature of the reduction in Weibel growth rate by increasing beam temperature. After the linear phase of growth, it

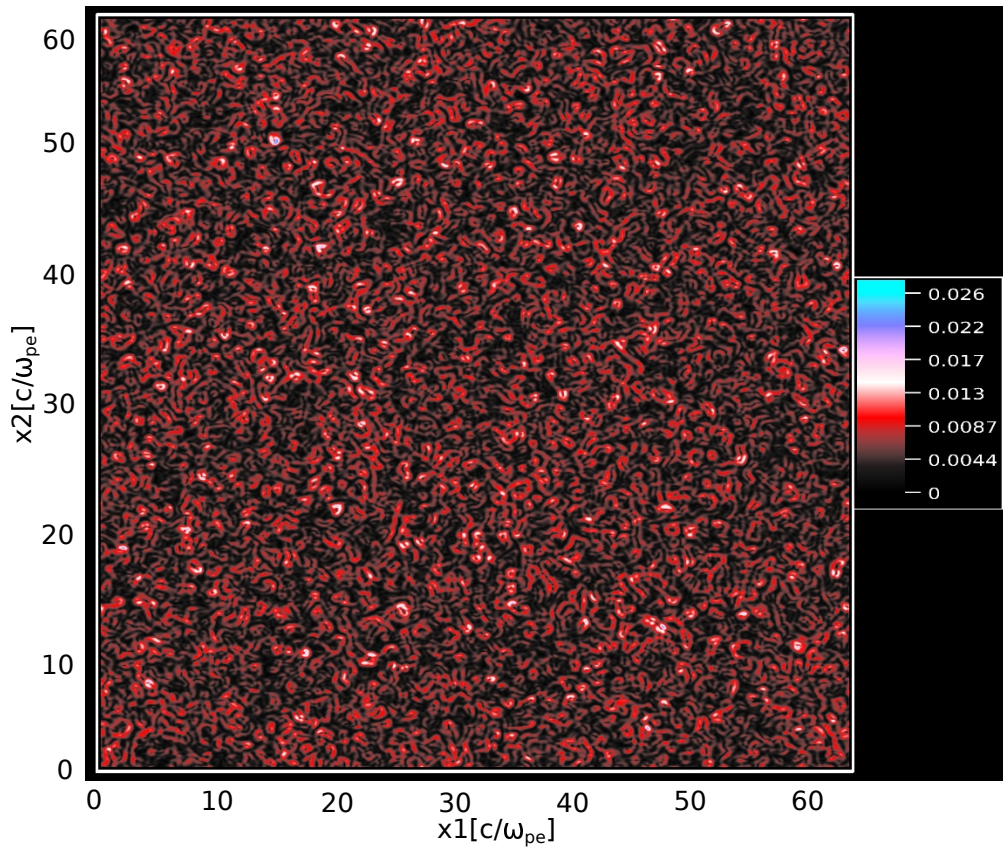


Figure 3.2: The transverse magnetic field $B_{\perp} = \sqrt{B_x^2 + B_y^2}$ [in unit of $m_e c \omega_{pe} / e$] at $t \omega_{pe} = 51$: The size of magnetic field structure in linear regime is the order of c / ω_{pe}

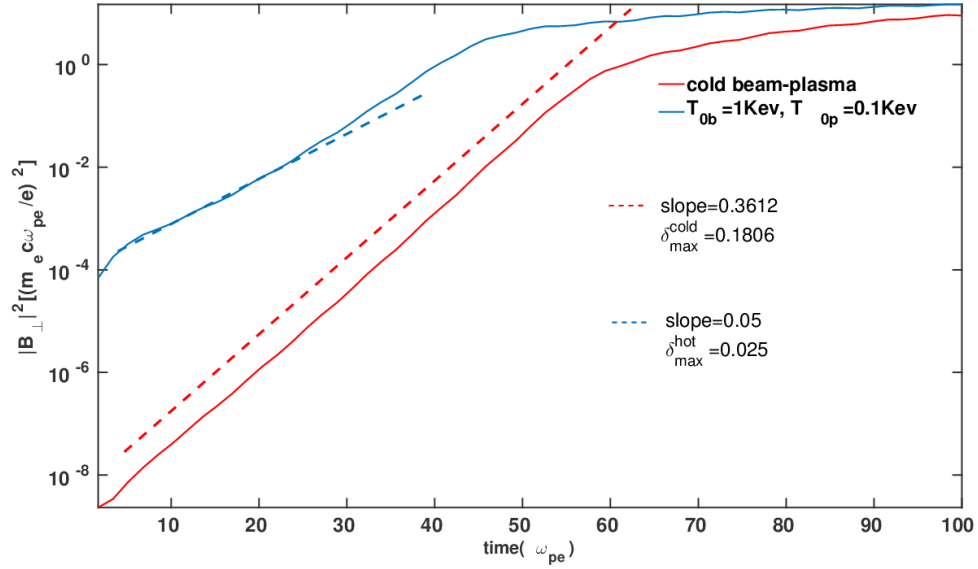


Figure 3.3: Calculation of linear growth rate from PIC simulation

can be observed from Fig.(3.3) that when the normalized magnetic energy becomes of the order of unity the increase in magnetic energy considerably slows down. This reflects the onset of the nonlinear regime. We discuss the nonlinear regime of the instability in the next section in detail.

3.4 Nonlinear stage of instability

When the Weibel separated magnetic fields acquire significant magnitude, they start influencing the dynamics of beam and plasma particles. This backreaction signifies the onset of nonlinear regime. The plot of the magnetic energy growth in Fig.(3.3) clearly, shows that at around $t \sim 50\omega_{pe}t$ (cold beam-plasma system) the system enters the nonlinear phase. The characteristics behaviour in the nonlinear regime has been described in the subsections below:

3.4.1 Current filaments

In the non-linear stage of WI, the current filaments, flowing in the same direction, merge with each other with time and organize as bigger size filaments. During the initial nonlinear stage magnetic field energy keeps growing, albeit at a rate

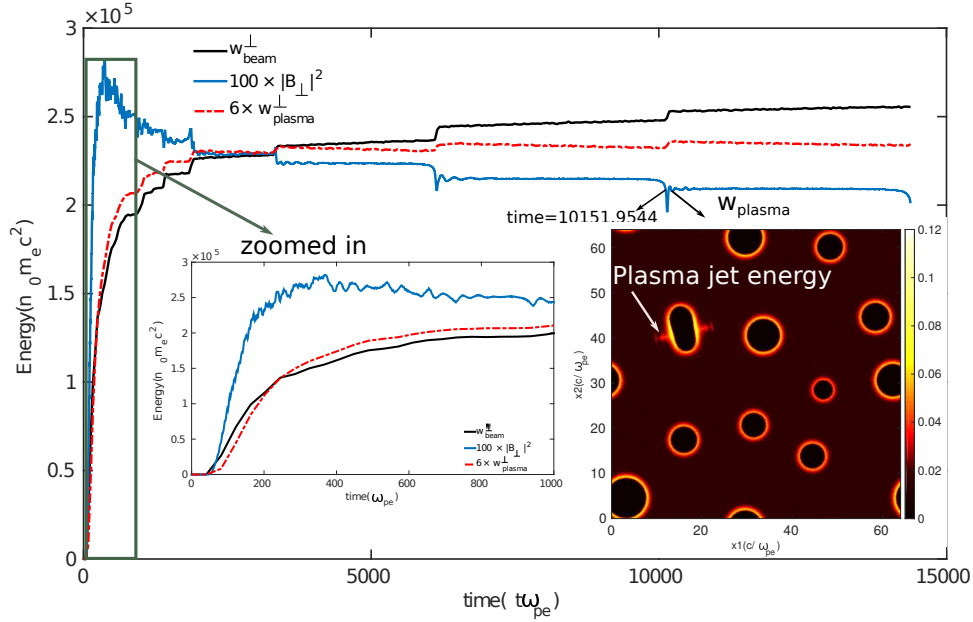


Figure 3.4: Evolution of energy (in unit of $n_0 m_e c^2$) with time: The solid blue curve shows the magnetic field energy $|B_{\perp}|^2 = |B_x^2 + B_y^2|$ and the decay in magnetic field energy at later time can be clearly seen. The solid black curve is for transverse kinetic energy W_{beam}^{\perp} of beam and dotted red curve is for transverse kinetic energy W_{plasma}^{\perp} of plasma. In the plots, we observe the gain in the transverse kinetic energy of plasma as well as beam at the same time when magnetic reconnection phenomena occurs and magnetic field energy decay. The color plot of kinetic energy of plasma particle has been shown in the inset of figure which shows the jet like structure.

which is much slower than the linear growth rate and then saturates (Fig. 3.4). Subsequently, the magnetic field energy decreases as can be observed from the plot of Fig.(3.4).

A rough estimate of the saturated magnetic field can be made by the following simple consideration. The spatial profile of the magnetic field in the current filament is mimicked as a sinusoidal function with k representation the inverse of the filament size. The amplitude of the magnetic field is B_0 which in the nonlinear regime significantly deflects the trajectories of the electrons. The transverse motion of an electron in the plane of the magnetic field is then given by

$$\frac{d^2 r}{dt^2} = \frac{ev_z}{mc\gamma_{0b}} B_0 \sin(kr) \quad (3.1)$$

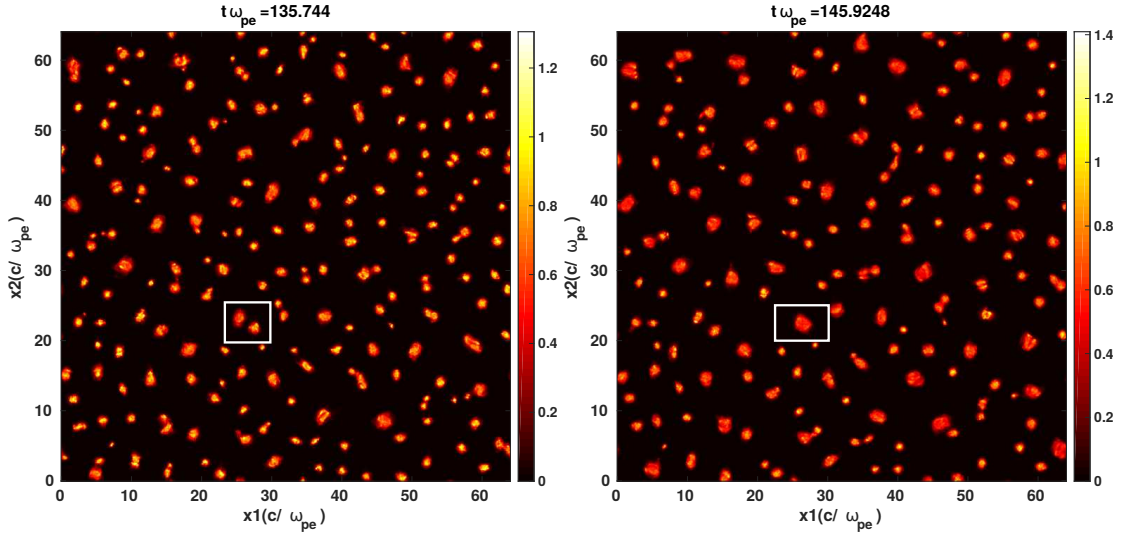


Figure 3.5: The merging of beam current filaments highlighted by white box

The bounce frequency of a magnetically trapped electron is thus

$$\omega_m^2 = \frac{ev_{0b}kB_0}{m_e c \gamma_{0b}} \quad (3.2)$$

the saturation would occur when the typical bounce frequency becomes equal to the maximum linear growth rate of instability. Therefore, the saturated magnetic field can be estimated by comparing the linear growth of filamentation instability to the bounce frequency ($\omega_m = \delta_m$). In case of mono-energetic distribution function, the saturated magnetic field is

$$B_{sat} \sim \left(\frac{m_e v_{0b} n_{0b}}{ekcn_{0p}} \right) \omega_p^2 \quad (3.3)$$

The estimate provided by the eq.(3.3) compares well with the observed saturated value of the magnetic field which is equal to 0.1.

3.4.2 Alfvén limited filaments

The process of merging of like current filaments can be seen from the plots of temporal evolution of the current densities shown in Fig.(3.5). The current in the filament is essentially due to the beam electrons as illustrated in Fig.(3.5). The

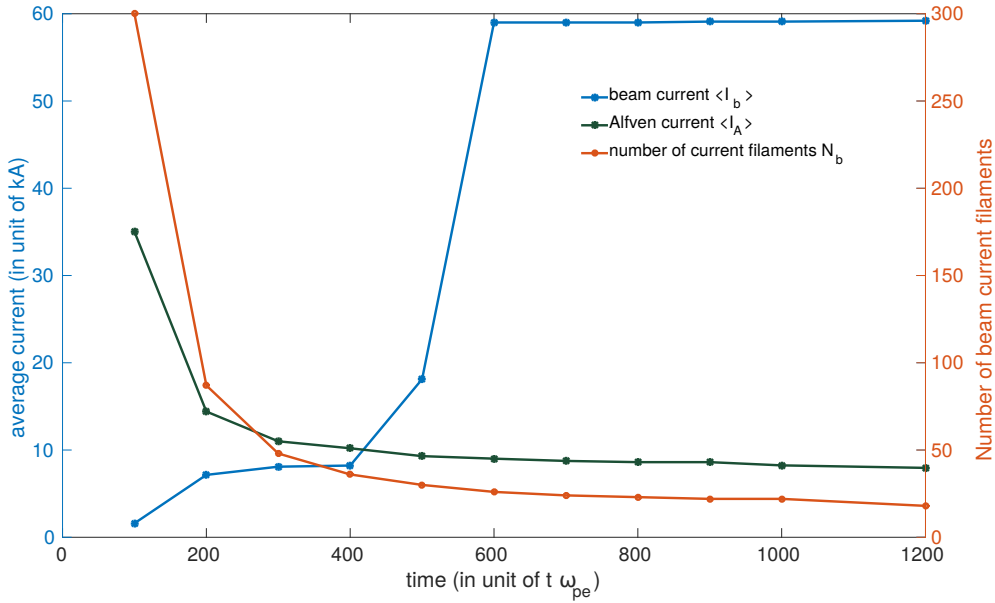


Figure 3.6: The time evolution of number of current filaments(solid red curve), average current per filament (solid blue curve) and Alfvén (solid green curve).

current in the filament, however, should not exceed the Alfvén limit. The value of the Alfvén limit for our simulations is $35kA$. In Fig.(3.6), we show the evolution of the beam current and the number of filaments in the simulation box.

The number of filaments keeps dropping slowly, however, the average beam current in the filament keeps increasing. Since the beam particles convert the partial kinetic energy into magnetic field energy and slow down, the Alfvén current limit drops with time and finally saturates. The magnetic field keep on increasing until the average beam current lower than Alfvén current limit and at particular time, the average beam current cross the Alfvén current limit. This is also the time after which there is no increase in the magnetic energy of the system. After the saturation of instability, the magnetic field energy ($|B_{\perp}|^2(n_0 m_e c^2)$ zoomed $100\times$ for better view) starts decaying as shown in Fig.(3.4). In fact, one observes that the magnetic energy reduces after this time. This decay in the magnetic field energy can be understood on the basis of magnetic reconnection phenomena.

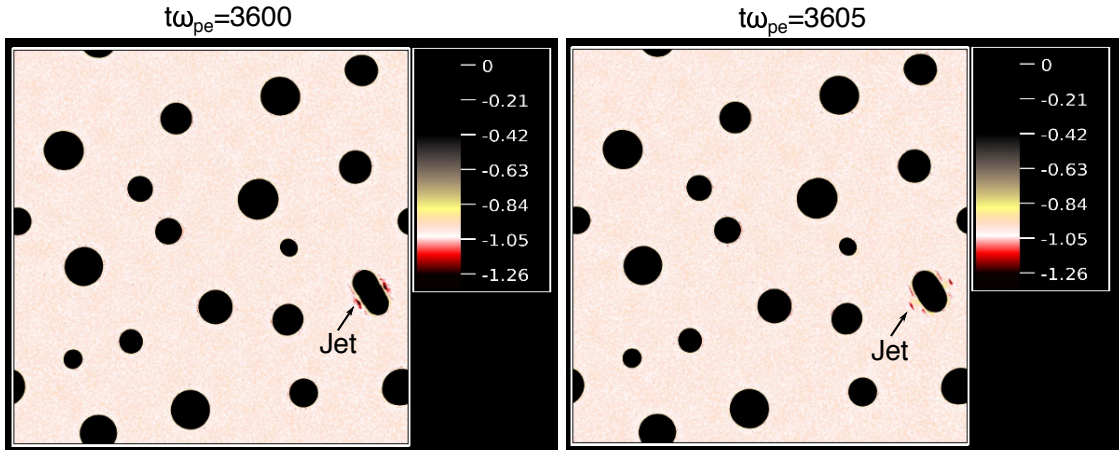


Figure 3.7: The formation of jet like structure during the magnetic reconnection process in background plasma charge density [highlighted by arrow]

3.4.3 Electron jet formation

At later times when only few filaments are left in the system, we can track each of the filaments individually. We choose two such filaments which are about to converge and observe their behaviour as they coalesce with each other in Fig.(3.7). The figures show the formation of electron jets in the plane as the two structures merge with each other.

The structures basically follow the EMHD^{156,157} dynamics. Thus as the filaments come near each other they carry the $\vec{B} - \nabla^2 \vec{B}$ with them. The filament scales being longer than electron skin depth, the magnetic field is essentially carried by the electron flow in the plane. However, when the filaments hit each other the magnetic fields get compressed against each other and scale sizes smaller than electron skin depth are formed. The collisionless inertia driven reconnection takes place and generating energetic electron jets in the direction orthogonal to the direction at which the filaments approach each other.

There is a change in magnetic field topology and accelerated electrons are observed. This is responsible for the reduction in magnetic field energy. In fact, each of the sudden drops in magnetic field energy can be times with such reconnection events in the simulation. The increase in the perpendicular energy of the electrons W_{\perp} has been shown in Fig.(3.4).

It is interesting to note that nature tries to use ingenious and rapid techniques to

relax a highly asymmetric system such as the one with inter-penetrating electron current flows along $\pm\hat{z}$. The system being collisionless it would not have been possible to convert W_{\parallel} (kinetic energy parallel to \hat{z} axis to W_{\perp}). The magnetic field provides an intermediary role to aid this process and symmetrize the system.

3.5 Conclusions

In this chapter, we have studied theoretically as well as numerically (PIC simulation) the Weibel instability in beam plasma system. We have shown that the linear stage of Weibel instability shows good agreement with PIC simulation results. In the non-linear stage, the current filaments having the flow in the same direction merge into each other. There is a rearrangement of the magnetic field lines through reconnection process leading to energetic electron jets in the plane. This has been clearly observed in the simulation. So ultimately the parallel flow energy gets converted into the perpendicular electron energy. Basically, the excitation of the instability and the nonlinear evolution tries to relax the configuration towards an isotropic configuration rapidly in a collisionless system.

4

Effect of finite beam size and initial current

In the previous chapters (Ch. 2 and Ch. 3), it has been shown that the combination of forward and return shielding currents is known to be susceptible to the Weibel destabilization process as observed from the PIC simulations for periodic infinite beam - plasma system.¹⁵⁸ Such a destabilization leads to spatially separated current filaments at the electron skin depth leading to magnetic field generation at commensurate scales. At later times, the current filaments created merge to form larger structures and hence, the long scale magnetic field structures are generated in the system through nonlinear inverse cascade mechanism. The choice of infinite periodic system is based on an inherent understanding that the boundary effects due to finite system would merely have small incremental impact. However, numerous laser-plasma experiments^{30,31} in last one decade suggests the generation of long scale magnetic field structures much before the conventional Weibel and other sheared flows instabilities like Kelvin-Helmholtz instabilities. The appearance of magnetic fields at scales longer than the skin depth during very early stage can never be accounted by conventional Weibel destabilization route of the beam plasma system. This remained a puzzle to us for nearly a decade which has never been well understood.

In this chapter *, we propose, simulate and experimentally demonstrate a new

* *Amita Das, Atul Kumar, Chandrasekhar Shukla, Ratan Kumar Bera, Deepa Verma, Bhavesh Patel, Y. Hayashi, K. A. Tanaka, Amit D. Lad, G. R. Kumar, and Predhiman Kaw, arXiv:1712.03099 [physics.plasm-ph] (2017)*

mechanism of long scale magnetic field generation in the context of laser plasma interaction. The mechanism relies on two realistic features which have been totally ignored in previous studies. These relate to the finite size of the laser generated electron beam and an initial current imbalance which would typically be present when energetic electrons push itself in a plasma medium. It is shown that magnetic fields of much longer scale lengths (comparable to the transverse beam dimension) get generated much before the conventional Weibel and Kelvin Helmholtz instabilities associated with the beam plasma system set in. This happens as a result of a radiative leakage at the boundaries of the finite beam wherein even a small but finite current imbalance plays a crucial role of a radiative antennae. These features have been absent in all conventional periodic systems considered in earlier simulations as well as theoretical analyses. Our study thus triggers a re-examination of hitherto prevalent ideas on magnetic field generation in plasmas and focus attention on the effects of finiteness in physical systems.

4.1 Introduction

The dynamical evolution of intense magnetic fields and associated current pulses plays an important role in a variety of plasma physics problems. These include plasma switches, design of novel radiation and charged particle sources, laser driven fusion and laboratory simulation of astrophysical phenomena etc.^{30,31,141,159–161} The current pulses may be generated and driven into a solid density plasma by an intense, femtosecond laser. It is now well known that massive current pulses produced in such an interaction induce return currents from the thermal plasma electrons and these two types of currents are fraught to electromagnetic instabilities. It is widely believed that the well known Weibel instability^{18,28,162} separates these initially superimposed counterstreaming currents and leads to strong magnetic field generation. Countless analytical and simulation studies have explored this instability and predicted that this instability generates magnetic field at the electron skin depth scale. The nonlinear inverse cascade mechanism subsequently leads to progressive generation of longer scales. In this manuscript, we provide convincing evidences that this is not a realistic physical situation but is merely an artefact of boundless beam plasma interaction in simulations as well as the-

oretical analyses. We demonstrate through laser plasma experiments and finite beam size simulations, using different variety of codes, that the energy is input preferentially into the magnetic field at the scale size of the beam (in the case of laser experiments this is at the spot size of the irradiating laser). We show that magnetic field generation caused by the electron currents first occurs at the scale size of the boundary and only much later does the Weibel instability kick in at the skin depth scale. This is a new mechanism of magnetic field generation which is triggered by a small current imbalance acting like an antenna causing radiative leakage from the two edges of the finite beam. When the plasma medium is overdense, the radiatively leaking fields accumulate at the beam edge giving rise to long scale magnetic fields. This mechanism of magnetic field generation dominates the Weibel instability at the initial stage and has its origin in the effect of radiative loss from negative energy waves in a manner analogous to the radiative instability of a leaky waveguide.^{163,164}

4.2 The new mechanism for long scale magnetic field generation

We have carried out theoretical analyses using two fluid model for an equilibrium configuration of the beam plasma system in 2-D $x - y$ plane as shown in Fig.1. The central region II from $-a \leq y \leq a$ carries the beam current and an oppositely flowing background plasma current, which balance each other. In region I and region III the plasma is static and at rest. The charge neutralization in equilibrium is achieved by balancing the total electron density by the background ion density, viz., $\sum_{\alpha} n_{0\alpha} = n_{0i}$ in all the three regions. The electron flow velocity in region I and III is zero, whereas in region II the two fluids flow in a fashion so as to have zero current, i.e. $\sum_{\alpha} n_{0\alpha} v_{0\alpha x} = 0$. Here the suffix α stands for b and p representing the beam and plasma electrons. The linearised perturbation of the momentum and continuity equations of the two fluids and the Maxwell set of equations around this equilibrium is considered. The perturbed fields are chosen to vary with respect to y and t only. The flow is confined in $x - y$ plane, so we have B_{1z} , E_{1x} and E_{1y} (where the suffix x, y , and z denotes the spatial components and B and E represent magnetic and electric field respectively) only as the perturbed dominant fields. The

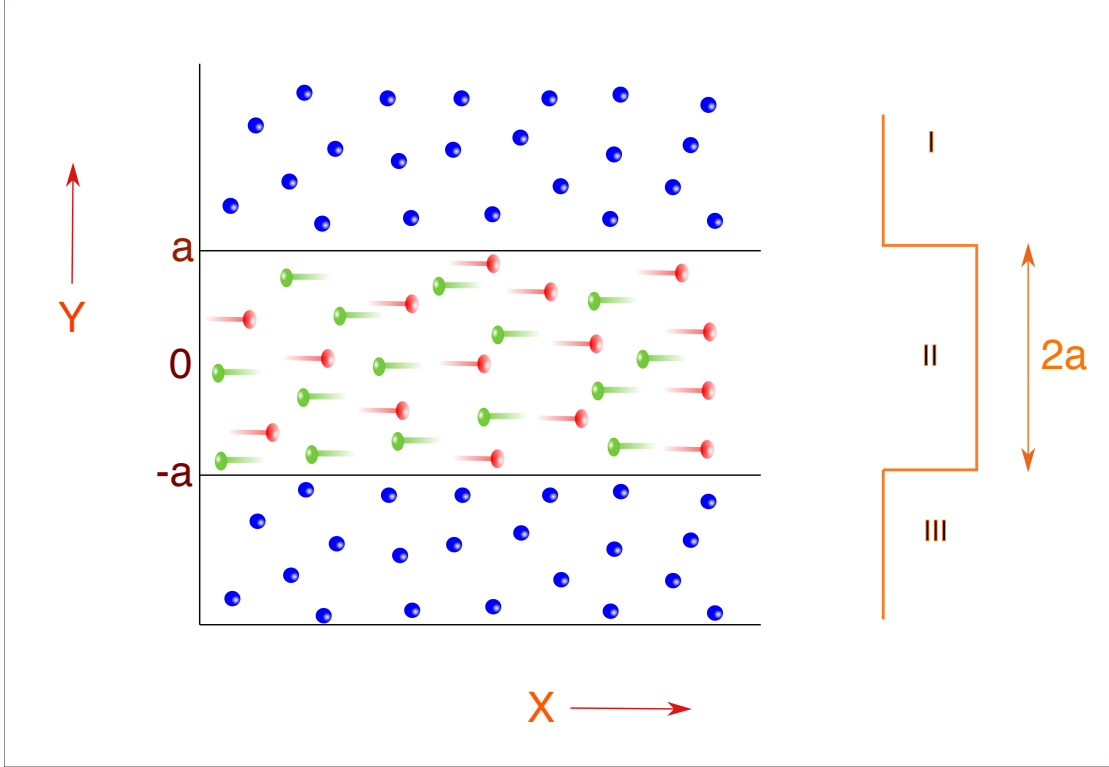


Figure 4.1: Schematics (not to scale) of 2D- equilibrium geometry of the beam plasma system where beam has finite width ' $2a$ ' in the transverse direction

linearised continuity equation for the species α can be written as:

$$\frac{\partial n_{1\alpha}}{\partial t} + \frac{\partial}{\partial y}(n_{0\alpha}v_{1\alpha y}) = 0 \quad (4.1)$$

Similarly, linearising the x and y components of momentum equation for the species α we have:

$$\frac{\partial}{\partial t}(m\gamma_{0\alpha}^3 v_{1\alpha x}) = -eE_{1x} \quad (4.2)$$

$$\frac{\partial}{\partial t}(m\gamma_{0\alpha} v_{1\alpha y}) = -eE_{1y} + ev_{0\alpha}B_{1z}/c; \quad (4.3)$$

where ' e ' is the magnitude of the electronic charge and ' m ' is the rest mass of an electron. The Faraday law gives the following relationship between the \hat{z} compo-

ment of magnetic field and the \hat{x} component of electric field:

$$B_{1z} = -\frac{k}{\omega}E_{1x} \quad (4.4)$$

Ampere's law can be written as,

$$\vec{\nabla} \times \vec{B} = \frac{4\pi}{c}\Sigma\vec{J}_{1\alpha} + \frac{1}{c}\frac{\partial\vec{E}_1}{\partial t}$$

or,

$$\vec{\nabla} \times \vec{\nabla} \times \vec{E} = -\frac{1}{c}\frac{\partial}{\partial t}(\vec{\nabla} \times \vec{B})$$

which can be further written after some algebraic steps as:

$$\left(\frac{\partial^2}{\partial y^2} + \frac{\omega^2}{c^2}\right)E_{1x} = -\frac{4\pi\iota\omega}{c^2}\Sigma J_{1\alpha x} \quad (4.5)$$

where,

$$\Sigma J_{1\alpha x} = -e\Sigma n_{0\alpha}v_{1\alpha x} - e\Sigma n_{1\alpha}v_{0\alpha x} \quad (4.6)$$

Employing the Fourier representation for the linearised fields (density, velocity, electric and magnetic field), we can cast the Eqs.(4.1 - 4.3) respectively to obtain:

$$n_{1\alpha} = \frac{k}{\omega}n_{0\alpha}v_{1\alpha y} \quad (4.7)$$

$$v_{1\alpha x} = -\frac{\iota}{\omega}\frac{eE_{1x}}{m_x\gamma_{0\alpha}^3} - \frac{\iota}{\omega}\frac{\frac{\partial}{\partial y}(\gamma_{0\alpha}v_{0\alpha x})}{\gamma_{0\alpha}^3}v_{1\alpha y} \quad (4.8)$$

$$v_{1\alpha y} = \frac{\iota e}{\omega\gamma_{0\alpha}c}\frac{v_{0\alpha x}}{m_e}B_{1z} \quad (4.9)$$

Substituting Eqs.(4.7 - 4.9) into Eq.(4.6), we obtain:

$$J_{1\alpha x} = en_{0\alpha}\left[\frac{\iota}{\omega}\frac{eE_{1x}}{m_e\gamma_{0\alpha}^3} + \frac{\iota}{\omega\gamma_{0\alpha}^3}\frac{\partial}{\partial y}(\gamma_{0\alpha}v_{0\alpha x})v_{1\alpha y}\right] + ev_{0\alpha x}\left[\frac{\iota}{\omega}n_{0\alpha}\frac{\partial}{\partial y}v_{1\alpha y}\right]$$

or,

$$J_{1\alpha x} = \frac{i n_{0\alpha} e^2}{m_e \gamma_{0\alpha}^3 \omega} E_{1x} + e n_{0\alpha} \frac{i}{\omega \gamma_{0\alpha}^3} \cdot \gamma_{0\alpha} \frac{\partial}{\partial y} (v_{0\alpha x}) \left[\frac{-e v_{0\alpha x}}{\gamma_{0\alpha} \omega^2 m_e} \frac{\partial E_{1x}}{\partial y} \right] + \frac{e v_{0\alpha x} n_{0\alpha} i}{\omega} \frac{\partial}{\partial y} \left[\frac{-e v_{0\alpha x}}{\gamma_{0\alpha} \omega^2 m_e} \frac{\partial E_{1x}}{\partial y} \right]$$

or,

$$J_{1\alpha x} = \frac{i \omega_{pe}^2 n_{0\alpha}}{4\pi n_0 \gamma_{0\alpha}^3 \omega} E_{1x} - \frac{i e^2 n_{0\alpha} v_{0\alpha x}}{\gamma_{0\alpha} m_e \omega^3} \frac{\partial E_{1x}}{\partial y} \frac{\partial}{\partial y} (v_{0\alpha x}) - \frac{i e^2 n_{0\alpha} v_{0\alpha x}}{m_e \omega^3} \frac{\partial}{\partial y} \left[\frac{v_{0\alpha x}}{\gamma_{0\alpha}} \frac{\partial E_{1x}}{\partial y} \right]$$

or,

$$J_{1\alpha x} = \frac{i \omega_{pe}^2 n_{0\alpha}}{4\pi n_0 \gamma_{0\alpha}^3 \omega} E_{1x} - \frac{i e^2 n_{0\alpha}}{m_e \omega^3} \left(\frac{v_{0\alpha x}}{\gamma_{0\alpha}} \frac{\partial E_{1x}}{\partial y} \right) \frac{\partial}{\partial y} (v_{0\alpha x}) - \frac{i e^2 n_{0\alpha}}{m_e \omega^3} (v_{0\alpha x}) \frac{\partial}{\partial y} \left[\frac{v_{0\alpha x}}{\gamma_{0\alpha}} \frac{\partial E_{1x}}{\partial y} \right]$$

or,

$$J_{1\alpha x} = \frac{i \omega_{pe}^2 n_{0\alpha}}{4\pi n_0 \gamma_{0\alpha}^3 \omega} E_{1x} - \frac{\partial}{\partial y} \left[\frac{i \omega_{pe}^2 n_{0\alpha}}{4\pi n_0 \gamma_{0\alpha}^3 \omega^3} v_{0\alpha x}^2 \frac{\partial E_{1x}}{\partial y} \right] \quad (4.10)$$

Substituting Eq.(4.10) into Eq.(4.5), we get the following expression:

$$\left(\frac{\partial^2}{\partial y^2} + \frac{\omega^2}{c^2} \right) E_{1x} + \frac{4\pi i \omega}{c^2} \Sigma \left\{ \frac{i \omega_{pe}^2 n_{0\alpha}}{4\pi n_0 \gamma_{0\alpha}^3 \omega} E_{1x} - \left[\frac{i \omega_{pe}^2 n_{0\alpha}}{4\pi n_0 \gamma_{0\alpha}^3 \omega^3} v_{0\alpha x}^2 \frac{\partial E_{1x}}{\partial y} \right]' \right\} = 0 \quad (4.11)$$

or,

$$\left[E_{1x}' + \frac{\omega_{pe}^2}{\omega^2 c^2} \Sigma \frac{n_{0\alpha} v_{0\alpha x}^2}{n_0 \gamma_{0\alpha}} E_{1x}' \right]' + \left(1 - \frac{\omega_{pe}^2}{\omega^2 c^2} \Sigma \frac{n_{0\alpha}}{n_0 \gamma_{0\alpha}^3} \right) \frac{\omega^2}{c^2} E_{1x} = 0$$

or,

$$\left[E_{1x}' \left(1 + \frac{\omega_{pe}^2}{\omega^2 c^2} \Sigma \frac{n_{0\alpha} v_{0\alpha x}^2}{n_0 \gamma_{0\alpha}} \right) \right]' + \left(1 - \frac{\omega_{pe}^2}{\omega^2 c^2} \Sigma \frac{n_{0\alpha}}{n_0 \gamma_{0\alpha}^3} \right) \frac{\omega^2}{c^2} E_{1x} = 0$$

or,

$$\left[E_{1x}' \left(1 + \frac{\omega_{pe}^2}{\omega^2 c^2} \Sigma \frac{n_{0\alpha} v_{0\alpha x}^2}{n_0 \gamma_{0\alpha}} \right) \right]' + \left(1 - \frac{\omega_{pe}^2}{\omega^2 c^2} \Sigma \frac{n_{0\alpha}}{n_0 \gamma_{0\alpha}^3} \right) \frac{\omega^2}{c^2} E_{1x} = 0 \quad (4.12)$$

We have chosen to normalize time with the inverse of electron plasma frequency, $\omega_{pe} = \sqrt{\frac{4\pi n_0 e^2}{m}}$ and length with the electron skin depth, $d_e = c/\omega_{pe}$ (*i.e.*, $t \cdot \omega_{pe}^{-1} \rightarrow t$ and $y \cdot d_e \rightarrow y$) to obtain the following differential equation expression Eliminating

all the perturbed fields in terms of E_{1x} :

$$[f_2 E'_{1x}]' - g_2 E_{1x} = 0 \quad (4.13)$$

Here

$$f_2 = 1 + \frac{S_4}{\omega^2} - \frac{S_3^2}{\omega^2(S_1 - \omega^2)} \quad (4.14)$$

$$g_2 = S_2 - \omega^2 \quad (4.15)$$

In addition, we have used the following definitions:

$$S_1 = \sum_{\alpha} \frac{n_{0\alpha}}{n_0 \gamma_{0\alpha}}; \quad S_2 = \sum_{\alpha} \frac{n_{0\alpha}}{n_0 \gamma_{0\alpha}^3} \quad (4.16)$$

$$S_3 = \sum_{\alpha} \frac{n_{0\alpha} v_{0\alpha}}{n_0 \gamma_{0\alpha}}; \quad S_4 = \sum_{\alpha} \frac{n_{0\alpha} v_{0\alpha}^2}{n_0 \gamma_{0\alpha}} \quad (4.17)$$

It should be noted that S_3 and S_4 are finite only when there is an equilibrium flow in the two fluid electron depiction. Furthermore, if the flow velocities of the two electron species are equal and opposite then $S_3 = 0$.

4.3 Existence of new finite beam instability

The homogeneous limit of Atul Kumar *et. al.*²⁸ (mentioned in Eq. 2.26, Chapter 2) can be easily recovered if we take Fourier transform of Eq.(4.13). The homogeneous equation yields the dispersion relation for the Weibel instability growth rate. We now seek the possibilities for obtaining purely growing modes in a finite system. For this purpose we multiply Eq.(4.13) by E_{1x} , replace $\omega^2 = -\Gamma^2$ (for purely growing modes) and integrate over y over region II, i.e. from $-a$ to a . This yields:

$$\int_{-a}^a [E_{1x}(f_2 E'_{1x})' - g_2 E_{1x}^2] dy = 0 \quad (4.18)$$

Upon integrating by parts we obtain

$$f_2 [E_{1x} E'_{1x}]|_{-a}^a - \int_{-a}^a \left\{ f_2 [E'_{1x}]^2 + g_2 E_{1x}^2 \right\} dy = 0 \quad (4.19)$$

In region II, f_2 and g_2 being constant, we can take them outside the integral. Thus Eq.(4.19) can be written as

$$f_2 [E_{1x} E'_{1x}] |_{-a}^a - f_2 \int_{-a}^a [E'_{1x}]^2 dy - g_2 \int_{-a}^a E_{1x}^2 dy = 0 \quad (4.20)$$

If the boundary term is absent, as in the case of an infinite homogeneous system, then Eq.(4.20) can be satisfied for a finite value of E_{1x} , provided second and third terms have opposite signs. The integrand being positive definite this is possible provided g_2 and f_2 have opposite signs. The definitions of g_2 and f_2 in terms of γ^2 are

$$f_2 = 1 + \frac{S_3^2}{\gamma^2(S_1 + \gamma^2)} - \frac{S_4}{\gamma^2}$$

$$g_2 = S_2 + \gamma^2$$

Since g_2 is positive, the only possible way for f_2 to be negative is to have S_4/γ^2 dominate over the first two terms of f_2 . Thus, the conventional Weibel gets driven by S_4 . It is also obvious that S_3 provides a stabilizing contribution making it more difficult for f_2 to become negative which is desired for Weibel destabilization.²⁸

For a finite system, an interesting thing happens when boundary contribution is retained. The boundary term $[E_{1x} E'_{1x}] |_{-a}^a$ represents the Poynting flux and is positive for the radiative flux moving outside region II. The sign of the boundary term thus gets determined by the sign of f_2 . Hence, another possibility for satisfying Eq.(4.20) with finite and positive value of first term balancing the other two negative terms exists.

It should be noted that the instability driven in this case is different from the Weibel mode as the boundary terms are responsible for it and the sign of f_2 is positive which is different from the Weibel case. Furthermore, it is interesting to observe that Equation(4.20) can be easily satisfied by the boundary contribution provided the variations in E_{1x} in the bulk is minimal as this leads to minimal (close to zero) contribution from the integrand of the second term. Thus the instability driven by the boundary term would have a preference for long scale excitation.

It is clear that for this mechanism to be operative, a finite beam with boundaries is essential. Also the radiative outward flux needs to be triggered.

We have clinched the evidences of long scale magnetic field structures that

gets generated via this new mechanism. We now show evidences of this instability through numerical simulations as well as experimental observations. PIC simulations using OSIRIS,^{46,47} PICPSI¹⁶⁵ and EPOCH¹⁶⁶ were carried out for the case of a forward beam current and a return plasma current with a slight mismatch between the two at $t = 0$. Both these conditions are realistic from the point of experiments. Care has been taken for the uncompensated current to be very weak so that the associated magnetic field initially is quite small.

4.4 Simulation and experimental details

4.4.1 Simulation details

The simulations were carried out in both 2-D and 3-D. In 3-D cylindrical beam currents of diameter $2a$ was chosen. The 2-D simulations were carried for a box size of $25c/\omega_{pe} \times 25c/\omega_{pe}$. The beam was chosen to be confined within an extent of $2a = 5c/\omega_{pe}$. The spatial resolution is taken to be 50 cells per c/ω_{pe} with 64 particles per cell which corresponds to a grid size of $\Delta x = 0.02c/\omega_{pe}$ and time step $\Delta t = 0.012\omega_{pe}^{-1}$. A small noise in terms of initial thermal velocity of $v_{th} = 0.0001397c$ in each of the two electron species has been introduced initially. Various choices of beam and background electron density have been chosen. In Fig.2, we have chosen to show the results (evolution of magnetic field as well as density) for beam electron density of $0.1n_0$ moving along \hat{x} with a proper velocity of $0.9c$ in a central region(from $y = 10c/\omega_{pe}$ to $y = 15c/\omega_{pe}$) i.e., with a transverse extent of $5c/\omega_{pe}$. In the same region, a shielding return current along $-\hat{x}$ of background electrons with density $0.9n_0$ has been taken to flow with a proper velocity of $0.1c$. Here, n_0 is the density of background ions which are at rest everywhere. In the remaining region from $y = 0$ to $10c/\omega_{pe}$ and 15 to $20 c/\omega_{pe}$ electrons and ions both with density n_0 are at rest. Thus, the plasma everywhere is neutral with electron density balancing the density of background plasma ions. In the central beam region, the beam current is slightly uncompensated by the return shielding current. We have also verified these results with other PIC codes EPOCH and PICPSI. The electromagnetic fluid simulations under LCPFCT framework has also been carried out by us to validate the above findings.

4.4.2 Experimental setup and methodology

The experiments[†] were carried out using a 20 TW Ti: Sapphire laser. The laser is capable of delivering 30fs, 800nm pulses at 10Hz. A p-polarized pump laser with 120mJ energy was focussed on an aluminium coated BK7 glass target with an $f/3$ off-axis parabola. The resulting peak intensity was $3 \times 10^{18} W/cm^2$. A second harmonic (400nm) probe pulse was time delayed with respect to the pump pulse. The intensity of probe pulse was adjusted to be $10^{11} W/cm^2$. A second harmonic probe can penetrate up to four times the critical density corresponding 800nm pump radiation.³¹ A magneto-optic Cotton-Mouton polarimetry set-up^{30,31} was utilized to spatially resolve ellipticity. The induced magnetic field is inferred from the ellipticity data.¹⁶⁷ The power spectra have been calculated as per Mondal *et. al.*³⁰ and shown to peak at the focal spot of the laser pulse right from the very beginning.

4.5 Evidences of long scale magnetic field structures

4.5.1 Simulation results

Snapshots of the evolution at various times have been depicted in Fig.(4.2) in the form of 2-D color plots for the z component of the magnetic field and the perturbed charge density respectively. From these plots, it is clearly evident that there are three distinct phases of evolution. During the first phase from $t = 0.12\omega_{pe}^{-1}$ to $t = 30\omega_{pe}^{-1}$ perturbed z component of magnetic field along \hat{z} (transverse to both flow and inhomogeneity) appear at the edges with opposite polarity. This magnetic field has no x dependence and is a function of y alone. The magnetic field perturbations are seen to grow with time and also expand in y from the edges in both the directions at the speed of light. The electron density perturbations, which also appear at the edge, on the other hand, remain confined at the edge during this phase. This first phase of the evolution thus can be characterized by the appearance of magnetic field perturbations with variations only along \hat{y} , the

[†]Performed by collaborators: Gaurab Chatterjee, Amit D. Lad, and G. Ravindra Kumar, Tata Institute of Fundamental Research, Mumbai, India

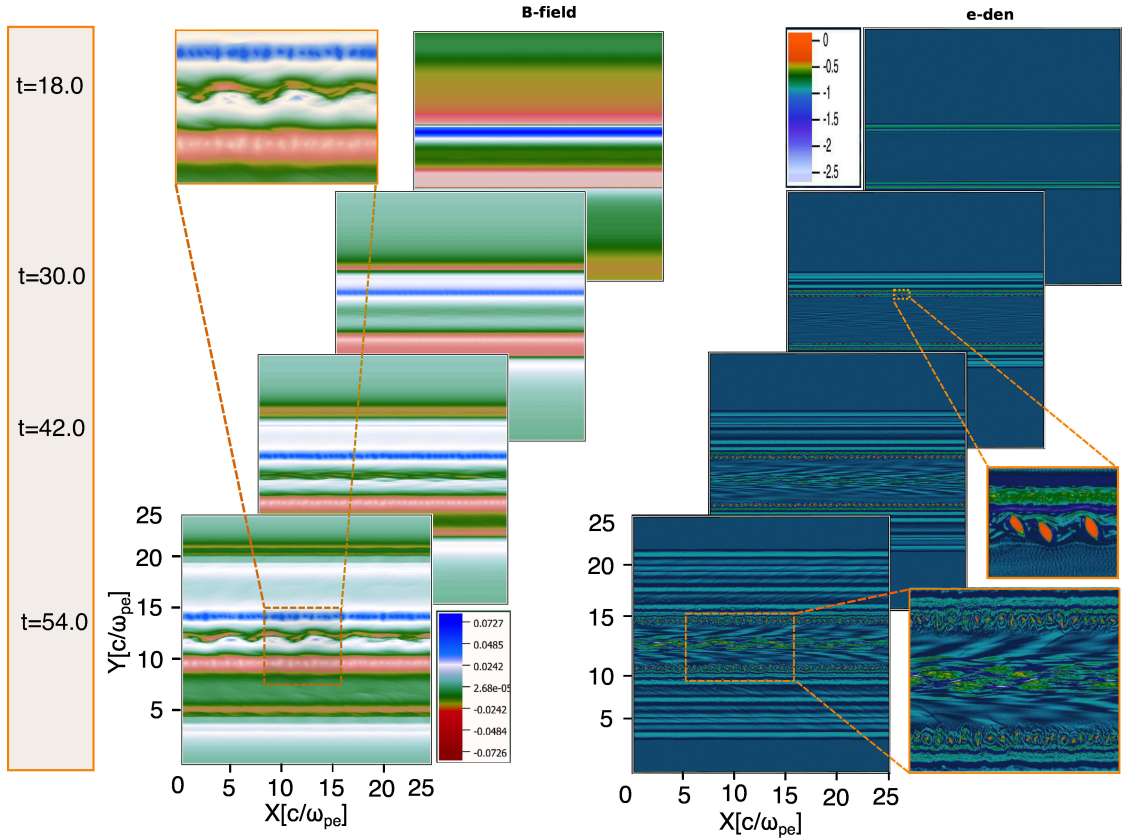


Figure 4.2: Snapshots of magnetic field B [in the units of $(mc\omega_{pe}/e)$] and electron density evolution in time t [in the unit of ω_{pe}^{-1}] for asymmetric flow configuration (*i.e.* for a finite value of S_3) has been depicted (prepared by Vapor [J. Clyne *et. al.*, *New Journal of Physics*, 9, 8, (2007); J. Clyne and M. Rast, *Electronic Imaging*, 284-295, (2005)]). Case(a) and Case(b) depicts the spatio temporal evolution of magnetic field B_z and the electron density respectively. At time $t = 18.0$, development of only long scale structures (B_z field with the opposite polarity) can be seen, at $t = 30$ KH mode at the beam edge and a faint Weibel instability in the bulk appears.

transverse direction. This fits the analytical description very well. Keeping in view that the structures do not seem to vary with respect to the x , the 1-D profiles along y have been shown in Fig.(4.3) for E_{1x} . As predicted theoretically, E_{1x} shows minimal variation inside the beam region. During the second phase from $t = 30\omega_{pe}^{-1}$ the Kelvin Helmholtz (KH) like perturbations appear at the edge of the current. Around this time one can also observe appearance of faint Weibel perturbations in the bulk central region. Both the KH and the Weibel mode have

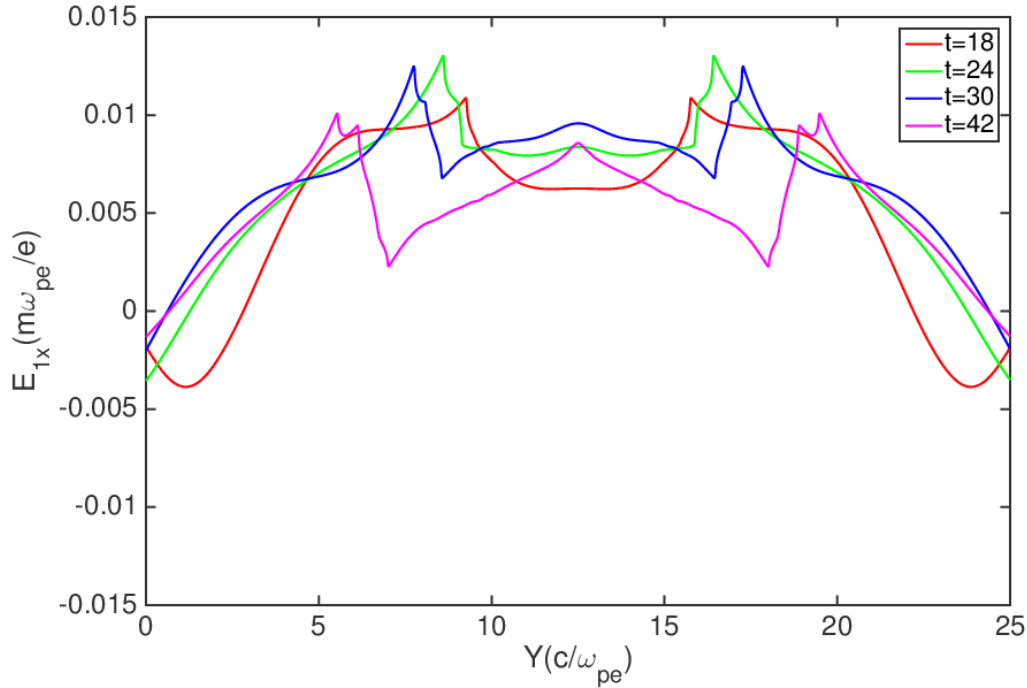


Figure 4.3: Evolution of E_{1x} profile as a function of y showing the minimal variation inside the beam region in the beginning in conformity with generation of long scale magnetic field structures.

variations along both \hat{y} and \hat{x} directions.

We have also carried out 3-D simulations and in Fig.(4.4) we show the magnetic field and density snapshot for a finite beam propagating in the plasma after a considerably later time in the simulations $t = 78.6\omega_{pe}^{-1}$ in which both long scale magnetic field and the Weibel mode can be observed. These observations with characteristics three phase developments have been repeatedly observed in both 2-D and 3-D studies from a variety of simulations carried out with different PIC as well as fluid codes.

A comparison of the evolution of the magnetic field spectra for the periodic system as well as the finite beam case has been provided at various times in Fig.(4.5). It is clear from the figure that for the periodic case the peak of spectral power appears at the electron skin depth scale initially. In this case, the spectral power only subsequently cascades towards longer scales via inverse cascade mechanism which is considerably slow. On the other hand, for the finite case, it can be clearly

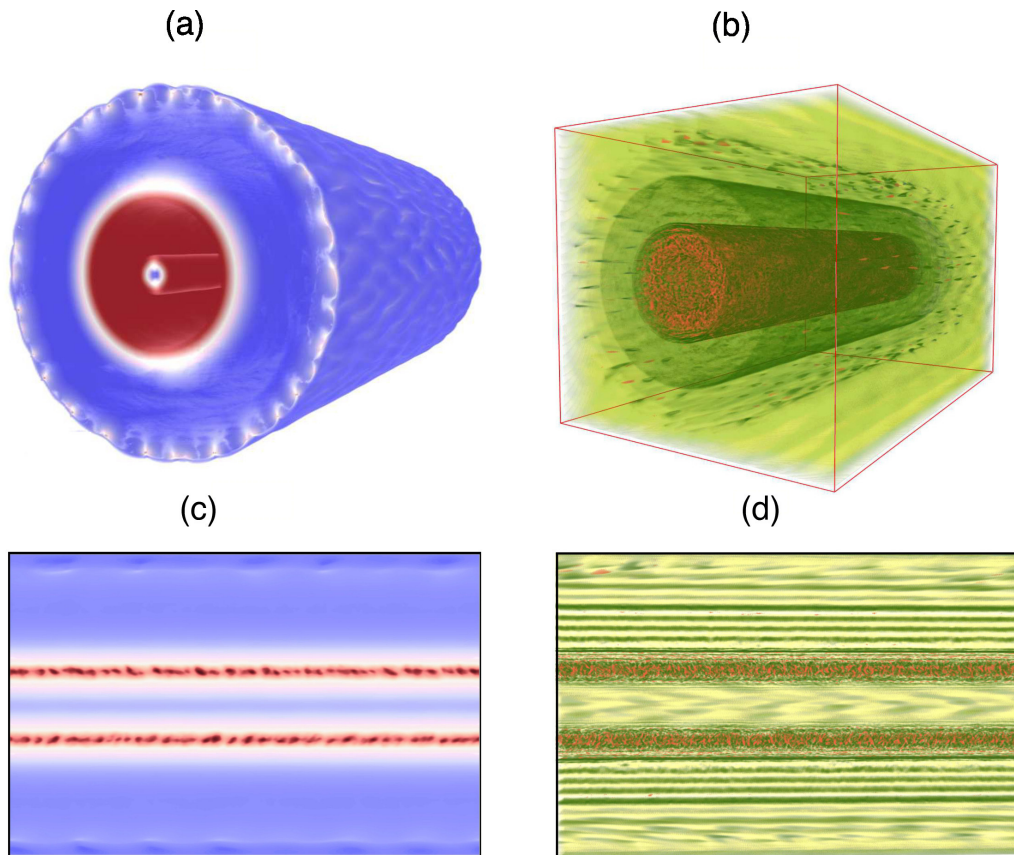


Figure 4.4: Snapshots of 3D PIC simulation with OSIRIS (prepared by Vapor [J. Clyne *et. al.*, *New Journal of Physics*, 9, 8, (2007); J. Clyne and M. Rast, *Electronic Imaging*, 284-295, (2005)]) at time $t = 78.6$ in the unit of ω_{pe}^{-1} . Subplots (a) and (b) depict 3D volume rendering of poloidal magnetic field and electron density respectively. In subplot (c) and (d) the cross sectional view in the $r - z$ plane have been shown for the magnetic field and the electron density respectively.

observed that the spectral peak appears at the beam size right from the very beginning.

4.5.2 Experimental results

In laboratory laser plasma experiments the electron beam width would always be finite, typically commensurate with the dimension of the laser focal spot. Also, there would typically be a mismatch between the forward and reverse shielding currents. Thus, evidence for finite beam instability in the laser plasma experi-

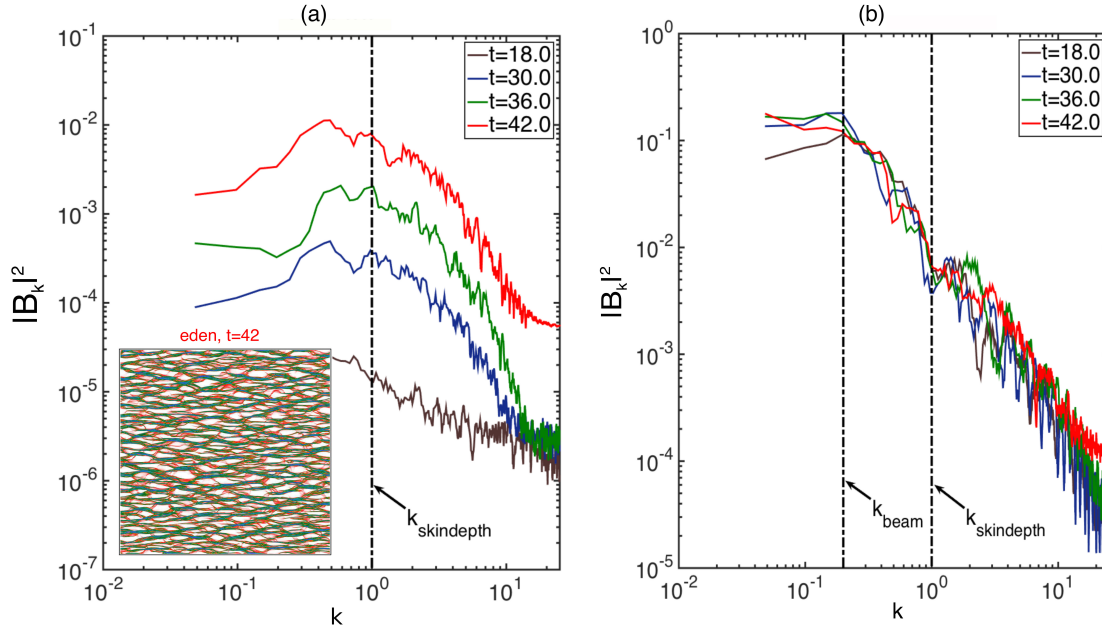


Figure 4.5: Evolution of Magnetic field spectra from PIC simulations with OSIRIS Case(a) Finite beam-plasma system was considered in simulation. The spectral maximum is at at the width of the beam right from the beginning; Case(b)-Periodic box simulations corresponding to infinite beam-plasma system where peak of the field spectra appears at the electron skin depth due to Weibel mode and the non-linear cascade towards long scale can be seen to be very slow.

ments should be apparent in experimental data. This is indeed so. The magnetic field spectra from experiments carried out at the Tata Institute of Fundamental Research have always shown to be higher at scales much longer than the electron skin depth even at very early times.^{30,31} Here in Fig.(6), we have shown a plot of magnetic field spectra at even earlier times (0.4 pico-seconds) from TIFR experiments. In this case too, the spectrum has a higher value at longer scales. The details about the experiment has been provided in method section. Thus, experiments provide yet another evidence for the existence of the long scale magnetic field structures.

The choice of a periodic beam - plasma system considered in earlier studies¹⁵⁸ is based on an inherent assumption that the boundary effects due to the finite system would merely have a small incremental impact. This assumption, however, turns out to be incorrect. We have shown with PIC as well as two-fluid simulations that

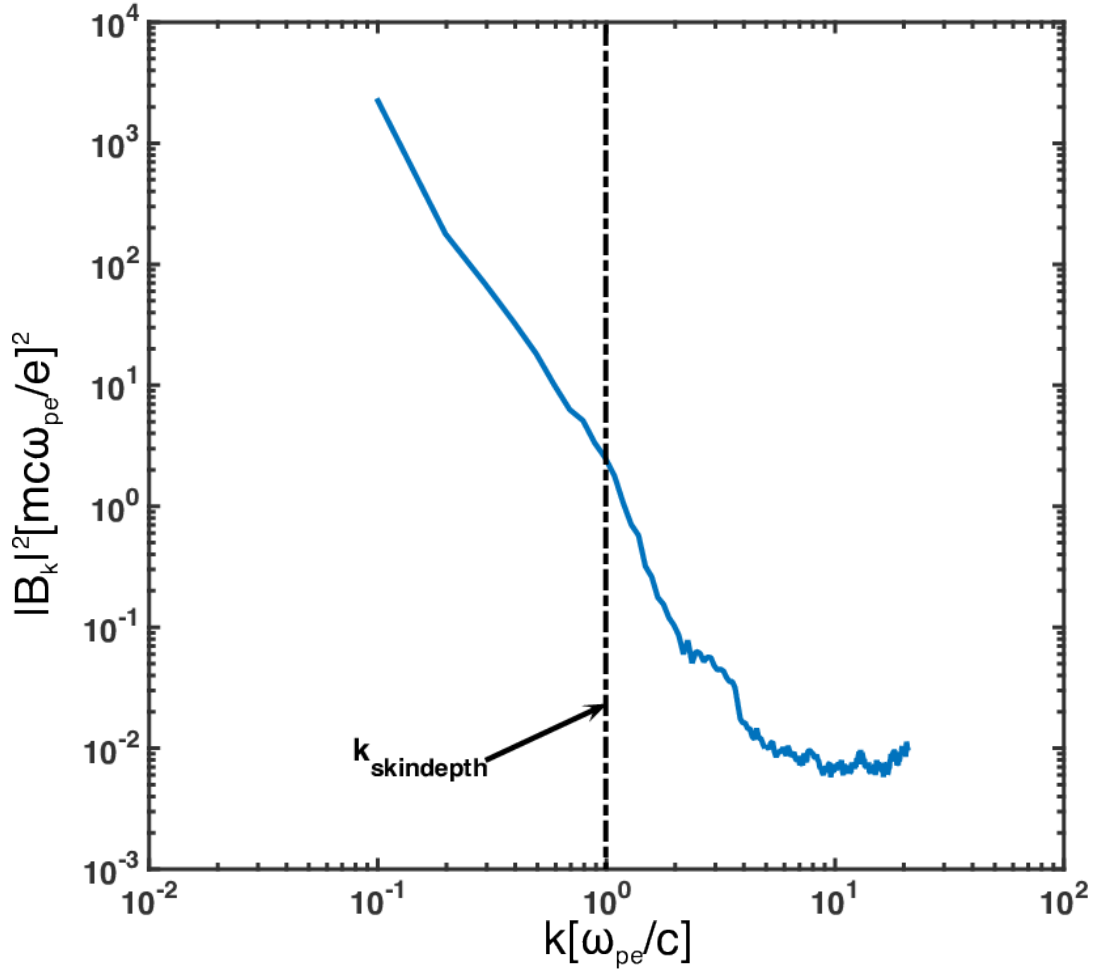


Figure 4.6: Power spectrum of magnetic field spatial profile measured at pump-probe delay of 0.4 picoseconds

when a beam with finite transverse extent is considered, an entirely new mechanism associated with the finite size of the beam appears which generates magnetic fields at the scale of the beam size right from the very beginning. Secondly, the sheared electron flow configuration at the two edges of the finite beam is seen to be susceptible to Kelvin Helmholtz instability.^{93,94} Weibel appears only in the bulk region of the beam at a later stage. Thus, there are three sources of the generation of magnetic fluctuations in a finite beam plasma system - the novel mechanism of long scale generation via radiative leakage and the KH instability operating at the edge and the usual Weibel destabilization process occurring in the bulk

region. The characteristic features of the observation in simulations (both PIC and fluid [LCPFCT¹⁶⁸]) match with the theoretical possibility of growing mode demonstrated in our analysis. Furthermore, the experimental data³⁰ where the appearance of magnetic field at the laser spot size (much larger than the skin depth) at very early stage can only be accounted by this novel mechanism. The conventional Weibel destabilization route of the beam plasma system can never account for such an effect.

4.6 Conclusion

While the KH and the Weibel modes are well known and have been discussed extensively in the literature, the FBI has neither been observed nor been described anywhere. This qualitatively new result arises because the infinite periodic approximation is unable to consider effects due to radiative leakage at the boundaries. The implications of this particular instability on magnetic field generation need to be evaluated in different contexts. For instance, it is likely that the finite size jets emanating from astrophysical objects are susceptible to this particular instability. This work also suggests that the finite size considerations in many other systems need to be looked afresh to unravel new effects which might have been overlooked so far.

Homogeneity and infinite extent are idealizations that permeate all physical models as they simplify descriptions because of the resulting uniformity and reduced dimensionality of the problem. Real systems, however, are finite and deviations from idealization can lead to novel physical effects. This lesson has been learned in a number of examples from time to time. For instance, the existence of Casimir effect^{169,170} leading to attractive force between two plates due to vacuum fluctuations, einzel lenses^{171,172} - which enables focussing of charged particles using fringing fields at capacitor edges, existence of surface plasmon modes¹⁷³ distinct from bulk modes, discrete eigen modes in wave - guides etc., are some examples of finite size boundaries leading to new effects. The present manuscript demonstrates another outstanding example in this context.

5

Direct coupling of laser to ions

The possibility of ion heating directly with short pulse, intense lasers has gained a significant interest in recent years because of their practical applications in a variety of contexts e.g. fast ignition scheme of laser fusion, proton radiography, biomedical applications etc.⁴⁴ Some of the well-known mechanisms in this regard are the RPA (Radiation Pressure Acceleration)⁵⁰ and TNSA (Target Normal Sheath Acceleration).⁵¹ In this chapter*, a new mechanism of ion heating with a p-polarized, pulsed CO_2 laser when incident normal to an over-dense plasma with sharp interface has been shown to be operative in presence of an external magneto-static field where other conventional laser absorption techniques fail to work. The external magnetic fields are chosen so as to restrict the electron motion and the heavier ions be allowed to respond to the laser electric field. The difference of electron and ion dynamics leads to charge separation and drives large amplitude ion plasma oscillations resonantly, thereby transferring the laser energy directly to heat ions (MeV). The proposed mechanism has been demonstrated by carrying out Particle-in-Cell (PIC) simulations under OSIRIS 4.0 framework using parameters for non-relativistic intensities $I = 3.46 \times 10^{14} W/cm^2$ (corresponding to $a_0 = 0.5$) of pulsed CO_2 laser for which the requirement of external magnetic field strength is smaller. Furthermore, the high power, pulsed CO_2 laser, because of its long wavelength ($10\mu m$), can deliver same energy ($I\lambda^2$) with 1/100 of laser intensity as compared to conventional solid state femtosecond lasers ($\lambda \sim 1\mu m$).

* **Atul Kumar**, Chandrasekhar Shukla, Deepa Verma, Amita Das, and Predhiman Kaw, *Plasma Phys. Control. Fusion*, in press (2018), <https://doi.org/10.1088/1361-6587/ab1408>

5.1 Introduction

The laser absorption into an overdense plasma has always been a topic of great interest because of its practical applications to fast ignition laser fusion,¹ generation of charge particle beams,^{2,3,58} bright source of X-rays^{4,59} and generation of higher order harmonics⁵ etc. The conventional methods of an intense, p-polarized laser absorption in inside an overdense plasma are vacuum heating, $\vec{J} \times \vec{B}$ heating, resonance absorption, collisional absorption etc. In collisional absorption case,^{103,104} laser energy gets coupled to plasma through collisions mostly between electrons and ions which leads to plasma heating. However, for high intensity lasers ($\sim I > 10^{15} \text{W/cm}^2$), collisional effects can be neglected.¹⁴⁷ For intense femtosecond/picosecond laser pulses, laser absorption is only possible through collisionless absorption mechanisms viz. $\vec{J} \times \vec{B}$ heating, resonance heating, vacuum heating etc. For highly intense lasers ($\sim I > 10^{18} \text{W/cm}^2$), relativistic effects becomes important. At such intensities, for a p-polarized, intense laser incident normal to a sharp vacuum plasma interface, absorption can only occur through $\vec{J} \times \vec{B}$ heating.¹⁰⁵ The laser absorption through this mechanism is typically small when non-relativistic laser intensities. In non-relativistic case, vacuum heating¹⁰⁶ is the only mechanism to couple laser energy to the collisionless, sharp interface plasma with steep density profile. In this case, a p-polarized laser is incident obliquely to a sharp interface plasma surface such that there is a component of electric field normal to the plasma surface. This normal component of electric field pulls out the electron in first half cycle of laser and sends them back inside the plasma with quiver velocity in its other half cycle. But this mechanism is not efficient when laser is incident normal to the plasma surface because of the absence any normal component of electric in this case. However, for an inhomogeneous, collisionless plasma medium, it is possible to couple laser energy to normal incident laser to plasma through resonance absorption process.^{107,174}

Laser energy is preferentially absorbed by the lighter electron species of the plasmas as they respond at the fast laser frequency. The energetic electrons thus generated are then often employed to heat ions in applications such as fast ignition etc., for creating hot spot in the plasma for ignition. This is a secondary process to heat ions and consequently somewhat inefficient. The propagation of

energetic electrons is marred by several instabilities which lead to their divergence and loss. Moreover, the Rutherford electron-ion collisional cross section to enable the transfer of energy reduces with increasing electron energy. It is thus desirable to have laser energy directly coupled to the heavier ion species. In addition there are also many other applications where ion acceleration/heating is of importance, e.g. proton radiography, biomedical applications.⁴¹⁻⁴⁴

The advantages of direct in-situ ion heating/acceleration are many. For instance, there would be (1) Efficient coupling directly to fusion species, viz. background DT species ; (2) Ions being non relativistic and total current being much less than Alfvén critical current for ions, magnetic fluctuations are expected to play negligible role in beam transport and beam stopping; (3) Classical collisional stopping of few MeV ions in dense core will be adequate; (4) Return currents, if any, will excite electrostatic ion acoustic modes leading to anomalous heating of the background plasma. Therefore, there is need to look for the possibility of new absorption mechanisms through which laser energy can directly be transferred to heavier species of plasma for efficient ion acceleration. This is the prime focus of our study here.

Some of the well-known mechanisms in this regard are the RPA (Radiation Pressure Acceleration)⁵⁰ and TNSA (Target Normal Sheath Acceleration).⁵¹ We show here the possibility of direct laser energy coupling to ions by applying an external magnetic field. The magnetic field amplitude is chosen appropriately so that the lighter electron species is magnetized at the laser frequency and its motion is severely restricted. On the other hand, the heavier ions remain unmagnetized. We choose a low frequency pulsed CO_2 laser for this task in our simulations to reduce the magnetic field requirement by a factor of 10, as compared to the conventional lasers. The other benefit of using CO_2 laser is because of its long wavelength ($10\mu m$), it can deliver same energy ($I\lambda^2$) with 1/100 of laser intensity as compared to conventional solid state femtosecond lasers ($\lambda \sim 1\mu m$). A 2-D Particle - In - Cell (PIC) simulations using OSIRIS4.0 was carried out for a CO_2 laser incident normally on an overdense plasma target. The simulations clearly show a development of charge separation leading to ion plasma oscillations. A clear enhancement of ion energy in the presence of an external magnetic field has been demonstrated. While

the special choice of CO_2 pulsed laser reduces the magnetic field requirement by a factor of 10, the short pulsed ensures that the table top set-up is adequate. With the recent advancements in building short pulse, CO_2 lasers¹⁰² and the attainment of magnetic field already of several kilo Tesla in laboratory,^{25, 54, 96–101} we believe that the experimental demonstration of our simulations are within reach in near future.

5.2 System configuration

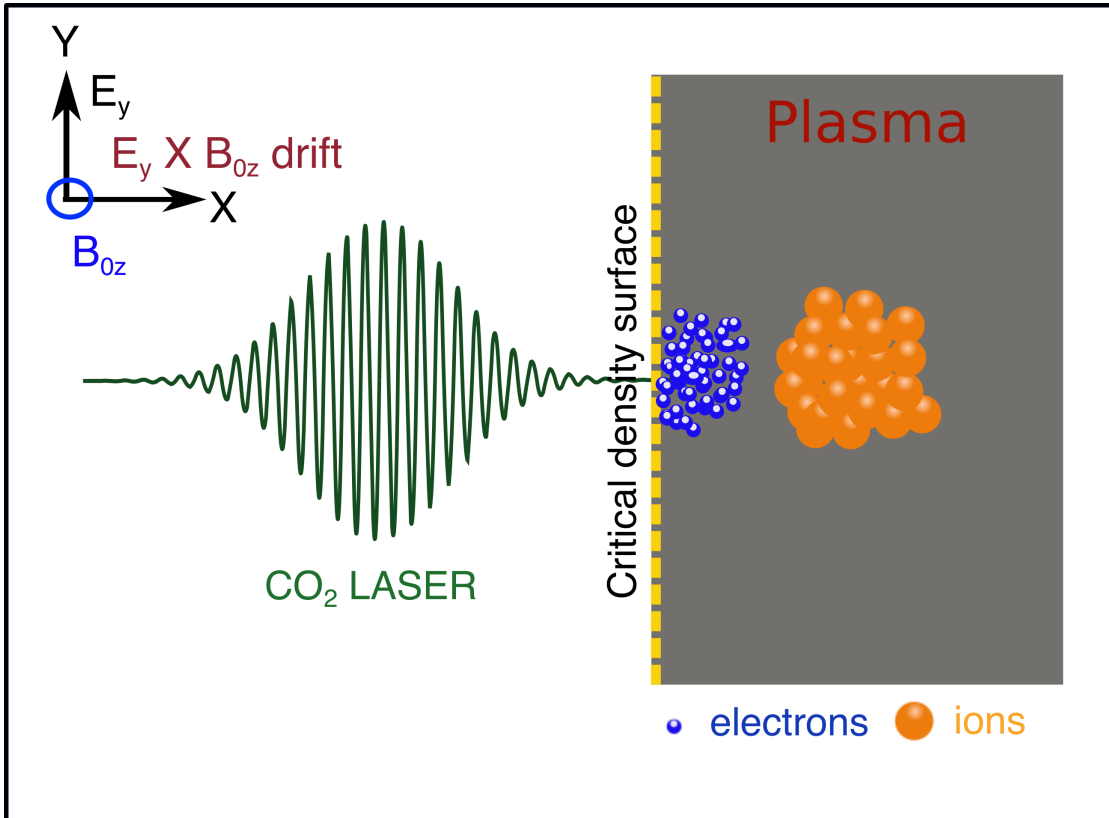


Figure 5.1: Schematic [not to the scale] representing charge separation and laser energy absorption via $\vec{E} \times \vec{B}$ drift with pulsed CO_2 laser in presence of an external magnetic field B_{0z}

In Fig.(5.1), we show the schematics of the geometry that has been used by us for the PIC simulations under OSIRIS-4.0 framework.^{46, 47, 176} The 2-D $x - y$ plane is shown in the figure. The applied magnetic field is along \hat{z} direction. We have

considered a system of electrons and ion plasma and chosen for simplicity and faster simulations, ions to be 25 times heavier than electrons (*i.e.* $m_i = 25m_e$, where m_i and m_e denotes the rest mass of the ion and electron species). For electrons to be strongly magnetized and ions to remain unmagnetized at the laser frequency, we have considered the magnetic field strength in such a fashion so as to satisfy the condition of $\omega_{ci} < \omega < \omega_{ce}$, where ω is the laser frequency and ω_{ci} and ω_{ce} are ion and electron cyclotron frequencies respectively and $\omega_{ps} = \sqrt{4\pi n_0 e^2 / m_s}$ is the plasma frequency for each species ‘s’. In particular we have chosen $\omega_{ci} = \omega/2$. The mass ratio being 25 implies $\omega_{ce} = 12.5\omega$ which also ensures that the electrons are strongly magnetized. A rectangular geometry of $1809.52 \times 30.16 \mu m^2$ (*i.e.* $6000c/\omega_{pe} \times 100c/\omega_{pe}$) in $x - y$ plane has been chosen for the simulation where plasma boundary starts from $150.79 \mu m$ (*i.e.* $500c/\omega_{pe}$). Thus there is vacuum between 0 and $150.79 \mu m$. The plasma density ($n_0 = 3.19 \times 10^{20} cm^{-3}$) is chosen such that the laser frequency $\omega = \omega_{pi}$ resonates with the ion plasma frequency. The plasma density is chosen to be at the critical ion density and $\omega_{ce} = 2.5\omega_{pe}$. Here ω_{pe} is the electron plasma frequency. The spatial resolution chosen in the simulation is 10 cells per electron skin depth ($0.3016 \mu m$) with 64 particles per cell for each species corresponding to a grid size $\Delta x = 0.03016 \mu m$ and time step $\Delta t = 0.07 fs$. The boundary conditions for electromagnetic fields and particles are periodic in \hat{y} direction and absorbing in \hat{x} direction. A p-polarized, plane X-mode CO_2 short pulse laser of wavelength $10 \mu m$, is incident from the left boundary at a sharp plasma surface at critical density along \hat{x} direction. A CO_2 laser pulse of intensity $I = 3.46 \times 10^{14} W/cm^2$ having Gaussian profile in time has been considered in the simulation with a rise and fall time of $204.6217 fs$ each (Here $1.0\omega_{pe}^{-1} \sim 1 fs$). A uniform and static external magnetic field of $B_0 = 14.13$ kilo-Tesla in transverse direction (\hat{z} direction) has been applied in the system.

5.3 Results and Analysis

It is well known that a p-polarised laser incident normally over the sharp plasma interface in an unmagnetized plasma would not be able to dump its energy to the plasma through the well known conventional mechanisms (e.g. resonance absorption,¹⁰⁷ Brunel mechanism,¹⁰⁶ $\vec{J} \times \vec{B}$ heating,¹⁰⁵ collisional absorption,^{103,104,147}

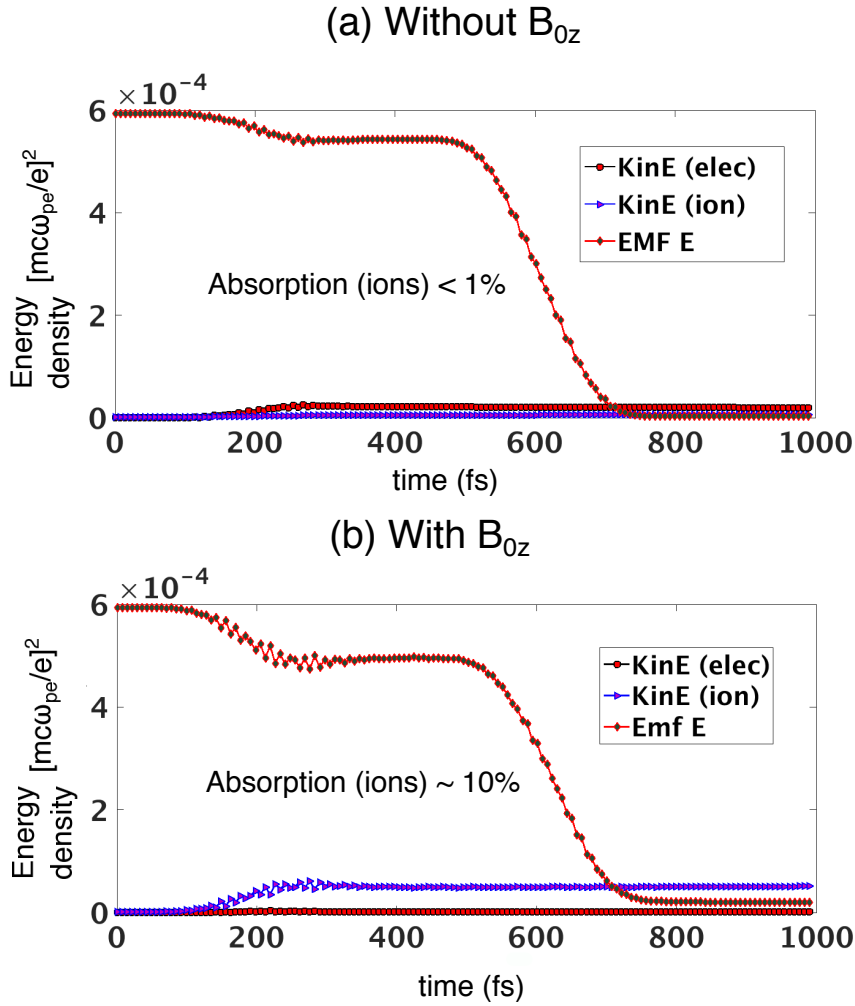


Figure 5.2: Laser energy evolution (red curve with square) and evolution of kinetic energy of plasma species viz. ions (blue solid curve with triangles) and electrons (blue solid line with red circles) via $\vec{E} \times \vec{B}$ drift with pulsed CO_2 laser in presence of an external magnetic field B_{0z}

etc.). However, when a strong magnetic field is applied so as to restrict the motion of electrons and ions be allowed to move, the laser energy has been observed to get absorbed significantly ($\sim 10\%$) to heavier species in overdense plasma with sharp interface. This has been confirmed in Fig.(5.2) where we have shown the laser energy evolution (red curve with square) of laser along with the kinetic energy evolution of plasma species viz. electrons (blue solid line with red circles) and ions (blue solid curve with triangles). It is evident from Fig.(5.2) that when there is no external magnetic field B_{0z} , the laser energy absorbed into the ions is less than

1% as expected. Electrons, in this case, take very small fraction of laser energy which less 4% and ions remains immobile. However, in presence of strong external magnetic field, the ions have gained around 10% of the laser energy at very early times. We have tabulated the above results which has been shown in Table-I.

TABLE I: Laser energy absorption into plasma species

Laser energy absorption	(a) Without B_{0z} (in %)	(b) With B_{0z} (in %)
Ions	0.97	8.34
Electrons	3.57	0.22
Electrons + ions	4.54	8.56

It is thus clear that not only the laser energy absorption has been increased in presence of the external magnetic field which ultimately leads to an irreversible transfer of the laser energy directly to ions species in plasma. Here, ions have gained significant amount of laser energy *i.e.* $\sim 10\%$ while electrons remain tied to the strong magnetic field lines. The subplots in Fig.(5.3) show the ion (red line with dots) and electron density (blue lines) profiles at two different times $t = 353.5fs$ and $t = 707fs$. The electron and ion densities for simulations carried out without the application of external magnetic field (termed as the case (a) shown in left sub-plots) and in the presence of magnetic field (termed as the case (b) shown in in right sub-plots) can be observed in the figure. The contrast between the two set of simulations is clearly evident. The space charge separation gets created in the case(b) leading to ion plasma oscillations. Furthermore, it can be observed from Fig.(5.4) that laser creates definite B field disturbances in the case (b) whereas in the case (a) such disturbances are absent. To investigate further whether this irreversible transfer of laser energy to ions is indeed cause heating, we have looked into the particle distributions in momentum space shown in Fig.(5.5) where the different circles corresponds to energy circles of $0.02MeV$ (magenta), $0.125MeV$ (green) and $0.5MeV$ (red). It is evident from Fig.(5.5) that in the case (a) when there is no external magnetic field applied in the system, the laser energy absorption by ions is negligible. The electrons acquire a tiny amount of energy which lies within the energy circle of $0.125MeV$. However, in the case (b), because

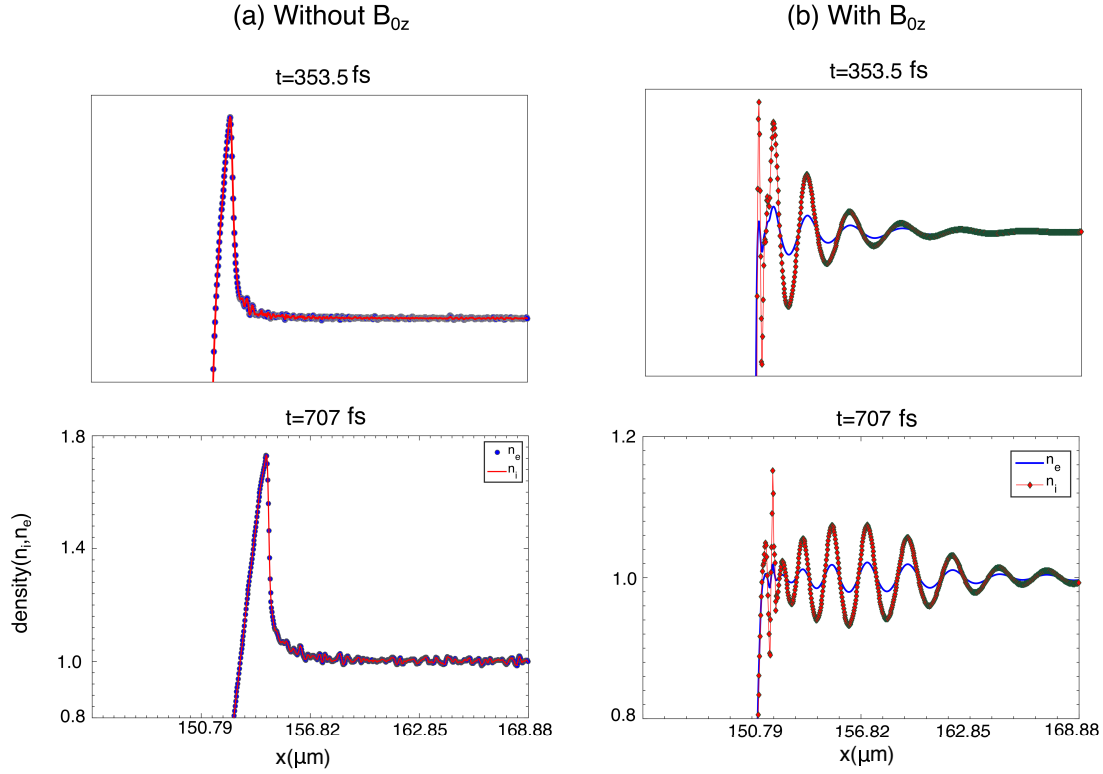


Figure 5.3: Temporal evolution of electron and ions density fluctuations with respect to x and averaged over \hat{y} direction (a) without magnetic field and (b) with magnetic field. Charge separation between two species, electrons and ions are clearly evident in right two sub-plots in presence of a transverse external magnetic field, B_{0z}

of the different $\vec{E} \times \vec{B}$ drifts of the electrons and ions, laser energy absorption by ions is significantly high and crosses well beyond the the energy circle of $0.5 MeV$. This isotropic distribution of particles in momentum space further confirms that this irreversible transfer of laser energy has caused heating in ions as shown in Fig.(ch4-fig4). This further confirmed in another diagnostics: Energy acquired by the species vs. species count as shown Fig.(5.6). Here also, the energy acquired by the ions in presence of strong magnetic field at initial stages of the simulations is very high as compared to the case when there is no magnetic field applied to the system.

Thus, it is evident from the above PIC simulation results that the presence of an external magnetic field can bind the electrons to the field lines and thereby, an irreversible and direct transfer of CO_2 laser energy (upto 10%) to heavier ion

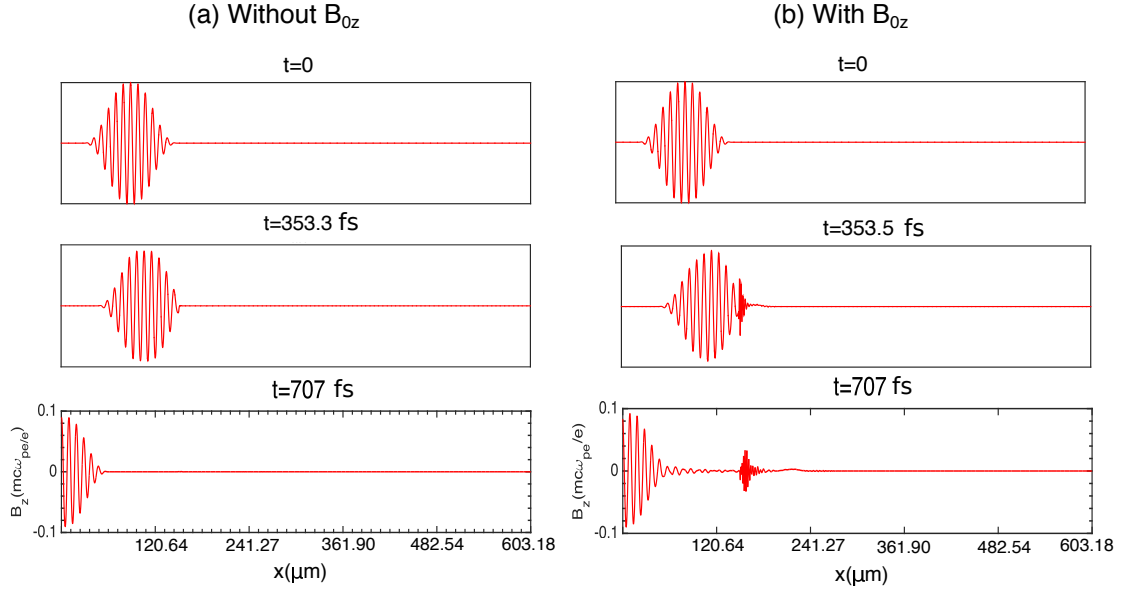


Figure 5.4: Temporal evolution of transverse magnetic field B_z with respect to x and averaged over \hat{y} direction (a) without magnetic field and (b) with magnetic field. It is obvious from the left two sub-plots that laser gets totally reflected back in absence of an external magnetic field B_{0z}

species in plasma can happen. One possible mechanism that can lead to the charge separation between the electrons and ions can be the $\vec{E} \times \vec{B}$ drift that acts differently on magnetized and unmagnetized species in plasma. Actually the presence of external magnetic field along with the condition of $\omega_{ci} < \omega < \omega_{ce}$ invokes a different $\vec{E} \times \vec{B}$ response between the two species, which is provided by

$$V_{\vec{E} \times \vec{B}, s} = \frac{\omega_{cs}^2}{\omega_{cs}^2 - \omega^2} \frac{\vec{E}(t) \times \vec{B}_0}{B_0^2} \quad (5.1)$$

The average drift for the two species is in opposite direction,¹⁷⁵ creating charge separation. Here $V_{\vec{E} \times \vec{B}, s}$ is the $\vec{E} \times \vec{B}$ drift velocities of the species 's' where 's' stands for electrons (e) and ions (i). Here \vec{B}_0 is the applied magnetic field and $\vec{E}(t)$ is the laser electric field. Also ω_{cs} is the gyro-frequency of the species $s = [i, e]$ and ω is the laser frequency. The charge separation thus created triggers can further leads to ion plasma oscillations in the system and can give rise to a new absorption mechanism wherein the laser energy can be also directly coupled to ions. However, this needs to be investigated further in detail.

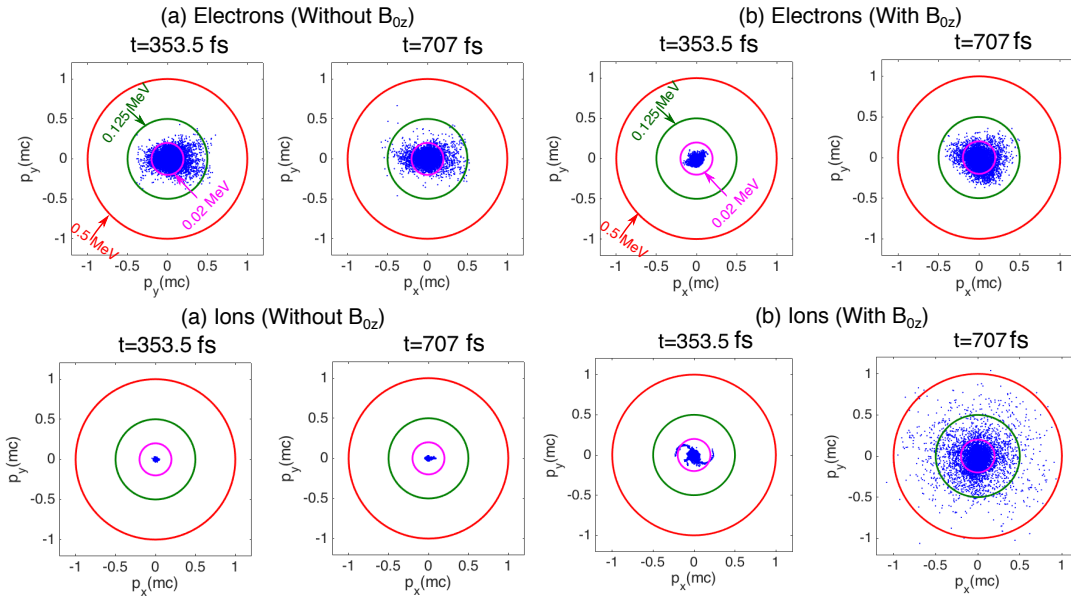


Figure 5.5: Temporal evolution of particles (electrons and ions) distributions in momentum species (a) without a magnetic field and (b) with magnetic field. It is obvious from the left two sub-plots that laser energy does not get absorbed by ions when there is no any external magnetic field B_{0z} and a slight heating in electrons is observed. However, in presence of a transverse external magnetic field, laser energy gets coupled to heavier ion species in the plasma, leading to a significant heating in ion species.

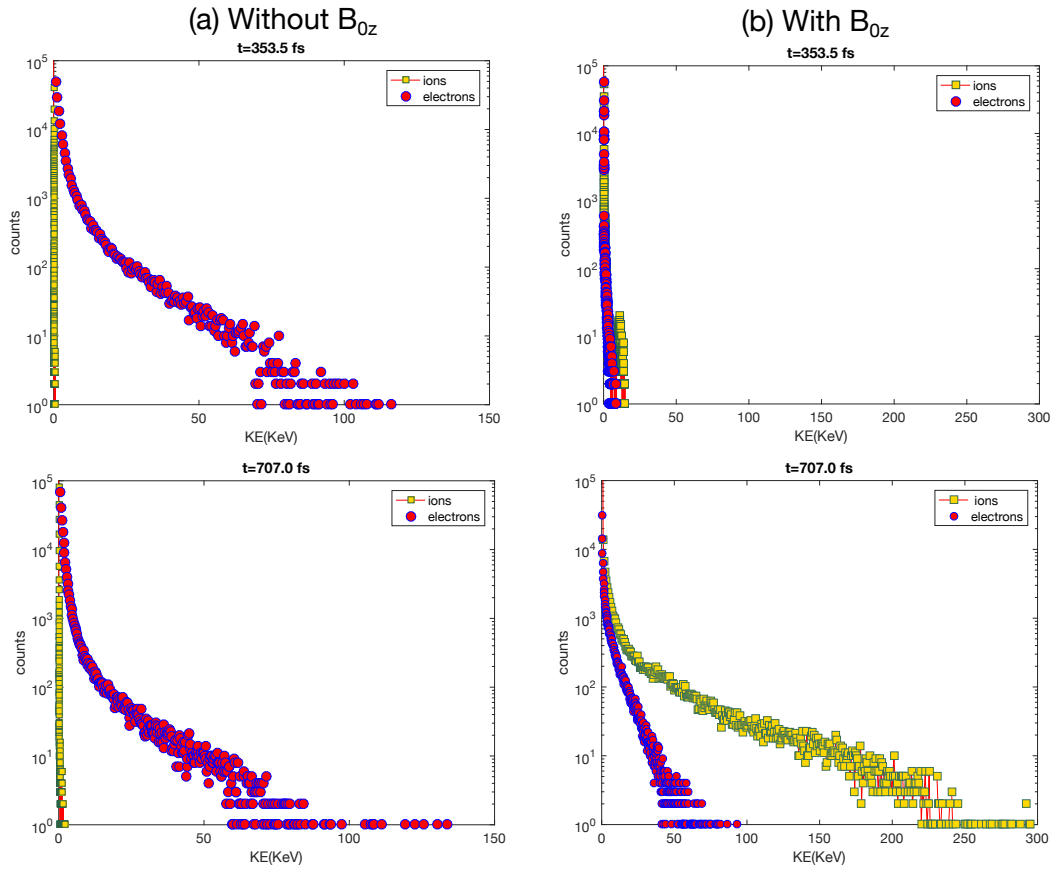


Figure 5.6: Temporal evolution of electrons and ions count from the simulation showing that the ions are accelerated significantly whereas the electrons motion is restricted when there is an applied external magnetic field in the system

5.4 Conclusions

In conclusion, we would like to state that CO_2 lasers till now have been considered as efficient industrial lasers in the market for continuous wave (CW) and relatively long pulse applications.^{86,177,178} The short pulse CO_2 lasers are now available¹⁰² but still they have not been as widely explored in the sub-nano or pico second domain. We demonstrate, with the help of PIC simulations, here as well as in a series of papers,¹⁷⁴ the immense possibilities that short pulse CO_2 lasers offer for physics explorations. In particular, here we have demonstrated the possibility of directly coupling of laser energy to the heavier ion species in the presence of an ambient magnetic field. We have, thereby, explored the ion dynamics dominated phenomena. The ion plasma oscillations were observed. Furthermore, ion heating up to $0.5MeV$ has been observed also.

6

Direct coupling of laser to ions: Magnetosonic excitations

In previous chapter, we proposed a new absorption technique through which laser energy ($3.46 \times 10^{14} W cm^{-2} \mu m^2$) even in non relativistic range where other conventional absorption techniques fail to work, can be directly coupled to heavier ion species in plasma. Ion plasma oscillations have also been shown to be excited via this new absorption technique. In this chapter *, it has been shown that at higher amplitude, the ion disturbances form magnetosonic solitons. A 2-D Particle - In - Cell (PIC) simulations for an incident laser beam normal to an overdense plasma target in the presence of an external magnetic field has been carried out. The external magnetic field has to be chosen such that the heavier ions remain unmagnetized but the lighter electron species get magnetized at the laser frequency. For conventional lasers of $\sim 1 \mu m$ wavelengths, the magnetic field requirement satisfying the aforementioned condition turns out to be of the order of several hundreds of kilo Tesla. This requirement goes down by one order if pulsed CO_2 lasers with wavelengths of $\sim 10 \mu m$ are employed. At present magnetic fields of several kilo Tesla have already been generated in the laboratory. It is thus only a matter of time when a factor of 10 enhancement in the magnetic field will bring the parameters in the right regime for experiments to test the new mechanism put forth here with pulsed CO_2 lasers. Keeping this in view, the simulations have been carried out for the pulsed CO_2 laser parameters with intensity $I = 7 \times 10^{17} W/cm^2$ (corre-

* **Atul Kumar**, Chandrasekhar Shukla, Deepa Verma, Amita Das, and Predhiman Kaw, *Plasma Phys. Control. Fusion*, in press (2018), <https://doi.org/10.1088/1361-6587/ab1408>

sponding to $a_0 = 7.0$ *i.e.* for relativistic laser intensities). The high power, pulsed CO_2 laser, because of its long wavelength ($10\mu m$), can deliver same energy ($I\lambda^2$) with 1/100 of laser intensity as compared to conventional solid state femtosecond lasers ($\lambda \sim 1\mu m$). For the choice of this laser intensity, it has been shown that the relativistic $\vec{J} \times \vec{B}$ absorption gets enhanced due to the $\vec{E} \times \vec{B}$ drift of the plasma species. Furthermore, it is shown that at a higher intensity of the laser, the ion disturbances acquire higher amplitude to excite Korteweg - de Vries (KdV) magnetosonic solitons. The solitons, as expected, propagate stably for several thousands of ion plasma periods. However, subsequently, they are seen to develop transverse modulations which grow with time.

6.1 Introduction

In general the conventional short pulse lasers are known to interact with the lighter electron species of the plasma. Therefore, the laser energy absorption through various mechanisms (resonance absorption,¹⁰⁷ Brunel mechanism,¹⁰⁶ $\vec{J} \times \vec{B}$ heating,¹⁰⁵ collisional absorption,^{103,104,147} etc.) transfer energy to electrons. The plasma modes excited by lasers are thus also typically dominated by electron dynamics, wherein ions merely play the role of a stationary neutralizing background. The energy transfer, if any to ions, occurs later and is mediated by the electrons. We show here the possibility of direct laser energy coupling to ions by applying an external magnetic field. The magnetic field amplitude is chosen appropriately so that the lighter electron species is magnetized at the laser frequency and its motion is severely restricted. On the other hand, the heavier ions remain unmagnetized. We choose a low frequency pulsed CO_2 laser for this task in our simulations to reduce the magnetic field requirement by a factor of 10, as compared to the conventional lasers. The other benefit of using CO_2 laser is because of its long wavelength ($10\mu m$), it can deliver same energy ($I\lambda^2$) with 1/100 of laser intensity as compared to conventional solid state femtosecond lasers ($\lambda \sim 1\mu m$). A 2-D Particle - In-Cell (PIC) simulations using OSIRIS4.0 was carried out for a CO_2 laser incident normally on an overdense plasma target. In the previous chapter, Ch.(5), development of charge separation leading to ion plasma oscillations has been shown in detail. A clear enhancement of ion energy in the presence of an external magnetic

field has been demonstrated. Furthermore, when the laser intensity is increased, ion plasma disturbances become nonlinear and the formation of a series coherent structures has been observed. It is shown in this chapter that these structures are essentially the KdV Magnetosonic solitons.

The solitons are nonlinear coherent structures and are well known for their robustness and the characteristic property of preserving their shape as they propagate in any medium. The generation of soliton in plasma and their role in formation of collisionless shock waves have attracted a significant amount of interest in recent years in a variety of contexts like astrophysics,^{179–183} solar and space physics,^{184,185} laboratory plasma experiments^{186–188} etc. They play a key role in charged particle acceleration and plasma heating.^{182,189–194} In the presence of an external magnetic field, soliton propagation with magnetosonic/Alfvén speed in plasma have been predicted. They are termed as magnetosonic solitons.^{195–197} Such structures have been observed in the Earth’s magnetosphere by cluster space crafts¹⁹⁸ etc. They are also believed to be present in pulsar wind, neutral star and the core of active galactic nuclei where the propagation speed is often relativistic.^{199,200} A number of studies in the context of short pulse lasers interacting with plasmas in laboratories have shown the formation of coherent solitonic structures involving electron species only as in these cases the laser usually interacts directly with the lighter electron species. In astrophysical context, however, the ion involvement is dominant. Often the question is posed about the possibility of utilizing short pulse lasers for replicating astrophysical phenomena. Here we illustrate the possibility of observing KdV solitons with such short pulse lasers.

Our studies illustrate that it is possible to excite linear oscillation as well as nonlinear solitonic structure, both dominated by the dynamics of the heavier ion species. This has been achieved by applying an external magnetic field of appropriate magnitude wherein the lighter electron species gets magnetized and the heavier ion component remains unmagnetized at the laser frequency. In our simulations we employ short pulse CO_2 lasers. While the special choice of CO_2 pulsed laser reduces the magnetic field requirement by a factor of 10, the short pulsed ensures that the table top setup is adequate. With the recent advancements in building short pulse, CO_2 lasers¹⁰² and the attainment of magnetic field already of several kilo Tesla in laboratory,^{25,54,96–101} we believe that the experimental demonstration of our simulations are within reach in near future.

6.2 Thoery of magnetosonic soliton in a cold plasma

The solitons are coherent solutions of nonlinear equations like Korteweg-de-Vries²⁰¹ equation, Klein-Gordon equation,²⁰² nonlinear Schrodinger equation etc.^{203,204} The MS solitons are the KdV solitons²⁰¹ which propagates with the magnetosonic speed perpendicular to the external magnetic field. Here, we have considered a 2D system consisting of electrons and ions. A strong magnetic field B_0 has been applied along \hat{z} direction such that electrons are strongly magnetized while ions still remain unmagnetized. The wave vector \vec{k} of the p-polarized, X-mode CO_2 laser is considered along \hat{x} direction (*i.e.* wave vector of laser, $\vec{k} = k\hat{x}$ and $\partial/\partial y = \partial/\partial z = 0$). Under these assumptions, continuity equation can be written as:

$$\frac{\partial}{\partial t}n_s + \frac{\partial}{\partial x}(n_s v_{sx}) = 0 \quad (6.1)$$

The momentum equation for each species in in \hat{x} and \hat{y} direction is expressed as:

$$m_s \left(\frac{\partial}{\partial t} + v_{sx} \frac{\partial}{\partial x} \right) v_{sx} = q_s (E_x + v_{sy} B_z) \quad (6.2)$$

$$m_s \left(\frac{\partial}{\partial t} + v_{sx} \frac{\partial}{\partial x} \right) v_{sy} = q_s (E_y - v_{sx} B_z) \quad (6.3)$$

Similarly, Faraday's law and Amperes's law for an electromagnetic wave can also be written as:

$$\frac{\partial}{\partial t} B_z = -\frac{\partial}{\partial x} E_y \quad (6.4)$$

$$\frac{\partial}{\partial x} B_z = -\frac{4\pi}{c} \sum_{s=e,i} (n_s v_{sy}) \quad (6.5)$$

Here, subscript 's' stands for electron and ion species, q_s and m_s is the charge and mass of each species respectively, v_{sx} and v_{sy} represents the velocities of each species in \hat{x} and \hat{y} directions respectively. Similarly, E_x and E_y are the perturbed electric fields in \hat{x} and \hat{y} directions respectively, and B_z is the perturbed magnetic field in \hat{z} direction. We use the normalizations, $x = \frac{x}{c/\omega_{pe}}$, $t = \frac{t}{c/v_A \omega_{pe}}$, $v_{s\alpha} = v_{s\alpha}/v_A$, $n = \frac{n}{n_0}$, $B_z = B_z/B_0$ and $E_\alpha = \frac{E_\alpha}{(v_A B_0)}$ where α stands for \hat{x} and \hat{y} directions, $v_A = \omega_{ci}/\omega_{pi}c$ is the Alfven velocity with $\omega_{ci} = eB_0/m_i c$ is the ion cyclotron frequency, $\omega_{ps} = \sqrt{4\pi n_0 e^2/m_s}$ is the plasma frequency for each species. Eqs. (6.1,

6.2, 6.3, 6.12 and 6.13) can then be solved using reductive-perturbative method²⁰⁵ using the above normalization can be written as follows:

$$\frac{\partial}{\partial t} n_e + \frac{\partial}{\partial x} (n_e v_{ex}) = 0 \quad (6.6)$$

$$\frac{\partial}{\partial t} n_i + \frac{\partial}{\partial x} (n_i v_{ix}) = 0 \quad (6.7)$$

$$\left(\frac{\partial}{\partial t} + v_{ex} \frac{\partial}{\partial x} \right) v_{ex} = -\eta^{-1} (E_x + v_{ey} B_z) \quad (6.8)$$

$$\left(\frac{\partial}{\partial t} + v_{ix} \frac{\partial}{\partial x} \right) v_{ex} = \eta (E_x + v_{iy} B_z) \quad (6.9)$$

$$\left(\frac{\partial}{\partial t} + v_{ey} \frac{\partial}{\partial x} \right) v_{ey} = -\eta^{-1} (E_y - v_{ey} B_z) \quad (6.10)$$

$$\left(\frac{\partial}{\partial t} + v_{iy} \frac{\partial}{\partial x} \right) v_{iy} = \eta (E_y - v_{iy} B_z) \quad (6.11)$$

$$\frac{\partial}{\partial t} B_z = -\frac{\partial}{\partial x} E_y \quad (6.12)$$

$$\frac{\partial}{\partial x} B_z = -\eta (n_i v_{iy} - n_e v_{ey}) \quad (6.13)$$

with $\eta = (m_e/m_i)^{1/2}$ the square root of the mass ratio. We now use transformed coordinates

$$\xi = \epsilon^{1/2} (x - t) \quad (6.14)$$

$$\tau = \epsilon^{3/2} t \quad (6.15)$$

such that

$$\frac{\partial(\cdot)}{\partial x} \rightarrow \epsilon^{1/2} \frac{\partial(\cdot)}{\partial \xi} \quad (6.16)$$

$$\frac{\partial(\cdot)}{\partial t} \rightarrow -\epsilon^{1/2} \frac{\partial(\cdot)}{\partial \xi} + \epsilon^{3/2} \frac{\partial(\cdot)}{\partial \tau} \quad (6.17)$$

Using the above transformtions, we can expand the plasma variables as,

$$B_z = 1 + \epsilon B_{1z} + \epsilon^2 B_{2z} + \dots \quad (6.18)$$

$$n_i = 1 + \epsilon n_{1i} + \epsilon^2 n_{2i} + \dots \quad (6.19)$$

$$n_e = 1 + \epsilon n_{1e} + \epsilon^2 n_{2e} + \dots \quad (6.20)$$

$$v_{ex} = 1 + \epsilon v_{1ex} + \epsilon^2 v_{2ex} + \dots \quad (6.21)$$

$$v_{ix} = 1 + \epsilon v_{1ix} + \epsilon^2 v_{2ix} + \dots \quad (6.22)$$

$$E_y = 1 + \epsilon E_{1y} + \epsilon^2 E_{2y} + \dots \quad (6.23)$$

$$E_x = \eta^{-1}(\epsilon^{3/2} E_{1x} + \epsilon^{5/2} E_{2x} + \dots) \quad (6.24)$$

$$v_{ey} = \eta^{-1}(\epsilon^{3/2} v_{1ey} + \epsilon^{5/2} v_{2ey} + \dots) \quad (6.25)$$

$$v_{iy} = \eta^{-1}(\epsilon^{3/2} v_{1iy} + \epsilon^{5/2} v_{2iy} + \dots) \quad (6.26)$$

Substituting the above equations 6.18 - 6.26 into equations 6.6 - 6.13, we obtain:

$$\epsilon^{3/2} \left[-\frac{\partial n_{1e}}{\partial \xi} + \frac{\partial v_{1ex}}{\partial \xi} \right] + \epsilon^{5/2} \left[-\frac{\partial n_{2e}}{\partial \xi} + \frac{\partial n_{1e}}{\partial \tau} + \frac{\partial v_{2ex}}{\partial \xi} + \frac{n_{1e} v_{1ex}}{\partial \xi} \right] + \dots = 0 \quad (6.27)$$

$$\epsilon^{3/2} \left[-\frac{\partial n_{1i}}{\partial \xi} + \frac{\partial v_{1ix}}{\partial \xi} \right] + \epsilon^{5/2} \left[-\frac{\partial n_{2i}}{\partial \xi} + \frac{\partial n_{1i}}{\partial \tau} + \frac{\partial v_{2ix}}{\partial \xi} + \frac{n_{1i} v_{1ex}}{\partial \xi} \right] + \dots = 0 \quad (6.28)$$

$$\eta^{-2} \epsilon^{3/2} [E_{1x} + v_{1ey}] + \eta^{-2} \epsilon^{5/2} [E_{2x} + v_{2ey} + v_{1ey} B_{1z}] + \dots = 0 \quad (6.29)$$

$$\begin{aligned} \epsilon^{3/2} \left[\frac{\partial v_{1ix}}{\partial \xi} + E_{1x} + v_{1iy} \right] + \left[\frac{\partial v_{2ix}}{\partial \xi} - \frac{\partial v_{1ix}}{\partial \tau} - v_{1ix} \frac{\partial v_{1ix}}{\partial \xi} + E_{2x} + v_{2iy} + v_{1iy} B_{1z} \right] \\ + \dots = 0 \end{aligned} \quad (6.30)$$

$$\eta^{-1} \epsilon [E_{1y} - v_{1ex}] + \eta^{-1} \epsilon^2 \left[\frac{\partial v_{1ey}}{\partial \xi} + E_{2y} - v_{2ex} - v_{1ex} B_{1z} \right] + \dots = 0 \quad (6.31)$$

$$\begin{aligned} \eta^{-1} \epsilon^2 \frac{\partial v_{1iy}}{\partial \xi} + \eta^{-1} \epsilon^3 \left[\frac{v_{2iy}}{\partial \xi} - \frac{\partial v_{1iy}}{\partial \tau} - v_{1ix} \frac{\partial v_{1iy}}{\partial \xi} \right] + \eta \epsilon [E_{1y} - v_{1ix}] \\ + \eta \epsilon^2 [E_{2y} - v_{2ix} - v_{1ix} B_{1z}] + \dots = 0 \end{aligned} \quad (6.32)$$

$$\epsilon^{3/2} \left[-\frac{\partial B_{1z}}{\partial \xi} + \frac{\partial E_{1y}}{\partial \xi} \right] + \epsilon^{5/2} \left[-\frac{\partial B_{2z}}{\partial \xi} + \frac{\partial B_{1z}}{\partial \tau} + \frac{\partial E_{2y}}{\partial \xi} \right] + \dots = 0 \quad (6.33)$$

$$\epsilon^{3/2} \left[\frac{\partial B_{1z}}{\partial \xi} + v_{1ix} - v_{1ex} \right] + \epsilon^{5/2} \left[\frac{B_{2z}}{\partial \xi} + n_{1i} v_{1ix} - n_{1e} v_{1ex} + v_{2ix} - v_{1ex} \right] + \dots = 0 \quad (6.34)$$

It is evident from the lowest order terms in Eqs. (6.27- 6.34) that $n_{1e} = v_{1ex} = E_{1y} = B_{1z}$ and $n_{1i} = v_{1ix}$. Furthermore, for $\eta \ll \epsilon \ll 1$ for lowest order terms in

Eqs. (6.27- 6.34), we obtain:

$$v_{1iy} = 0 \quad (6.35)$$

$$v_{1ix} = B_{1z} \quad (6.36)$$

$$v_{1ey} = -E_x = \frac{\partial B_{1z}}{\partial \xi} \quad (6.37)$$

The ϵ and ϵ^2 terms in the expansion of Ampere's law along the x direction gives $v_{1ex} = v_{1ix}$ and $v_{2ex} = v_{2ix}$. Substituting these results into the $\mathcal{O}(\epsilon^{5/2})$ term of Eq.(6.30) yeilds:

$$\frac{B_{1z}}{\partial \tau} - \frac{\partial v_{2ex}}{\partial \xi} + \frac{1}{2} \frac{\partial (B_{1z})^2}{\partial \xi} - E_{2x} = 0 \quad (6.38)$$

Eqs.(6.38), together with the $\mathcal{O}(\eta^{-2}\epsilon^{5/2})$ terms in Eq.(6.29), the $\mathcal{O}(\eta^{-1}\epsilon^2)$ term is Eq.(6.31), the $\mathcal{O}(\epsilon^{5/2})$ term in Eq.(6.33) and, the $\mathcal{O}(\epsilon^{5/2})$ term in Eq.(6.34) are then used to eliminate second order coefficients v_{2ex} , v_{2ey} , E_{2x} , E_{2y} and B_{2z} to obtain the evolution equation for B_{1z} which has a KdV form for the perturbed magnetic field along \hat{z} -direction,

$$\frac{\partial B_{1z}}{\partial t} + \frac{3}{2} B_{1z} \frac{\partial B_{1z}}{\partial \xi} + \frac{1}{2} \frac{\partial^3 B_{1z}}{\partial \xi^3} = 0 \quad (6.39)$$

The general solution to the Eq.(6.39) can also be written as:

$$B_{1z} = \epsilon \operatorname{sech}^2 \left[\frac{\sqrt{\epsilon}}{2} \left(\xi - \frac{\epsilon}{2} \tau \right) \right] \quad (6.40)$$

Similarly, the electric fields E_x (electrostatic component) and E_y (electromagnetic component) can be expressed as:

$$\begin{aligned} E_x &= (m_e/m_i)^{-1} \left[\epsilon^{3/2} \operatorname{sech}^2 \left(\frac{\sqrt{\epsilon}}{2} [x - t(1 - \epsilon/2)] \right) \right. \\ &\quad \left. \times \tanh \left(\frac{\sqrt{\epsilon}}{2} [x - t(1 - \epsilon/2)] \right) \right] + \mathcal{O}(\epsilon^{5/2}) \end{aligned} \quad (6.41)$$

$$E_y = \epsilon \operatorname{sech}^2 \left(\frac{\sqrt{\epsilon}}{2} [x - t(1 - \epsilon/2)] \right) + \mathcal{O}(\epsilon^2) \quad (6.42)$$

Furthermore, these magnetosonic solitons are quasi-neutral with $n_e \sim n_i$, both

having the secant hyperbolic profile in space and can be expressed as:

$$n = n_e = n_i = 1 + \epsilon \operatorname{sech}^2\left(\frac{\sqrt{\epsilon}}{2}[x - t(1 - \epsilon/2)]\right) + \mathcal{O}(\epsilon^2) \quad (6.43)$$

These structures propagate typically with the Alfvén speed v_A in cold magnetized plasma case as can be seen by writing the solution Eq.(6.39) in dimensionless form.

$$n(x, t) = n_0 \left[1 + \epsilon \operatorname{sech}^2\left(\frac{\omega_{pe}}{2c} \sqrt{\epsilon}[x - v_A t(1 - \epsilon/2)]\right) + \mathcal{O}(\epsilon^2) \right] \quad (6.44)$$

6.3 System configuration

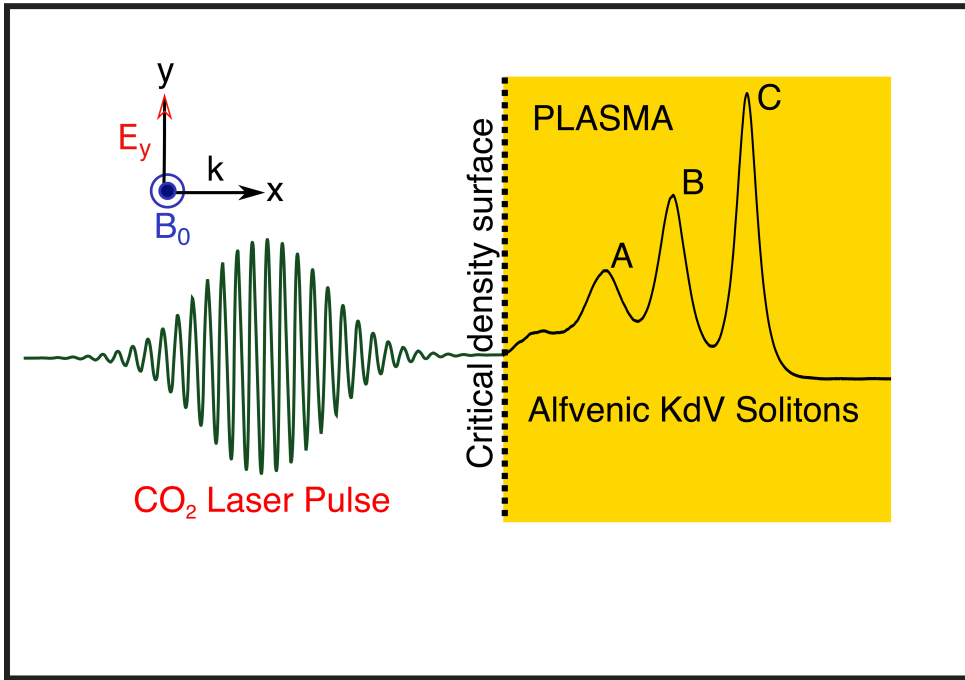


Figure 6.1: Schematic (not to the scale) which shows the system configuration for the excitation of magnetosonic KdV solitons with pulsed CO_2 laser in presence of an external magnetic field B_{0z}

In Fig.(6.1), we show the schematics of the geometry that has been used by us for the PIC simulations under OSIRIS-4.0 framework.^{46,47,176} The 2-D $x - y$ plane is shown in the figure. The applied magnetic field is along \hat{z} direction. We have

considered a system of electrons and ion plasma and chosen for simplicity and faster simulations, ions to be 25 times heavier than electrons (*i.e.* $m_i = 25m_e$, where m_i and m_e denotes the rest mass of the ion and electron species). For electrons to be strongly magnetized and ions to remain unmagnetized at the laser frequency, we have considered the magnetic field strength in such a fashion so as to satisfy the condition of $\omega_{ci} < \omega < \omega_{ce}$, where ω is the laser frequency and ω_{ci} and ω_{ce} are ion and electron cyclotron frequencies respectively and $\omega_{ps} = \sqrt{4\pi n_0 e^2 / m_s}$ is the plasma frequency for each species 's'. In particular we have chosen $\omega_{ci} = \omega/2$. The mass ratio being 25 implies $\omega_{ce} = 12.5\omega$ which also ensures that the electrons are strongly magnetized. A rectangular geometry of $1809.52 \times 30.16\mu m^2$ (*i.e.* $6000c/\omega_{pe} \times 100c/\omega_{pe}$) in $x - y$ plane has been chosen for the simulation where plasma boundary starts from $150.79\mu m$ (*i.e.* $500c/\omega_{pe}$). Thus there is vacuum between 0 and $150.79\mu m$. The plasma density ($n_0 = 3.19 \times 10^{20} cm^{-3}$) is chosen such that the laser frequency $\omega = \omega_{pi}$ resonates with the ion plasma frequency. The plasma density is chosen to be at the critical ion density and $\omega_{ce} = 2.5\omega_{pe}$. Here ω_{pe} is the electron plasma frequency. The spatial resolution chosen in the simulation is 10 cells per electron skin depth ($0.3016\mu m$) with 64 particles per cell for each species corresponding to a grid size $\Delta x = 0.03016\mu m$ and time step $\Delta t = 0.07fs$. The boundary conditions for electromagnetic fields and particles are periodic in \hat{y} direction and absorbing in \hat{x} direction. A p-polarized, plane X-mode CO_2 short pulse laser of wavelength $10\mu m$, is incident from the left boundary at a sharp plasma surface at critical density along \hat{x} direction. A CO_2 laser pulse with a higher intensity, $I = 7.0 \times 10^{17} W/cm^2$ having gaussian profile in time has been considered in the simulation with a rise and fall time of $204.6217fs$ each (Here $1.0\omega_{pe}^{-1} \sim 1fs$). A uniform and static external magnetic field of $B_0 = 14.13$ kilo-Tesla in transverse direction (\hat{z} direction) has been applied in the system.

6.4 Results and analysis

When the intensity of laser is increased *e.g.* for a choice of intensity, $I = 7 \times 10^{17} W/cm^2$, we observe the formation of magnetosonic solitons. The laser intensity being high, the amplitude of electron-ion separation increases as the $\vec{E} \times \vec{B}$ drift is higher. However, for this intensity the electron quiver motion can be rel-

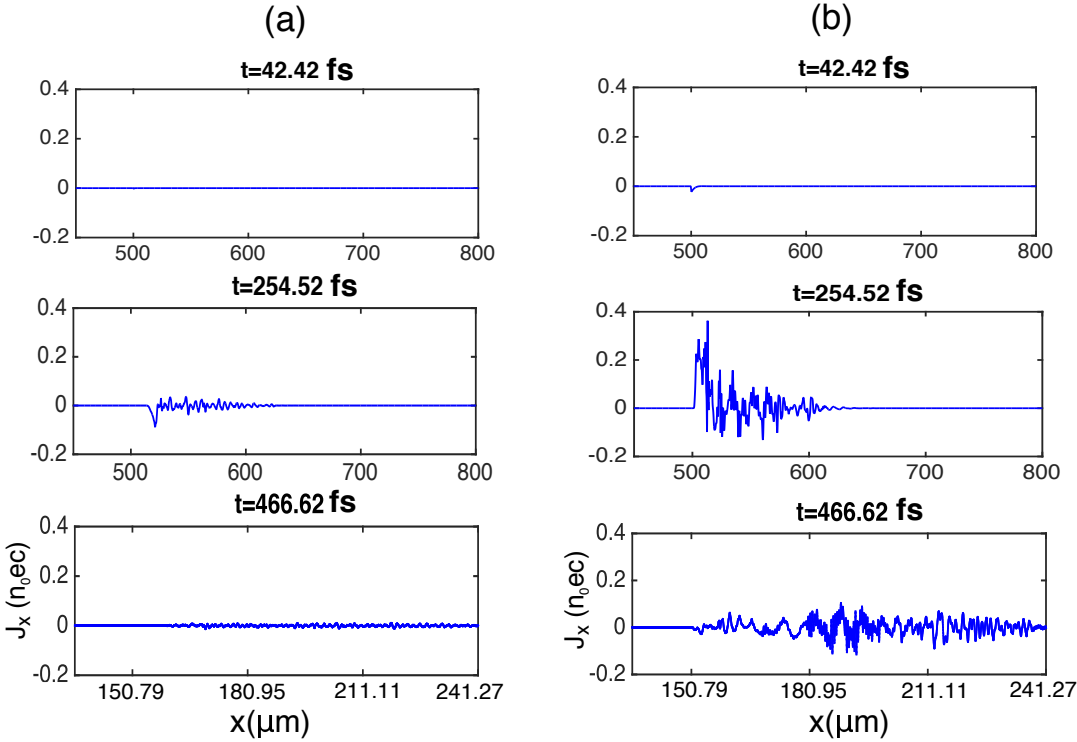


Figure 6.2: Temporal evolution of plasma current with respect to x and averaged over \hat{y} direction (a) without magnetic field and (b) with magnetic field. It is clear from the left and right subplots that a significant amount of plasma current is generated when there is an external magnetic field and for higher intensities of CO_2 laser. Even when laser intensity is relativistic, the plasma current generated by $\vec{J} \times \vec{B}$ heating mechanism is negligible in absence of the external magnetic field

ativistic and one may also expect the $\vec{J} \times \vec{B}$ heating mechanism to be operative for absorption. We have plotted the current density for the two cases of (a) and (b) in Fig.(6.2). The amplitude of current density perturbation is much weaker in the case (a) when compared to the case (b). The electrostatic disturbances thus created are clearly observed to be enhanced. It can also be observed from Fig.(6.2) that the high amplitude laser pulse triggers a large amplitude ion plasma disturbance.

This disturbance ultimately breaks in three pulses and propagate reasonably stably inside the plasma. This coherent structure formation and its stable propagation is observed in all the fields, namely the ion density (n_i), magnetic field B_z , transverse electric field E_y and electron density (n_e) (see Fig.(6.3), Fig. (6.4) and

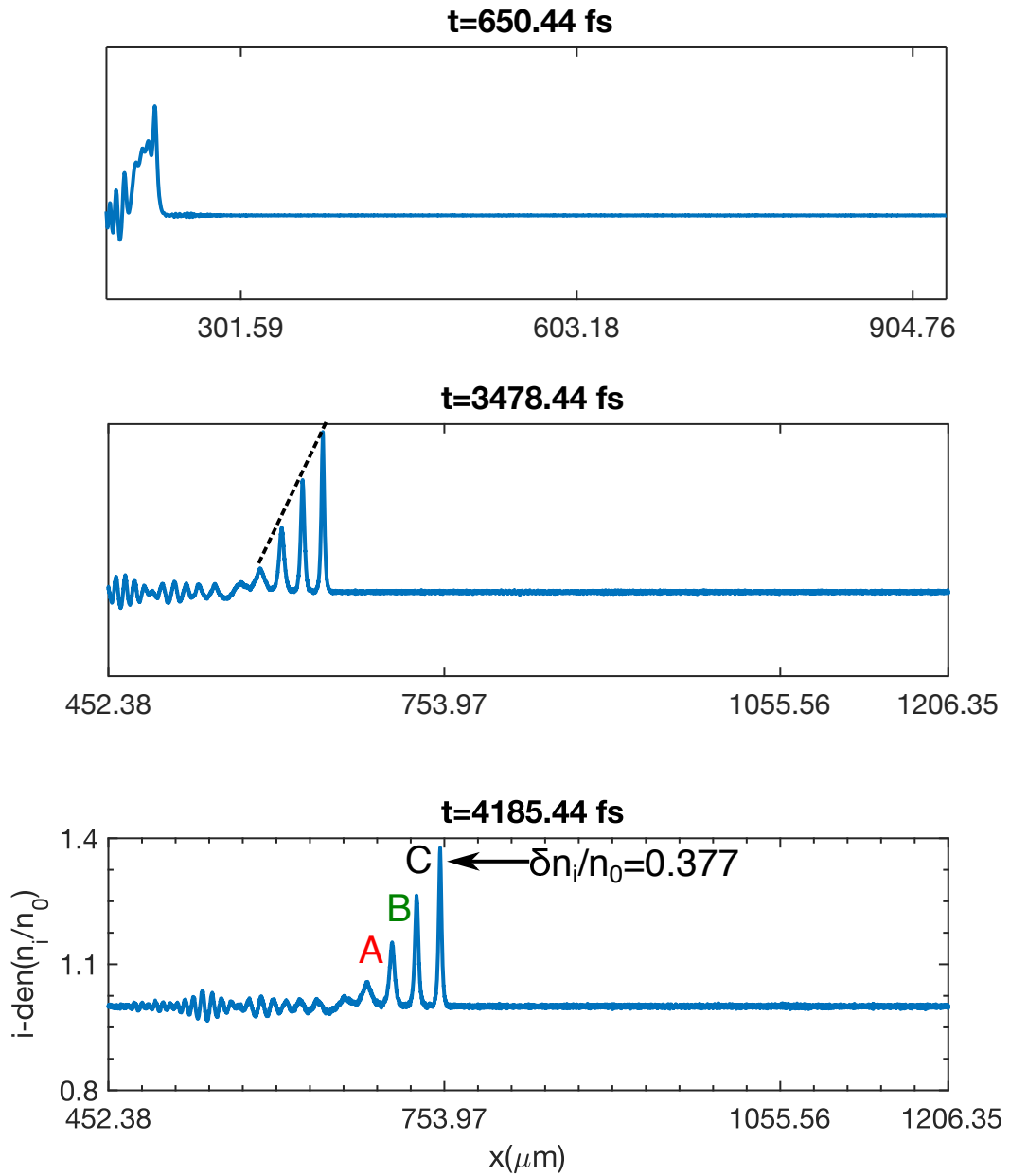


Figure 6.3: Temporal evolution of the ion density with respect to x and averaged over \hat{y} direction where three solitary structures A, B, and C are shown for higher intensities of pulsed CO_2 laser.

Fig. (6.5) respectively).

The three pulses termed as (A, B and C), in all these fields are observed to arrange in increasing amplitude with time in a straight line. This is a characteristic

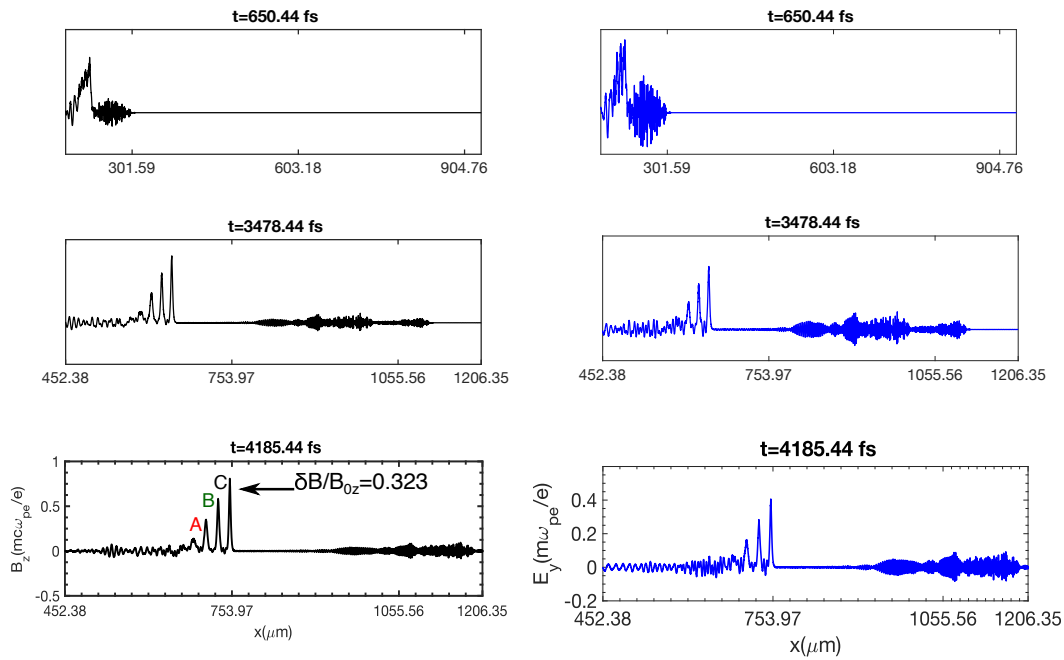


Figure 6.4: Temporal evolution of the perturbed electromagnetic fields B_z and E_y corresponding to the magnetosonic KdV solitons with respect to x and averaged over \hat{y} direction

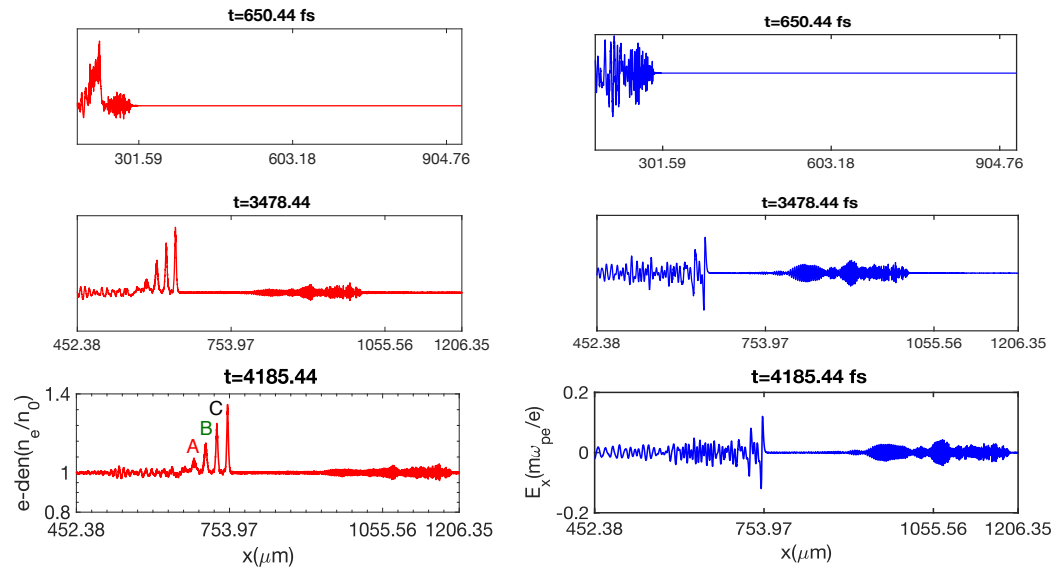


Figure 6.5: Temporal evolution of the electron density n_e and electrostatic field E_x with respect to x and averaged over \hat{y} direction.

feature of the KdV solitons that seems to get formed in this case as we show now. The higher amplitude solitons travel faster and are able to overtake the lower amplitude solitonic structures. It is for this reason the three pulses shown in Figs.(6.3-6.4) termed as (A , B and C), are observed to arrange one ahead of other in increasing amplitude forming a straight line. The propagation speed of these solitons are thus very close to the Alfvén speed in a cold magnetized plasma. We measured the propagation speed of these solitonic structures from our simulations and found them to be $v_{sim,A} = 0.4653c$, $v_{sim,B} = 0.4795c$, and $v_{sim,C} = 0.4950c$ for the three structures A , B , and C respectively. These propagation speed match closely with the Alfvén speed of the medium which is $v_A = (m_e/m_i)^{1/2}\omega_{ce}/\omega_{pe} = 0.5c$ for our choice of parameters of the medium. The unaltered stable propagation of the three structures for a long time, several thousands of ion plasma periods also suggest that the structures are solitons.

The KdV solitons²⁰¹ also have an interesting property that for solitons with different amplitudes a their width L vary in such a fashion so as to have aL^2 as constant. We have evaluated the same for the three structures observed in the simulation at various time and have shown it in TABLE I.

TABLE I

The parameter aL^2 changes very little in simulations and essentially remains constant for the observed magnetosonic KdV solitons A , B and C . The percentage variation in a is 61.05% L^2 is 65.39% but aL^2 only varies by 15.46% in the data shown below.

<i>Soliton</i>	$t(fs)$	$a(\delta n_i/n_0)$	$L(\times 0.3016\mu m)$	aL^2
A	2771.44	0.148	17.0	42.77
	3478.44	0.149	16.5	43.06
	4185.44	0.148	17.0	42.77
B	2771.44	0.266	13.0	44.95
	3478.44	0.266	12.7	42.90
	4185.44	0.265	13.0	44.78
C	2771.44	0.380	10	38.00
	3478.44	0.380	10	38.00
	4185.44	0.378	10.2	38.32

It is clear from the TABLE I that despite considerable difference in the amplitudes and width of the three solitons, the parameter aL^2 remains relatively unaltered. While the amplitude a of the different solitons differ by as much as 61.05%, and the square of the width L^2 by 65.39%; the variation in aL^2 in the observations is only about 15.46%. This clearly suggests that the structures which have formed in the simulations are essentially KdV solitons. The slight variations occur as the conditions of the medium changes with time and the KdV solitons are essentially approximate solutions in the small amplitude reductive perturbative expansion limit of the full set of MHD equations in the weakly dispersive, nonlinear regime. Our studies, therefore, confirm that the magnetosonic KdV solitons can be excited in a laboratory by using pulsed CO_2 lasers along with an externally applied magnetic field. Fig.(6.6) shows the 1D plot of ion density with different

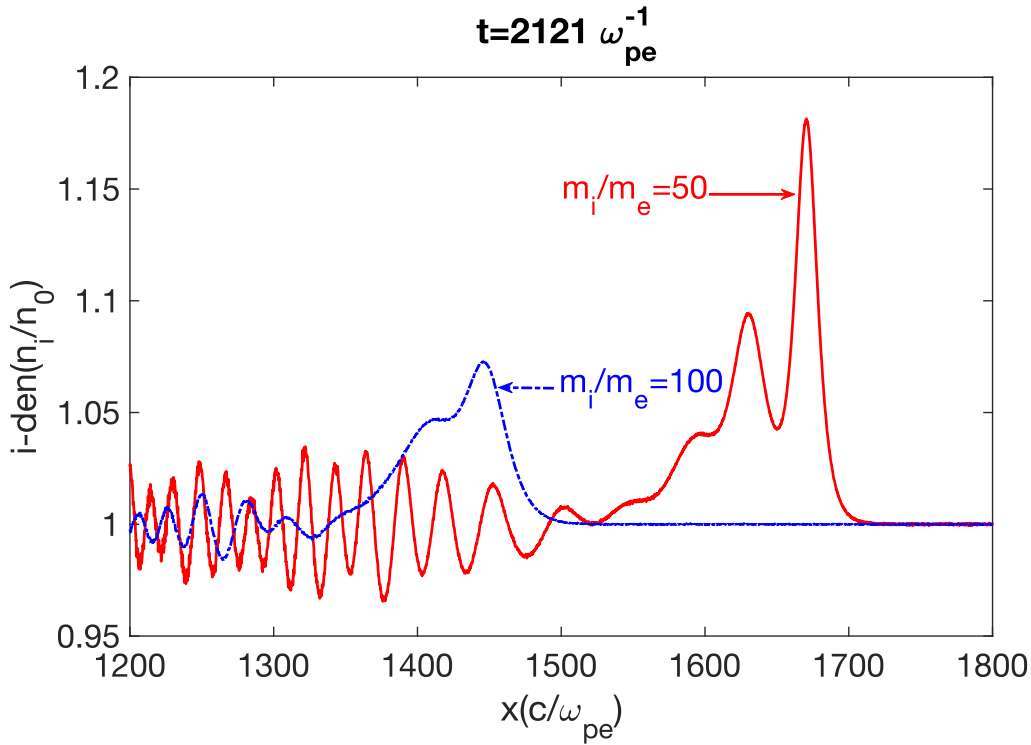


Figure 6.6: 1D plot Ion density with respect to x and averaged over \hat{y} direction. It is evident from this plot that magnetosonic solitons do get excited with different mass ratios.

ion to electron mass ratios ($m_i/m_e = 50, 100$). It has been observe that in these cases too, the solitonic structure gets excited. However, the number of solitons ex-

cited get reduced with increasing mass ratio. This is so because higher amplitude disturbances lead to the nonlinear soliton formation. With increasing mass ratio the required laser intensity needs to be increased to disturb the ions strongly at similar intensity then the number of solitons gets reduced.

Our simulations being carried out in 2-D, we observe that the solitonic structures which are of 1-D nature, after a long time (~ 400 ion plasma periods) transverse modulations in the other direction are observed. These modulations are observed to increase with time as shown in Fig. (6.7), signifying a development of an instability and ultimately seem to form transverse modulational structures.

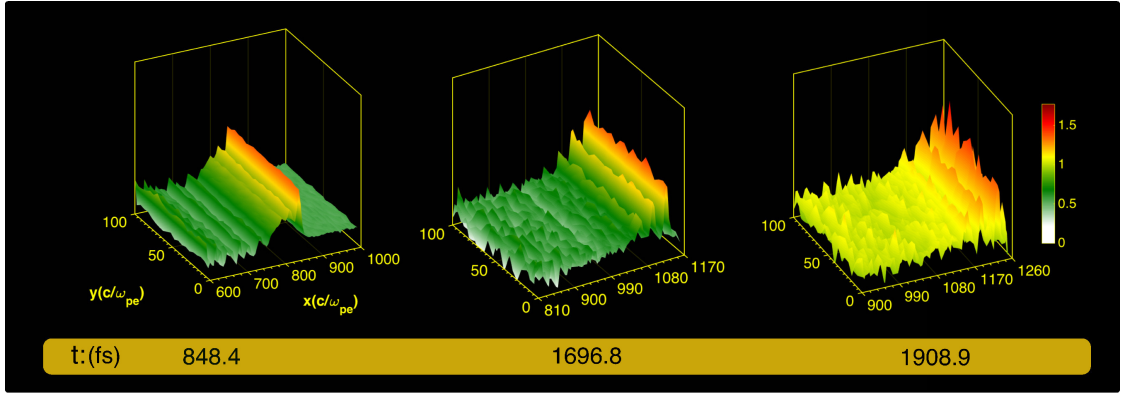


Figure 6.7: Surface plot of the ion charge density. Transverse filamentation of each peak of the ion charge density of the magnetosonic KdV soliton is quite evident from this figure. It has been shown that at $t = 1696.8 fs$, transverse filamentation starts and it continues to grow with time

6.5 Conclusion

In conclusion, we have demonstrated in this work that how next-generation pulsed CO_2 laser can be further utilized to excite magnetosonic solitons laboratory laser-plasma experiments for higher intensities. These are solitary structures found to propagate stably upto several thousands of ion plasma periods. It has been shown with the help of 2-D PIC simulations that these solitons in higher dimensions show density modulations which grows further grows with time. Furthermore, it has been shown that the density fluctuation with respect to the background plasma and the number of solitary pulses that gets excited depend on the laser intensity.

With the recent advent of high power, pulsed CO_2 laser and magnetic field upto $10KT$, ion dominated phenomena are ready to be tested in laboratory in near future.

7

Conclusion and future scope

With the advancement of laser technologies, several newer regimes of physics exploration concerning fast ignition laser fusion,¹ generation of charged particle beams,^{2,3} bright source of X-rays⁴ and Gamma-ray flashes and generation of higher order harmonics,⁵ promising source of positron emitters for PET (positron emission tomography),⁶ cosmic accelerations (ultra-high energy cosmic rays)⁷ etc. have become a topic of prime importance.

In the present thesis, theoretical and numerical investigations using the Particle-in-Cell code OSIRIS-4.0 have been carried out to understand the laser generated electron beam propagation inside the plasma and possibility of new absorption techniques based on pulsed CO_2 laser for direct ion accelerations. In the preceding chapters, the detail descriptions of some of the studies carried out by us have been presented. We briefly provide a summary of the major findings of the thesis here. The future scope of work has also been identified.

7.1 Main results of this thesis

7.1.1 Energy principle for beam plasma system instabilities

The energy principle utilizes the energy cost associated with the perturbed equilibria to ascertain whether the growth of a particular mode is energetically favourable or not. This technique often provides an interesting physical insight and has been extensively employed in the context of plasma systems governed by Magnetohydrodynamics. Recently, it has been invoked for understanding the electrostatic

two stream instability.

In this study, we have shown that an energy principle argument can be put forth for the electromagnetic Weibel mode in the context of beam plasma system. The perturbations in linear regime provide both positive and negative energy contributions in the system. This is essential for the instability, as for conservative system the total energy of the system is constant. The system should allow the possibility of the growth of perturbations without any additional cost of energy. This can happen only when the perturbations merely transfer energy from one form to another. Thus causing one form of energy to grow at the cost of another. For the beam filamentation instability, the electromagnetic field energy in the perturbed state grows at the cost of kinetic energy of the equilibrium flow. We have identified $S_4 = \sum_{\alpha} \frac{n_{0\alpha} v_{0\alpha}^2}{n_0 \gamma_{0\alpha}}$ as the coefficient of the negative energy contributing term and is crucial for the instability. We have also shown that a finite value of $S_3 = \sum_{\alpha} \frac{n_{0\alpha} v_{0\alpha}}{n_0 \gamma_{0\alpha}}$ is responsible for generating the electric field transverse to the flow profile and in fact, costs energy. It is clear that S_3 is finite only in the relativistic case and for the case when the flow profile is asymmetric (beam and background plasma have different densities). The finite value of S_3 suppresses the filamentation mode. This has been verified by comparing the growth rates for various cases in this manuscript. For instance, it has been shown that for a constant value of S_4 the growth rate is maximum for $|S_3| = 0$ and reduces monotonically with increasing value of $|S_3|$. We have also carried out 2-D PIC simulations to illustrate the difference between symmetric and asymmetric flow configurations. We have chosen two flow parameters for which S_4 is same. The value of S_3 is zero for one case and is finite for the other case corresponding to symmetric and asymmetric configurations respectively. We have observed that even in the presence of 2-D perturbations (permitted by the 2-D PIC simulations carried out by us) the symmetric case has higher growth rate. Furthermore, the nonlinear saturation level of the perturbed magnetic field is also observed to be higher for the symmetric flow configuration.

7.1.2 Nonlinear regime of beam plasma instability

The relativistic electron beam (REB) propagation in plasma is fraught with beam plasma instabilities. The prominent amongst them is the collisionless Weibel desta-

bilization which spatially separates the forward propagating REB and the return shielding currents. This results in the formation of REB current filaments which are typically of the size of electron skin depth during the linear stage of the instability. It has been observed that in the nonlinear stage the filaments size increases as they merge with each other. With the help of 2-D PIC simulations in the plane perpendicular to the REB propagation, it is shown that these mergers occur in two distinct nonlinear phases. In the first phase, the total magnetic energy increases. Subsequently, however, during the second phase, one observes a reduction in magnetic energy. It is shown that the transition from one nonlinear regime to another occurs when the typical current associated with individual filaments hits the Alfvén threshold. In the second nonlinear regime, therefore, the filaments can no longer permit any increase in current. Magnetic reconnection events then dissipate the excess current (and its associated magnetic energy) that would result from a merger process leading to the generation of energetic electrons jets in the perpendicular plane. At later times when there are only few filaments left the individual reconnection events can be clearly identified. It is observed that in between such events the magnetic energy remains constant and shows a sudden drop as and when two filaments merge. The electron jets released in these reconnection events are thus responsible for the transverse heating which has been mentioned in some previous studies

7.1.3 Effect of finite beam size and initial current

The all pervading and often enigmatic presence of the magnetic field in many natural phenomena has aroused great curiosity and spawned many efforts to understand its generation. In this chapter, we propose, simulate and experimentally demonstrate a new mechanism of long scale magnetic field generation in the context of laser plasma interaction. The mechanism relies on two realistic features which have been totally ignored in previous studies. These relate to the finite size of the laser generated electron beam and an initial current imbalance which would typically be present when energetic electrons push itself in a plasma medium. It is shown that magnetic fields of much longer scale lengths (comparable to the transverse beam dimension) get generated much before the conventional Weibel and Kelvin Helmholtz instabilities associated with the beam plasma system set in.

This happens as a result of a radiative leakage at the boundaries of the finite beam wherein even a small but finite current imbalance plays a crucial role of a radiative antennae. These features have been absent in all conventional periodic systems considered in earlier simulations as well as theoretical analyses. Our study thus triggers a re-examination of hitherto prevalent ideas on magnetic field generation in plasmas and focus attention on the effects of finiteness in physical systems.

7.1.4 Direct coupling of laser to ions

The possibility of ion heating directly with a laser has been another topic of interest. Some of the well-known mechanisms in this regard are the RPA (Radiation Pressure Acceleration) and TNSA (Target Normal Sheath Acceleration) . We have demonstrated another mechanism of ion heating by employing external magnetic fields. The external magnetic field is chosen so as to constrain the electron movement and have them tied to the magnetic field. The heavier ions remain unmagnetized and respond to the laser electric field. The difference of electron and ion dynamics lead to charge separation and drives ion plasma oscillations, thereby transferring the laser energy to ions to a great extent directly. A 2-D Particle - In - Cell (PIC) simulations for an incident laser beam normal to an overdense plasma target in the presence of an external magnetic field has been carried out. The external magnetic field has to be chosen such that the heavier ions remain unmagnetized but the lighter electron species get magnetized at the laser frequency. For conventional lasers of $\sim 1\mu m$ wavelengths, the magnetic field requirement satisfying the aforementioned condition turns out to be of the order of several hundreds of kilo Tesla. This requirement goes down by one order if pulsed CO_2 lasers with wavelengths of $\sim 10\mu m$ are employed. At present magnetic fields of several kilo Tesla has already been generated in the laboratory. It is thus only a matter of time when a factor of 10 enhancement in the magnetic field will bring the parameters in the right regime for experiments to test the new mechanism put forth here with pulsed CO_2 lasers.

7.1.5 Direct coupling of laser to ions: Magnetosonic excitations

We continue our studies on direct energy absorption of the laser by ions further and show that when the laser power is increased in addition to exciting ion plasma oscillations, the excitation of Korteweg - de Vries (KdV) magnetosonic solitons are also observed. Keeping this in view, the simulations have been carried out for the pulsed CO_2 laser parameters with intensity $I = 7 \times 10^{17} W/cm^2$). It is shown that at a higher intensity of the laser, the ion disturbances acquire higher amplitude to excite Korteweg - de Vries (KdV) magnetosonic solitons. The solitons, as expected, propagate stably for several thousands of ion plasma periods. However, subsequently, they are seen to develop transverse modulations which grow with time.

7.2 Future scope of these works

This thesis provides many directions for theoretical as well experimental explorations.

7.2.1 Theoretical and Numerical explorations

7.2.1.1 Effect of radiation reaction on beam-plasma system

In the near future many new facilities worldwide are poised to become operational (e.g ELI, XCELS, SULF, SEL etc.^{6,55-57}) to study the on laser-solid interactions where the intensity and timescale limit would be pushed to even higher limits namely that of intensities $\geq 10^{24} W/cm^2$ and attosecond scales respectively. Such an intense laser impinging over an overdense target generates a highly energetic electrons. Any accelerating charged particle loses its energy through radiation. As a result, a charged particle loses its momenta and slows down. This effective force on charged particles causing the loss in momenta of the particles is called "radiation reaction". Generally effect of radiation reaction is negligible, however, it becomes significant and comparable to in magnitude to the Lorentz force when γE approaches E_{cr} where E is the electric field acting on the particle

with the Lorentz factor γ and $E_{cr} = 1.3 \times 10^{18} Vm^{-1}$ is the critical field of quantum electrodynamics. With next generation $10PW$ laser facilities and in several astrophysical contexts, it is possible to generate electrons with such an energy that it may feel the effect of radiation reaction. Therefore, the effect of radiation reaction on the streaming instabilities like current filamentation/Weibel instability, Kelvin-Helmholtz instabilities studied in typical typical becomes of prime importance and needs to be addressed which are planned in our future work. We have also planned to develop a EMHD type model set of fluid equations for quantum hydrodynamic plasma also.

In the second nonlinear phase of Weibel instability, the magnetic energy of the beam-plasma system decreases and an increase in kinetic energy is observed. This happens because of the magnetic reconnection process which leads to the generation of electron jets in the plane transverse to the plasma flows. These highly energetic electrons jets will also feel the effect of radiation reaction which needs to be addressed. The understanding of Weibel mediated magnetic reconnection process and generation of energetic electrons jets in the reconnection process are now a plan for our future work.

7.2.1.2 Role of finite boundary of the beam in a beam-plasma system

The magnetic field generation is an important issue in a variety of contexts. In a beam plasma system it is typically believed that the Weibel destabilization process causes the generation of magnetic fields at the electron skin depth scales. It has recently been shown, however, that a finite transverse size of the beam leads to the generation of magnetic field at the long scale length of the beam ([arXiv.org,1704.00970v1](https://arxiv.org/abs/1704.00970v1) [physics.plasm-ph], 2017). This has been attributed to a new mechanism for the generation of long scale magnetic field structures in this context. In a realistic situation the beam in addition to having a finite transverse extent would also have a finite temporal width. Keeping this in view, we plan to work in the future where a finite longitudinal extent of the beam has also been considered.

Some laboratory experiments have now been able to explore the regime of ion response for the generation of turbulent magnetic fields. In this context, it will be interesting to extend beam-plasma simulations with ion response and characterize

the behaviour of turbulence in detail.

7.2.1.3 Lower hybrid type in-situ ion heating

In magnetic confinement fusion, direct heating of ions via lower hybrid resonance heating is always desirable as it is the ion species (D-T species) which participate in fusion producing an enormous amount of energy and ion energy confinement time is generally longer than that of the electrons. It is achieved by launching an extraordinary mode of an electromagnetic wave at a frequency higher or equal to the lower hybrid mode of the plasma in the Tokamaks using phased wave guide array.²⁰⁶ As the wave gets tunnelled from the cut-off region, a part of it get converted into electrostatic lower hybrid wave which further leads to an in-situ ion heating near lower hybrid resonance.^{113-115,206-208} The similar mechanism in the case of fast ignition scheme of Inertial confinement fusion can be applied to energise ions directly but have been overlooked till date. As a part of our future work, we have planned to look for the possibility of lower hybrid type in-situ ion heating with X-mode pulsed CO_2 laser. We are also studying how ion cyclotron resonance heating can be utilized in fast ignition scheme of laser fusion.

7.2.2 Experimental explorations

The CO_2 lasers till now have been considered as efficient industrial lasers in the market for continuous wave (CW) and relatively long pulse applications.^{86,177,178} Recently, the short pulse CO_2 lasers are now available (BESTIA laser¹⁰²) but still they have not been as widely explored in the sub-nano or picoseconds domain. We demonstrate, with the help of PIC simulations, in this thesis as well as in a series of papers,¹⁷⁴ the immense possibilities that short pulse CO_2 lasers offer for physics explorations. In particular, here we have demonstrated the possibility of directly coupling of laser energy to the heavier ion species in the presence of an ambient magnetic field. With the recent advent of several Kilo Tesla magnetic field in the laboratory, it can be possible to realize the ion acceleration mechanisms proposed in this thesis in near future.

Bibliography

- ¹ Max Tabak, James Hammer, Michael E. Glinsky, William L. Kruer, Scott C. Wilks, John Woodworth, E. Michael Campbell, Michael D. Perry, and Rodney J. Mason. Ignition and high gain with ultrapowerful lasers*. *Physics of Plasmas*, 1(5):1626–1634, 1994.
- ² S. Kar, A. P. L. Robinson, D. C Carroll, O Lundh, K. Markey, P. McKenna, P. Norreys, and M. Zepf. Guiding of relativistic electron beams in solid targets by resistively controlled magnetic fields. *Phys. Rev. Lett.*, 102:055001, Feb 2009.
- ³ J. Fuchs, P. Antici, E. D’Humières, E. Lefebvre, M. Borghesi, E. Brambrink, C. A. Cecchetti, M. Kaluza, V. Malka, M. Manclossi, S. Meyroneinc, P. Mora, J. Schreiber, T. Toncian, H. Pépin, and P. Audebert. Laser-driven proton scaling laws and new paths towards energy increase. *Nature Physics*, 2(1):48–54, 2006.
- ⁴ L. M. Chen, F. Liu, W. M. Wang, M. Kando, J. Y. Mao, L. Zhang, J. L. Ma, Y. T. Li, S. V. Bulanov, T. Tajima, Y. Kato, Z. M. Sheng, Z. Y. Wei, and J. Zhang. Intense high-contrast femtosecond k -shell x-ray source from laser-driven ar clusters. *Phys. Rev. Lett.*, 104(215004), May 2010.
- ⁵ U. Teubner and P. Gibbon. High-order harmonics from laser-irradiated plasma surfaces. *Rev. Mod. Phys.*, 81(445–479), Apr 2009.
- ⁶ E. Amato, A. Italiano, D. Margarone, B. Pagano, S. Baldari, and G. Korn. Future laser-accelerated proton beams at eli-beamlines as potential source of positron emitters for pet. *Journal of Instrumentation*, 11(04):C04007, 2016.
- ⁷ Gerard A. Mourou, Toshiki Tajima, and Sergei V. Bulanov. Optics in the relativistic regime. *Rev. Mod. Phys.*, 78:309–371, Apr 2006.
- ⁸ A. Di Piazza, C. Müller, K. Z. Hatsagortsyan, and C. H. Keitel. Extremely high-intensity laser interactions with fundamental quantum systems. *Rev. Mod. Phys.*, 84:1177–1228, Aug 2012.
- ⁹ T.Y. Brian Yang, William L. Kruer, Richard M. More, and A. Bruce Langdon. Absorption of laser light in overdense plasmas by sheath inverse bremsstrahlung. *Physics of Plasmas*, 2(3146), 1995.

- ¹⁰ T.Y. Brian Yang, William L. Kruer, A. Bruce Langdon, and Tudor W. Johnston. Mechanisms for collisionless absorption of light waves obliquely incident on overdense plasmas with steep density gradients. *Physics of Plasmas*, 3(2702), 1996.
- ¹¹ D. W. Forslund, J. M. Kindel, Kenneth Lee, E. L. Lindman, and R. L. Morse. Theory and simulation of resonant absorption in a hot plasma. *Phys. Rev. A*, 11(679), Feb 1975.
- ¹² F. Brunel. Not-so-resonant, resonant absorption. *Phys. Rev. Lett.*, 59(52), Jul 1987.
- ¹³ W. L. Kruer and Kent Estabrook. Jxb heating by very intense laser light. *Physics of Fluids*, 28(430), 1985.
- ¹⁴ S. C. Wilks, W. L. Kruer, M. Tabak, and A. B. Langdon. Absorption of ultra-intense laser pulses. *Phys. Rev. Lett.*, 69(1383), Aug 1992.
- ¹⁵ G. Malka and J. L. Miquel. Experimental confirmation of ponderomotive-force electrons produced by an ultrarelativistic laser pulse on a solid target. *Phys. Rev. Lett.*, 77(75), Jul 1996.
- ¹⁶ Z.-M. Sheng, K. Mima, Y. Sentoku, M. S. Jovanović, T. Taguchi, J. Zhang, and J. Meyer-ter Vehn. Stochastic heating and acceleration of electrons in colliding laser fields in plasma. *Phys. Rev. Lett.*, 88(055004), Jan 2002.
- ¹⁷ J. F. Drake, P. K. Kaw, Y. C. Lee, G. Schmid, C. S. Liu, and Marshall N. Rosenbluth. Parametric instabilities of electromagnetic waves in plasmas. *Physics of Fluids*, 17(778), 1974.
- ¹⁸ Erich S. Weibel. Spontaneously growing transverse waves in a plasma due to an anisotropic velocity distribution. *Phys. Rev. Lett.*, 2:83–84, Feb 1959.
- ¹⁹ B. Ramakrishna, S. Kar, A. P. L. Robinson, D. J. Adams, K. Markey, M. N. Quinn, X. H. Yuan, P. McKenna, K. L. Lancaster, J. S. Green, R. H. H. Scott, P. A. Norreys, J. Schreiber, and M. Zepf. Laser-driven fast electron collimation in targets with resistivity boundary. *Phys. Rev. Lett.*, 105(135001), Sep 2010.

-
- ²⁰ A. P. L. Robinson and M. Sherlock. Magnetic collimation of fast electrons produced by ultraintense laser irradiation by structuring the target composition. *Physics of Plasmas*, 14(083105), 2007.
- ²¹ Gourab Chatterjee, Prashant Kumar Singh, Saima Ahmed, A. P. L. Robinson, Amit D. Lad, Sudipta Mondal, V. Narayanan, Iti Srivastava, Nikhil Koratkar, John Pasley, A. K. Sood, and G. Ravindra Kumar. Macroscopic transport of mega-ampere electron currents in aligned carbon-nanotube arrays. *Phys. Rev. Lett.*, 108:235005, Jun 2012.
- ²² S. K. Mishra, Predhiman Kaw, A. Das, S. Sengupta, and G. Ravindra Kumar. Stabilization of beam–weibel instability by equilibrium density ripples. *Physics of Plasmas (1994-present)*, 21(012108), 2014.
- ²³ Chandrasekhar Shukla and Amita Das. Observation of enhanced absorption of laser radiation by nanostructured targets in pic simulations. *Physics of Plasmas*, 24(9):093118, 2017.
- ²⁴ A. Grassi, M. Grech, F. Amiranoff, F. Pegoraro, A. Macchi, and C. Riconda. Electron weibel instability in relativistic counterstreaming plasmas with flow-aligned external magnetic fields. *Phys. Rev. E*, 95:023203, Feb 2017.
- ²⁵ M. Bailly-Grandvaux, J. J. Santos, C. Bellei, P. Forestier-Colleoni, S. Fujioka, L. Giuffrida, J. J. Honrubia, D. Batani, R. Bouillaud, M. Chevrot, J. E. Cross, R. Crowston, S. Dorard, J. L. Dubois, M. Ehret, G. Gregori, S. Hulin, S. Kojima, E. Loyez, J. R. Marques, A. Morace, Ph. Nicolai, M. Roth, S. Sakata, G. Schaubmann, F. Serres, J. Serval, V. T. Tikhonchuk, N. Woolsey, and Z. Zhang. Guiding of relativistic electron beams in dense matter by longitudinally imposed strong magnetic fields. *Nature Communications*, 9(102), 2018.
- ²⁶ C Thauray, E Guillaume, A Döpp, R Lehe, A Lifschitz, K Ta Phuoc, J Gautier, J-P Goddet, A Tafzi, A Flacco, F Tissandier, S Sebban, A Rousse, and V Malka. Demonstration of relativistic electron beam focusing by a laser-plasma lens. *Nature Communications*, 6:6860, apr 2015.
- ²⁷ C. N. Lashmore-Davies. Two-stream instability, wave energy, and the energy principle. *Physics of Plasmas*, 14(9), 2007.

- ²⁸ Atul Kumar, Chandrasekhar Shukla, Amita Das, and Predhiman Kaw. Energy principle for excitations in plasmas with counterstreaming electron flows. *AIP Advances*, 8(5):055213, 2018.
- ²⁹ Chandrasekhar Shukla, Atul Kumar, Amita Das, and Bhavesh G. Patel. Merger and reconnection of Weibel separated relativistic electron beam. *Physics of Plasmas*, 25(2), 2018.
- ³⁰ Sudipta Mondal, V. Narayanan, Wen Jun Ding, Amit D. Lad, Biao Hao, Saima Ahmad, Wei Min Wang, Zheng Ming Sheng, Sudip Sengupta, Predhiman Kaw, Amita Das, and G. Ravindra Kumar. Direct observation of turbulent magnetic fields in hot, dense laser produced plasmas. *Proceedings of the National Academy of Sciences*, 109(21):8011–8015, 2012.
- ³¹ Gourab Chatterjee, Kevin M Schoeffler, Prashant Kumar Singh, Amitava Adak, Amit D Lad, Sudip Sengupta, Predhiman Kaw, Luis O Silva, Amita Das, and G Ravindra Kumar. Magnetic turbulence in a table-top laser-plasma relevant to astrophysical scenarios. 8:15970, jun 2017.
- ³² D. G. Stearns, O. L. Landen, E. M. Campbell, and J. H. Scofield. Generation of ultrashort x-ray pulses. *Phys. Rev. A*, 37(1684), Mar 1988.
- ³³ O. Culfa, G. J. Tallents, E. Wagenaars, C. P. Ridgers, R. J. Dance, A. K. Rossall, R. J. Gray, P. McKenna, C. D. R. Brown, S. F. James, D. J. Hoarty, N. Booth, A. P. L. Robinson, K. L. Lancaster, S. A. Pikuz, A. Ya. Faenov, T. Kampfer, K. S. Schulze, I. Uschmann, and N. C. Woolsey. Hot electron production in laser solid interactions with a controlled pre-pulse. *Physics of Plasmas*, 21(043106), 2014.
- ³⁴ G. Kulcsár, D. AlMawlawi, F. W. Budnik, P. R. Herman, M. Moskovits, L. Zhao, and R. S. Marjoribanks. Intense picosecond x-ray pulses from laser plasmas by use of nanostructured “velvet” targets. *Phys. Rev. Lett.*, 84(5149), May 2000.
- ³⁵ Subhendu Kahaly, S. K. Yadav, W. M. Wang, S. Sengupta, Z. M. Sheng, A. Das, P. K. Kaw, and G. Ravindra Kumar. Near-complete absorption of intense,

- ultrashort laser light by sub- λ gratings. *Phys. Rev. Lett.*, 101(145001), Sep 2008.
- ³⁶ P. P. Rajeev, P. Taneja, P. Ayyub, A. S. Sandhu, and G. Ravindra Kumar. Metal nanoplasmas as bright sources of hard x-ray pulses. *Phys. Rev. Lett.*, 90(115002), Mar 2003.
- ³⁷ A. L. Lei, K. A. Tanaka, R. Kodama, G. R. Kumar, K. Nagai, T. Norimatsu, T. Yabuuchi, and K. Mima. Optimum hot electron production with low-density foams for laser fusion by fast ignition. *Phys. Rev. Lett.*, 96(255006), Jun 2006.
- ³⁸ C. Gahn, G. Pretzler, A. Saemann, G. D. Tsakiris, K. J. Witte, D. Gassmann, T. Schätz, U. Schramm, P. Thirolf, and D. Habs. MeV γ - ray yield from solid targets irradiated with fs-laser pulses. *Applied Physics Letters*, 73(3662), 1998.
- ³⁹ Lihua Cao, Yuqiu Gu, Zongqing Zhao, Leifeng Cao, Wenzhong Huang, Weimin Zhou, X. T. He, Wei Yu, and M. Y. Yu. Enhanced absorption of intense short-pulse laser light by subwavelength nanolayered target. *Physics of Plasmas*, 17(4):043103, 2010.
- ⁴⁰ Alden Curtis, Chase Calvi, James Tinsley, Reed Hollinger, Vural Kaymak, Alexander Pukhov, Shoujun Wang, Alex Rockwood, Yong Wang, Vyacheslav N Shlyaptsev, and Jorge J Rocca. Micro-scale fusion in dense relativistic nanowire array plasmas. *Nature Communications*, 9(1):1077, 2018.
- ⁴¹ S.V Bulanov, T.Zh Esirkepov, V.S Khoroshkov, A.V Kuznetsov, and F Pegoraro. Oncological hadrontherapy with laser ion accelerators. *Physics Letters A*, 299(2):240 – 247, 2002.
- ⁴² A. J. Mackinnon, Y. Sentoku, P. K. Patel, D. W. Price, S. Hatchett, M. H. Key, C. Andersen, R. Snavely, and R. R. Freeman. Enhancement of proton acceleration by hot-electron recirculation in thin foils irradiated by ultraintense laser pulses. *Phys. Rev. Lett.*, 88:215006, May 2002.
- ⁴³ K. Zeil, M. Baumann, E. Beyreuther, T. Burris-Mog, T. E. Cowan, W. Enghardt, L. Karsch, S. D. Kraft, L. Laschinsky, J. Metzkes, D. Naumburger, M. Oppelt, C. Richter, R. Sauerbrey, M. Schürer, U. Schramm, and J. Pawelke.

- Dose-controlled irradiation of cancer cells with laser-accelerated proton pulses. *Applied Physics B*, 110(4):437–444, Mar 2013.
- ⁴⁴ Andrea Macchi, Marco Borghesi, and Matteo Passoni. Ion acceleration by superintense laser-plasma interaction. *Rev. Mod. Phys.*, 85:751–793, May 2013.
- ⁴⁵ Atul Kumar, Chandrasekhar Shukla, Deepa Verma, Predhiman Kaw, and Amita Das. Excitation of KdV magnetosonic solitons in plasma in the presence of an external magnetic field. *submitted to Plasma Phys. Control. Fusion*, 2018.
- ⁴⁶ R. A. Fonseca, L. O. Silva, F. S. Tsung, V. K. Decyk, W. Lu, C. Ren, W. B. Mori, S. Deng, S. Lee, T. Katsouleas, and J. C. Adam. *OSIRIS: A Three-Dimensional, Fully Relativistic Particle in Cell Code for Modeling Plasma Based Accelerators*, pages 342–351. Springer Berlin Heidelberg, Berlin, Heidelberg, 2002.
- ⁴⁷ R A Fonseca, S F Martins, L O Silva, J W Tonge, F S Tsung, and W B Mori. One-to-one direct modeling of experiments and astrophysical scenarios: pushing the envelope on kinetic plasma simulations. *Plasma Physics and Controlled Fusion*, 50(12):124034, 2008.
- ⁴⁸ M. Honda, J. Meyer-ter Vehn, and A. Pukhov. Collective stopping and ion heating in relativistic-electron-beam transport for fast ignition. *Phys. Rev. Lett.*, 85:2128–2131, Sep 2000.
- ⁴⁹ Amita Das, Atul Kumar, Chandrasekhar Shukla, Ratan Kumar Bera, Deepa Verma, Bhavesh Patel, Y. Hayashi, K. A. Tanaka, Amit D. Lad, G. R. Kumar, and Predhiman Kaw. Evidence of new finite beam plasma instability for magnetic field generation. pages 1–11, 2017.
- ⁵⁰ A. Henig, S. Steinke, M. Schnürer, T. Sokollik, R. Hörlein, D. Kiefer, D. Jung, J. Schreiber, B. M. Hegelich, X. Q. Yan, J. Meyer-ter Vehn, T. Tajima, P. V. Nickles, W. Sandner, and D. Habs. Radiation-pressure acceleration of ion beams driven by circularly polarized laser pulses. *Phys. Rev. Lett.*, 103:245003, Dec 2009.
- ⁵¹ L Robson, PT Simpson, P McKenna, KWD Ledingham, RJ Clarke, T McCanny, D Neely, Olle Lundh, Filip Lindau, Claes-Göran Wahlström, and M Zepf. Scal-

- ing of proton acceleration driven by petawatt-laser-plasma interactions. *Nature Physics*, 3(58):58–62, 2007.
- ⁵² Shinsuke Fujioka, Zhe Zhang, Kazuhiro Ishihara, Keisuke Shigemori, Youichiro Hironaka, Tomoyuki Johzaki, Atsushi Sunahara, Naoji Yamamoto, Hideki Nakashima, Tsuguhiro Watanabe, Hiroyuki Shiraga, Hiroaki Nishimura, and Hiroshi Azechi. Kilotessa Magnetic Field due to a Capacitor-Coil Target Driven by High Power Laser. *Scientific Reports*, 3:1170, jan 2013.
- ⁵³ K. D. Xiao, C. T. Zhou, H. Zhang, T. W. Huang, R. Li, B. Qiao, J. M. Cao, T. X. Cai, S. C. Ruan, and X. T. He. Generation of ten kilotesla longitudinal magnetic fields in ultraintense laser-solenoid target interactions. *arXiv1803.06868[physics-plasm]*, pages 1–5, 2018.
- ⁵⁴ D. Nakamura, A. Ikeda, H. Sawabe, Y. H. Matsuda, and S. Takeyama. Record indoor magnetic field of 1200 t generated by electromagnetic flux-compression. *Review of Scientific Instruments*, 89(9):095106, 2018.
- ⁵⁵ G A Mourou, C L Labaune, M Dunne, N Naumova, and V T Tikhonchuk. Relativistic laser-matter interaction: from attosecond pulse generation to fast ignition. *Plasma Physics and Controlled Fusion*, 49(12B):B667, 2007.
- ⁵⁶ Editorial. Extreme light. *Nature Materials*, 15(1):1, 2015.
- ⁵⁷ By Edwin Cartlidge. Physicists are planning to build lasers so powerful they could rip apart empty space. *Science*, 2018.
- ⁵⁸ R. B. Stephens, R. A. Snavely, Y. Aglitskiy, F. Amiranoff, C. Andersen, D. Batani, S. D. Baton, T. Cowan, R. R. Freeman, T. Hall, S. P. Hatchett, J. M. Hill, M. H. Key, J. A. King, J. A. Koch, M. Koenig, A. J. MacKinnon, K. L. Lancaster, E. Martinolli, P. Norreys, E. Perelli-Cippo, M. Rabec Le Gloahhec, C. Rousseaux, J. J. Santos, and F. Scianitti. K_α fluorescence measurement of relativistic electron transport in the context of fast ignition. *Phys. Rev. E*, 69:066414, Jun 2004.
- ⁵⁹ Antoine Rousse, Christian Rischel, and Jean-Claude Gauthier. Femtosecond x-ray crystallography. *Rev. Mod. Phys.*, 73:17–31, Jan 2001.

- ⁶⁰ B J B Crowley, R Bingham, R G Evans, D O Gericke, O L Landen, C D Murphy, P A Norreys, S J Rose, Th Tschentscher, C H.-T Wang, J S Wark, and G Gregori. Testing quantum mechanics in non-Minkowski space-time with high power lasers and 4th generation light sources. *Scientific Reports*, 2:491, jul 2012.
- ⁶¹ I Felix Mirabel and Luis F Rodriguez. Sources of relativistic jets in the galaxy. *Annual Review of Astronomy and Astrophysics*, 37(1):409–443, 1999.
- ⁶² A. R. Bell. The acceleration of cosmic rays in shock fronts-i. *Monthly Notices of the Royal Astronomical Society*, 182(2):147, 1978.
- ⁶³ M. Ackermann, M. Ajello, A. Allafort, L. Baldini, J. Ballet, G. Barbiellini, M. G. Baring, D. Bastieri, K. Bechtol, R. Bellazzini, R. D. Blandford, E. D. Bloom, E. Bonamente, A. W. Borgland, E. Bottacini, T. J. Brandt, J. Bregeon, M. Brigida, P. Bruel, R. Buehler, G. Busetto, S. Buson, G. A. Caliandro, R. A. Cameron, P. A. Caraveo, J. M. Casandjian, C. Cecchi, Ö. Çelik, E. Charles, S. Chaty, R. C. G. Chaves, A. Chekhtman, C. C. Cheung, J. Chiang, G. Chiaro, A. N. Cillis, S. Ciprini, R. Claus, J. Cohen-Tanugi, L. R. Cominsky, J. Conrad, S. Corbel, S. Cutini, F. D’Ammando, A. de Angelis, F. de Palma, C. D. Dermer, E. do Couto e Silva, P. S. Drell, A. Drlica-Wagner, L. Falletti, C. Favuzzi, E. C. Ferrara, A. Franckowiak, Y. Fukazawa, S. Funk, P. Fusco, F. Gargano, S. Germani, N. Giglietto, P. Giommi, F. Giordano, M. Giroletti, T. Glanzman, G. Godfrey, I. A. Grenier, M.-H. Grondin, J. E. Grove, S. Guiriec, D. Hadasch, Y. Hanabata, A. K. Harding, M. Hayashida, K. Hayashi, E. Hays, J. W. Hewitt, A. B. Hill, R. E. Hughes, M. S. Jackson, T. Jogler, G. Jóhannesson, A. S. Johnson, T. Kamae, J. Kataoka, J. Katsuta, J. Knödlseeder, M. Kuss, J. Lande, S. Larsson, L. Latronico, M. Lemoine-Goumard, F. Longo, F. Loparco, M. N. Lovellette, P. Lubrano, G. M. Madejski, F. Massaro, M. Mayer, M. N. Mazziotta, J. E. McEnery, J. Mehault, P. F. Michelson, R. P. Mignani, W. Mitthumsiri, T. Mizuno, A. A. Moiseev, M. E. Monzani, A. Morselli, I. V. Moskalenko, S. Murgia, T. Nakamori, R. Nemmen, E. Nuss, M. Ohno, T. Ohsugi, N. Omodei, M. Orienti, E. Orlando, J. F. Ormes, D. Paneque, J. S. Perkins, M. Pesce-Rollins, F. Piron, G. Pivato, S. Rainò, R. Rando, M. Razzano, S. Razzaque, A. Reimer, O. Reimer, S. Ritz, C. Romoli, M. Sánchez-Conde, A. Schulz,

- C. Sgrò, P. E. Simeon, E. J. Siskind, D. A. Smith, G. Spandre, P. Spinelli, F. W. Stecker, A. W. Strong, D. J. Suson, H. Tajima, H. Takahashi, T. Takahashi, T. Tanaka, J. G. Thayer, J. B. Thayer, D. J. Thompson, S. E. Thorsett, L. Tibaldo, O. Tibolla, M. Tinivella, E. Troja, Y. Uchiyama, T. L. Usher, J. Vandenbroucke, V. Vasileiou, G. Vianello, V. Vitale, A. P. Waite, M. Werner, B. L. Winer, K. S. Wood, M. Wood, R. Yamazaki, Z. Yang, and S. Zimmer. Detection of the characteristic pion-decay signature in supernova remnants. *Science*, 339(6121):807–811, 2013.
- ⁶⁴ A. H. Bridle. Sidedness, field configuration, and collimation of extragalactic radio jets. *Astron. J.*, 89:979–986, Jul 1984.
- ⁶⁵ C M Huntington, F Fiuza, J S Ross, A B Zylstra, R P Drake, D H Froula, G Gregori, N L Kugland, C C Kuranz, M C Levy, C K Li, J Meinecke, T Morita, R Petrasso, C Plechaty, B A Remington, D D Ryutov, Y Sakawa, A Spitkovsky, H Takabe, and H.-S. Park. Observation of magnetic field generation via the Weibel instability in interpenetrating plasma flows. *Nature Physics*, 11(2):173–176, 2015.
- ⁶⁶ I. B. Bernstein, E. A. Frieman, M. D. Kruskal, and R. M. Kulsrud. An energy principle for hydromagnetic stability problems. *Proceedings of the Royal Society of London A: Mathematical, Physical and Engineering Sciences*, 244(1236):17–40, 1958.
- ⁶⁷ E. Frieman and Manuel Rotenberg. On hydromagnetic stability of stationary equilibria. *Rev. Mod. Phys.*, 32:898–902, 1960.
- ⁶⁸ R. Kulsrud. General stability theory in plasma physics. In M. N. Rosenbluth, editor, *Advanced Plasma Theory*, volume 1, page 54, 1964.
- ⁶⁹ M. B. Isichenko. Nonlinear hydrodynamic stability. *Phys. Rev. Lett.*, 80:972–975, 1998.
- ⁷⁰ Eliezer Hameiri. Variational principles for equilibrium states with plasma flow. *Physics of Plasmas*, 5(9):3270–3281, 1998.
- ⁷¹ P. A. DAVIDSON. An energy criterion for the linear stability of conservative flows. *Journal of Fluid Mechanics*, 402:329–348, 2000.

- ⁷² G. Laval, C. Mercier, and R. Pellat. Necessity of the energy principles for magnetostatic stability. *Nuclear Fusion*, 5(2):156, 1965.
- ⁷³ J.P. Freidberg. *Ideal magnetohydrodynamics*. Plenum Press, New York, NY, 1987.
- ⁷⁴ Eliezer Hameiri. Dynamically accessible perturbations and magnetohydrodynamic stability. *Physics of Plasmas*, 10(7):2643–2648, 2003.
- ⁷⁵ A. V. Kats. Canonical description of ideal magnetohydrodynamic flows and integrals of motion. *Phys. Rev. E*, 69:046303, Apr 2004.
- ⁷⁶ I. V. Khalzov, A. I. Smolyakov, and V. I. Ilgisonis. Energy of eigenmodes in magnetohydrodynamic flows of ideal fluids. *Physics of Plasmas*, 15(5):054501, 2008.
- ⁷⁷ J. W. Van Dam, M. N. Rosenbluth, and Y. C. Lee. A generalized kinetic energy principle. *The Physics of Fluids*, 25(8):1349–1354, 1982.
- ⁷⁸ A. Bhattacharjee, R. L. Dewar, A. H. Glasser, M. S. Chance, and J. C. Wiley. Energy principle with global invariants: Applications. *The Physics of Fluids*, 26(2):526–534, 1983.
- ⁷⁹ Russell M Kulsrud and James W K Mark. Collective instabilities and waves for inhomogeneous stellar systems. I. The necessary and sufficient energy principle. *The Astrophysical Journal*, 160(May):471–484, 1970.
- ⁸⁰ J. P. Goedbloed. Variational principles for stationary one- and two-fluid equilibria of axisymmetric laboratory and astrophysical plasmas. *Physics of Plasmas*, 11(12):L81–L84, 2004.
- ⁸¹ Oleg Polomarov, Igor Kaganovich, and Gennady Shvets. Merging of superalfvénic current filaments during collisionless weibel instability of relativistic electron beams. *Phys. Rev. Lett.*, 101:175001, Oct 2008.
- ⁸² F. Califano, N. Attico, F. Pegoraro, G. Bertin, and S. V. Bulanov. Fast formation of magnetic islands in a plasma in the presence of counterstreaming electrons. *Phys. Rev. Lett.*, 86:5293–5296, Jun 2001.

- ⁸³ S. Zenitani and M. Hesse. The role of the weibel instability at the reconnection jet front in relativistic pair plasma reconnection. *Physics of Plasmas*, 15(2):022101, 2008.
- ⁸⁴ W Theobald, A A Solodov, C Stoeckl, K S Anderson, F N Beg, R Epstein, G Fiksel, E M Giraldez, V Yu. Glebov, H Habara, S Ivancic, L C Jarrott, F J Marshall, G McKiernan, H S McLean, C Mileham, P M Nilson, P K Patel, F Pérez, T C Sangster, J J Santos, H Sawada, A Shvydky, R B Stephens, and M S Wei. Time-resolved compression of a capsule with a cone to high density for fast-ignition laser fusion. *Nature Communications*, 5:5785, dec 2014.
- ⁸⁵ L C Jarrott, M S Wei, C McGuffey, A A Solodov, W Theobald, B Qiao, C Stoeckl, R Betti, H Chen, J Delettrez, T Döppner, E M Giraldez, V Y Glebov, H Habara, T Iwawaki, M H Key, R W Luo, F J Marshall, H S McLean, C Mileham, P K Patel, J J Santos, H Sawada, R B Stephens, T Yabuuchi, and F N Beg. Visualizing fast electron energy transport into laser-compressed high-density fast-ignition targets. *Nature Physics*, 12:499, jan 2016.
- ⁸⁶ F. N. Beg, A. R. Bell, A. E. Dangor, C. N. Danson, A. P. Fews, M. E. Glinsky, B. A. Hammel, P. Lee, P. A. Norreys, and M. Tatarakis. A study of picosecond laser-solid interactions up to $10^{19} \text{W}/\text{cm}^2$. *Physics of Plasmas*, 4(2):447–457, feb 1997.
- ⁸⁷ Sc Wilks, Wl Kruer, M. Tabak, and Ab Langdon. Absorption of ultra-intense laser pulses. *Physical review letters*, 69(9):1383–1386, 1992.
- ⁸⁸ O. Buneman. Dissipation of currents in ionized media. *Phys. Rev.*, 115:503–517, Aug 1959.
- ⁸⁹ T. F. Bell and O. Buneman. Plasma instability in the whistler mode caused by a gyrating electron stream. *Phys. Rev.*, 133:A1300–A1302, Mar 1964.
- ⁹⁰ K. V. Roberts and H. L. Berk. Nonlinear evolution of a two-stream instability. *Phys. Rev. Lett.*, 19:297–300, Aug 1967.
- ⁹¹ A. Bret. Weibel, two-stream, filamentation, oblique, bell, buneman...which one grows faster? *Astrophysical Journal*, 699(2):990–1003, 2009.

- ⁹² A. Bret, L. Gremillet, and M. E. Dieckmann. Multidimensional electron beam-plasma instabilities in the relativistic regime. *Physics of Plasmas*, 17(12), 2010.
- ⁹³ Amita Das and Predhiman Kaw. Nonlocal sausage-like instability of current channels in electron magnetohydrodynamics. *Physics of Plasmas*, 8(10):4518–4523, 2001.
- ⁹⁴ Chandrasekhar Shukla, Amita Das, and Kartik Patel. Particle-in-cell simulation of two-dimensional electron velocity shear driven instability in relativistic domain. *Physics of Plasmas*, 23(8):082108, 2016.
- ⁹⁵ A Grassi, M Grech, F Amiranoff, F Pegoraro, A Macchi, and C Riconda. Electron Weibel instability in relativistic counterstreaming plasmas with flow-aligned external magnetic fields. *Physical Review E*, 95(2):023203, feb 2017.
- ⁹⁶ Z. M. Sheng and J. Meyer-ter Vehn. Inverse faraday effect and propagation of circularly polarized intense laser beams in plasmas. *Phys. Rev. E*, 54:1833–1842, Aug 1996.
- ⁹⁷ J. P. Knauer, O. V. Gotchev, P. Y. Chang, D. D. Meyerhofer, O. Polomarov, R. Betti, J. A. Frenje, C. K. Li, M. J.-E. Manuel, R. D. Petrasso, J. R. Rygg, and F. H. SÁlguin. Compressing magnetic fields with high-energy lasers. *Physics of Plasmas*, 17(5):056318, 2010.
- ⁹⁸ Hitoki Yoneda, Tomonori Namiki, Akinori Nishida, Ryosuke Kodama, Youichi Sakawa, Yasuhiro Kuramitsu, Taichi Morita, Kento Nishio, and Takao Ide. Strong compression of a magnetic field with a laser-accelerated foil. *Phys. Rev. Lett.*, 109:125004, Sep 2012.
- ⁹⁹ H. Nagatomo, T. Johzaki, A. Sunahara, H. Sakagami, K. Mima, H. Shiraga, and H. Azechi. Computational study of strong magnetic field generation in a nonspherical, cone-guided implosion. *Nuclear Fusion*, 53(6), 2013.
- ¹⁰⁰ Shinsuke Fujioka, Yasunobu Arikawa, Sadaoki Kojima, Tomoyuki Johzaki, Hideo Nagatomo, Hiroshi Sawada, Seung Ho Lee, Takashi Shiroto, Naofumi Ohnishi, Alessio Morace, Xavier Vaisseau, Shohei Sakata, Yuki Abe, Kazuki Matsuo, King Fai Farley Law, Shota Tosaki, Akifumi Yogo, Keisuke Shigemori, Yoichiro Hironaka, Zhe Zhang, Atsushi Sunahara, Tetsuo Ozaki, Hitoshi

- Sakagami, Kunioki Mima, Yasushi Fujimoto, Kohei Yamanoi, Takayoshi Norimatsu, Shigeki Tokita, Yoshiki Nakata, Junji Kawanaka, Takahisa Jitsuno, Noriaki Miyanaga, Mitsuo Nakai, Hiroaki Nishimura, Hiroyuki Shiraga, Kotaro Kondo, Mathieu Bailly-Grandvaux, Claudio Bellei, João Jorge Santos, and Hiroshi Azechi. Fast ignition realization experiment with high-contrast kilo-joule peta-watt LFEX laser and strong external magnetic field. *Physics of Plasmas*, 23(5), 2016.
- ¹⁰¹ Kazuki Matsuo, Hideo Nagatomo, Zhe Zhang, Philippe Nicolai, Takayoshi Sano, Shohei Sakata, Sadaoki Kojima, Seung Ho Lee, King Fai Farley Law, Yasunobu Arikawa, Youichi Sakawa, Taichi Morita, Yasuhiro Kuramitsu, Shinsuke Fujioka, and Hiroshi Azechi. Magnetohydrodynamics of laser-produced high-energy-density plasma in a strong external magnetic field. *Physical Review E*, 95(5), 2017.
- ¹⁰² Igor V. Pogorelsky, Markus Babzien, Ilan Ben-Zvi, John Skaritka, and Mikhail N. Polyanskiy. BESTIA - The next generation ultra-fast CO_2 laser for advanced accelerator research. *Nuclear Instruments and Methods in Physics Research, Section A: Accelerators, Spectrometers, Detectors and Associated Equipment*, 829:432–437, 2016.
- ¹⁰³ P. K. Kaw and J. M. Dawson. Laser-induced anomalous heating of a plasma. *The Physics of Fluids*, 12(12):2586–2591, 1969.
- ¹⁰⁴ John Dawson and Carl Oberman. Effect of ion correlations on high-frequency plasma conductivity. *The Physics of Fluids*, 6(3):394–397, 1963.
- ¹⁰⁵ W. L. Kruer and Kent Estabrook. ω heating by very intense laser light. *The Physics of Fluids*, 28(1):430–432, 1985.
- ¹⁰⁶ F. Brunel. Not-so-resonant, resonant absorption. *Phys. Rev. Lett.*, 59:52–55, Jul 1987.
- ¹⁰⁷ J. P. Freidberg, R. W. Mitchell, R. L. Morse, and L. I. Rudinski. Resonant absorption of laser light by plasma targets. *Phys. Rev. Lett.*, 28:795–799, Mar 1972.

- ¹⁰⁸ L. Spitzer. Physics of fully ionized gases. *Interscience Publishers, Inc., New York*, 1956.
- ¹⁰⁹ R. G. Meyerand and A. F. Haught. Gas breakdown at optical frequencies. *Phys. Rev. Lett.*, 11(401), Nov 1963.
- ¹¹⁰ S. Rand. Inverse bremsstrahlung with high-intensity radiation fields. *Phys. Rev.*, 136(B231), Oct 1964.
- ¹¹¹ K. Warren R. . Falcone M. Murnane R. More, Z. Zinamon. Heating of solids with ultra-short laser pulses. *Journal de Physique Colloques*, 49(C7-43-C7-51.), 1988.
- ¹¹² K. G. Budden. Radio waves in the ionosphere. *Cambridge University Press*, 46(358):319, 1961.
- ¹¹³ V E Golant and A D Piliya. Linear transformation and absorption of waves in a plasma. *Soviet Physics Uspekhi*, 14(4):413–437, 1972.
- ¹¹⁴ R B White and F F Chen. Amplification and absorption of electromagnetic waves in overdense plasmas. *Plasma Physics*, 16(7):565–587, jul 1974.
- ¹¹⁵ P. Bellan and M. Porkolab. Excitation of Lower-Hybrid Waves by a slow-Wave Structure. *Physical Review Letters*, 1(18), 1975.
- ¹¹⁶ H. M. Milchberg, R. R. Freeman, S. C. Davey, and R. M. More. Resistivity of a simple metal from room temperature to 10^6 k. *Phys. Rev. Lett.*, 61(2364), Nov 1988.
- ¹¹⁷ J. A. Cobble, G. A. Kyrala, A. A. Hauer, A. J. Taylor, C. C. Gomez, N. D. Delamater, and G. T. Schappert. Kilovolt x-ray spectroscopy of a subpicosecond-laser-excited source. *Phys. Rev. A*, 39(454), Jan 1989.
- ¹¹⁸ M. I. K. Santala, M. Zepf, I. Watts, F. N. Beg, E. Clark, M. Tatarakis, K. Krushelnick, A. E. Dangor, T. McCanny, I. Spencer, R. P. Singhal, K. W. D. Ledingham, S. C. Wilks, A. C. Machacek, J. S. Wark, R. Allott, R. J. Clarke, and P. A. Norreys. Effect of the plasma density scale length on the direction of fast electrons in relativistic laser-solid interactions. *Phys. Rev. Lett.*, 84(1459), Feb 2000.

-
- ¹¹⁹ Q. L. Dong and J. Zhang. Electron acceleration by static and oscillating electric fields produced in the interaction between femtosecond laser pulses and solid targets. *Physics of Plasmas*, 8(1025), 2001.
- ¹²⁰ J. Kupersztych, M. Raynaud, and C. Riconda. Electron acceleration by surface plasma waves in the interaction between femtosecond laser pulses and sharp-edged overdense plasmas. *Physics of Plasmas*, 11(1669), 2004.
- ¹²¹ M. Raynaud, J. Kupersztych, C. Riconda, J. C. Adam, and A. Heron. Strongly enhanced laser absorption and electron acceleration via resonant excitation of surface plasma waves. *Physics of Plasmas*, 14, 2007.
- ¹²² K. Eidmann, R. Rix, T. Schlegel, and K. Witte. Absorption of intense high-contrast sub-picosecond laser pulses in solid targets. *EPL (Europhysics Letters)*, 55(3), 2001.
- ¹²³ Edward A. Startsev and Ronald C. Davidson. Two-stream instability for a longitudinally compressing charged particle beam. *Physics of Plasmas*, 13(6):062108, 2006.
- ¹²⁴ F. Califano, R. Prandi, F. Pegoraro, and S. V. Bulanov. Nonlinear filamentation instability driven by an inhomogeneous current in a collisionless plasma. *Phys. Rev. E*, 58:7837–7845, Dec 1998.
- ¹²⁵ F. Pegoraro, S. V. Bulanov, F. Califano, and M. Lontano. Nonlinear development of the weibel instability and magnetic field generation in collisionless plasmas. *Physica Scripta*, T63(3):262–265, 1996.
- ¹²⁶ Irving Langmuir. Scattering of electrons in ionized gases. *Phys. Rev.*, 26(585), Nov 1925.
- ¹²⁷ J. R. Pierce. Possible fluctuations in electron streams due to ions. *Journal of Applied Physics*, 19(3):231–236, 1948.
- ¹²⁸ D. Bohm and E. P. Gross. Theory of plasma oscillations. a. origin of medium-like behavior. *Phys. Rev.*, 75:1851–1864, Jun 1949.
- ¹²⁹ Burton D. Fried. Mechanism for instability of transverse plasma waves. *Physics of Fluids*, 2(3), 1959.

- ¹³⁰ Laurent Gremillet, Guy Bonnaud, and Francois Amiranoff. Filamented transport of laser-generated relativistic electrons penetrating a solid target. *Physics of Plasmas*, 9(941), 2002.
- ¹³¹ P. A. Norreys, F. N. Beg, Y. Sentoku, L. O. Silva, R. A. Smith, and R. M. G. M. Trines. Intense laser-plasma interactions: New frontiers in high energy density physics. *Physics of Plasmas*, 16(041002), 2009.
- ¹³² Martin V. Goldman. Theory of stability of large periodic plasma waves. *The Physics of Fluids*, 13(5):1281–1289, 1970.
- ¹³³ C. B. Wharton, J. H. Malmberg, and T. M. O’Neil. Nonlinear effects of large amplitude plasma waves. *The Physics of Fluids*, 11(8):1761–1763, 1968.
- ¹³⁴ R. L. Morse and C. W. Nielson. One-, two-, and three-dimensional numerical simulation of two-beam plasmas. *Phys. Rev. Lett.*, 23:1087–1090, Nov 1969.
- ¹³⁵ L. Muschietti, I. Roth, C. W. Carlson, and R. E. Ergun. Transverse instability of magnetized electron holes. *Phys. Rev. Lett.*, 85:94–97, Jul 2000.
- ¹³⁶ S. D. Bale, P. J. Kellogg, D. E. Larsen, R. P. Lin, K. Goetz, and R. P. Lepping. Bipolar electrostatic structures in the shock transition region: Evidence of electron phase space holes. *Geophysical Research Letters*, 25(15):2929–2932.
- ¹³⁷ G. Sarri, M. E. Dieckmann, C. R. D. Brown, C. A. Cecchetti, D. J. Hoarty, S. F. James, R. Jung, I. Kourakis, H. Schamel, O. Willi, and M. Borghesi. Observation and characterization of laser-driven phase space electron holes. *Physics of Plasmas*, 17(1):010701, 2010.
- ¹³⁸ C. Ruyer and F. Fiuza. Disruption of Current Filaments and Isotropization of the Magnetic Field in Counterstreaming Plasmas. *Physical Review Letters*, 120(24):245002, jun 2018.
- ¹³⁹ A. Modena, Z. Najmudin, A. Dangor, C. Clayton, K. A. Marsh, C. Joshi, V. Malka, C. Darrow, C. Danson, D. Neely, and F. N. Walsh. Electron acceleration from the breaking of relativistic plasma waves. *Nature*, 377:606–608, Sep 1995.

- ¹⁴⁰ F. Brunel. Anomalous absorption of high intensity subpicosecond laser pulses. *Physics of Fluids*, 31(9):2714, 1988.
- ¹⁴¹ K. B. Wharton, S. P. Hatchett, S. C. Wilks, M. H. Key, J. D. Moody, V. Yanovsky, A. A. Offenberger, B. A. Hammel, M. D. Perry, and C. Joshi. Experimental measurements of hot electrons generated by ultraintense laser-plasma interactions on solid-density targets. *Phys. Rev. Lett.*, 81:822–825, Jul 1998.
- ¹⁴² A. Bret, M. C. Firpo, and C. Deutsch. Characterization of the initial filamentation of a relativistic electron beam passing through a plasma. *Physical Review Letters*, 94(11):1–4, 2005.
- ¹⁴³ W. Fox, G. Fiksel, A. Bhattacharjee, P. Y. Chang, K. Germaschewski, S. X. Hu, P. M. Nilson, Tzi-cheng Lai, S. X. Luan, W. Yu, F. Y. Li, Dong Wu, Z. M. Sheng, M. Y. Yu, and J. Zhang. Filamentation Instability of Counterstreaming Laser-Driven Plasmas W. *Physical Review E - Statistical, Nonlinear, and Soft Matter Physics*, 111(22):1–5, 2013.
- ¹⁴⁴ J. A. Stamper, K. Papadopoulos, R. N. Sudan, S. O. Dean, E. A. McLean, and J. M. Dawson. Spontaneous magnetic fields in laser-produced plasmas. *Phys. Rev. Lett.*, 26:1012–1015, Apr 1971.
- ¹⁴⁵ K. B. Wharton, S. P. Hatchett, S. C. Wilks, M. H. Key, J. D. Moody, V. Yanovsky, A. A. Offenberger, B. A. Hammel, M. D. Perry, and C. Joshi. *Phys. Rev. Lett.*, 81(822), Jul 1998.
- ¹⁴⁶ M. Tabak, D. S. Clark, S. P. Hatchett, M. H. Key, B. F. Lasinski, R. A. Snavely, S. C. Wilks, R. P. J. Town, R. Stephens, E. M. Campbell, R. Kodama, K. Mima, K. A. Tanaka, S. Atzeni, and R. Freeman. Review of progress in fast ignitiona. *Physics of Plasmas*, 12(057305), 2005.
- ¹⁴⁷ Stefano Atzeni and JÃijrgen Meyer ter Vehn. The physics of inertial fusion: Beamplasma interaction, hydrodynamics, hot dense matter. *Oxford University press*, page 480, 2009.

- ¹⁴⁸ Toshihiro Taguchi, Thomas M. Antonsen, Chuan S. Liu, and Kunioki Mima. Structure formation and tearing of an mev cylindrical electron beam in a laser-produced plasma. *Phys. Rev. Lett.*, 86:5055–5058, May 2001.
- ¹⁴⁹ Jeremy Martin Hill, Michael H. Key, Stephen P. Hatchett, and Richard R. Freeman. Beam-weibel filamentation instability in near-term and fast-ignition experiments. *Physics of Plasmas (1994-present)*, 12(082304), 2005.
- ¹⁵⁰ M. Lazar, R. Schlickeiser, R. Wielebinski, and S. Poedts. Cosmological effects of weibel-type instabilities. *The Astrophysical Journal*, 693(2):1133, 2009.
- ¹⁵¹ C. M. Huntington, F. Fiuza, J. S. Ross, A. B. Zylstra, R. P. Drake, D. H. Froula, G. Gregori, N. L. Kugland, C. C. Kuranz, M. C. Levy, C. K. Li, J. Meinecke, T. Morita, R. Petrasso, C. Plechaty, B. A. Remington, D. D. Ryutov, Y. Sakawa, A. Spitkovsky, H. Takabe, and H.-S. Park. Observation of magnetic field generation via the weibel instability in interpenetrating plasma flows. *Nature Physics*, 11(173–176), 2015.
- ¹⁵² Mikhail V. Medvedev and Abraham Loeb. Generation of magnetic fields in the relativistic shock of gamma-ray burst sources. *The Astrophysical Journal*, 526(2):697, 1999.
- ¹⁵³ Mikhail V. Medvedev, Massimiliano Fiore, Ricardo A. Fonseca, Luis O. Silva, and Warren B. Mori. Long-time evolution of magnetic fields in relativistic gamma-ray burst shocks. *The Astrophysical Journal Letters*, 618(2):L75, 2005.
- ¹⁵⁴ LuÃs O. Silva, Ricardo A. Fonseca, John W. Tonge, Warren B. Mori, and John M. Dawson. On the role of the purely transverse weibel instability in fast ignitor scenarios. *Physics of Plasmas*, 9(6):2458–2461, 2002.
- ¹⁵⁵ Brendan B. Godfrey, William R. Shanahan, and Lester E. Thode. Linear theory of a cold relativistic beam propagating along an external magnetic field. *The Physics of Fluids*, 18(3):346–355, 1975.
- ¹⁵⁶ R. L. Stenzel, M. C. Griskey, J. M. Urrutia, and K. D. Strohmaier. Three-dimensional electron magnetohydrodynamic reconnection. i. fields, currents, and flows. *Physics of Plasmas*, 10(7):2780–2793, 2003.

-
- ¹⁵⁷ Amita Das. Nonlinear aspects of two-dimensional electron magnetohydrodynamics. *Plasma Physics and Controlled Fusion*, 41(3A):A531, 1999.
- ¹⁵⁸ Y. Sentoku, K. Mima, Z. M. Sheng, P. Kaw, K. Nishihara, and K. Nishikawa. Three-dimensional particle-in-cell simulations of energetic electron generation and transport with relativistic laser pulses in overdense plasmas. *Phys. Rev. E*, 65:046408, Mar 2002.
- ¹⁵⁹ Keith A. Brueckner and Siebe Jorna. Laser-driven fusion. *Rev. Mod. Phys.*, 46:325–367, Apr 1974.
- ¹⁶⁰ R. Betti and O. A. Hurricane. Inertial-confinement fusion with lasers. *Nature Physics*, 12(May):435–448, 2016.
- ¹⁶¹ A. B. Remington, Arnett David, Paul R., Drake, and Takabe Hideaki. Modeling astrophysical phenomena in the laboratory with intense lasers. *Science*, 284(5419):1488–1493, 1999.
- ¹⁶² F Pegoraro, S V Bulanov, F Califano, and M Lontano. Nonlinear development of the weibel instability and magnetic field generation in collisionless plasmas. *Physica Scripta*, T63(3):262–265, 1996.
- ¹⁶³ Mitsunobu Miyagi. Bending losses in hollow and dielectric tube leaky waveguides. *Appl. Opt.*, 20(7):1221–1229, Apr 1981.
- ¹⁶⁴ D. Botez, L. Mawst, P. Hayashida, G. Peterson, and T. J. Roth. High-power, diffraction-limited beam operation from phase-locked diode-laser arrays of closely spaced leaky waveguides (antiguides). *Applied Physics Letters*, 53(6):464–466, 1988.
- ¹⁶⁵ Chandrasekhar Shukla, Amita Das, and Kartik Patel. Effect of finite beam width on current separation in beam plasma system: Particle-in-Cell simulations. arxiv:1508.07701[physics.plasm-ph]:1–8, 2015.
- ¹⁶⁶ T D Arber, K Bennett, C S Brady, A Lawrence-Douglas, M G Ramsay, N J Sircombe, P Gillies, R G Evans, H Schmitz, A R Bell, and C P Ridgers. Contemporary particle-in-cell approach to laser-plasma modelling. *Plasma Physics and Controlled Fusion*, 57(11):113001, 2015.

- ¹⁶⁷ A. S. Sandhu, A. K. Dharmadhikari, P. P. Rajeev, G. R. Kumar, S. Sengupta, A. Das, and P. K. Kaw. Laser-generated ultrashort multimegagauss magnetic pulses in plasmas. *Phys. Rev. Lett.*, 89:225002, Nov 2002.
- ¹⁶⁸ J.P. Boris, A.M. Landsberg, E.S. Oran, and J.H. Gardner. Lcpfct - a flux-corrected transport algorithm for solving generalized continuity equations. Technical Report NRL Memorandum Report 93-7192., Navel Research Laboratory, 1993.
- ¹⁶⁹ H. B. G. Casimir and D. Polder. The influence of retardation on the london-van der waals forces. *Phys. Rev.*, 73:360–372, Feb 1948.
- ¹⁷⁰ H. B. G. Casimir. On the attraction between two perfectly conducting plates. *Proc. K. Ned. Akad. Wet.*, 51:793–795, 1948.
- ¹⁷¹ H. Liebl. *Applied Charged Particle Optics*. Springer-Verlag, Berlin, 2008.
- ¹⁷² R. Feynman, R. B. Leighton, and M. Sands. *The Feynman Lectures on Physics*, volume 2. Addison-Wesley, Reading, Massachusetts, 1964.
- ¹⁷³ E. A. Stern and R. A. Ferrell. Surface plasma oscillations of a degenerate electron gas. *Phys. Rev.*, 120:130–136, Oct 1960.
- ¹⁷⁴ Atul Kumar, Chandrasekhar Shukla, Predhiman Kaw, and Amita Das. Fast Ignition Laser Fusion Using In-Situ Ion Acceleration With Pulsed CO2 Lasers. *arXiv:1804.02200v2 [physics.plasm-ph]*, 2018.
- ¹⁷⁵ K. Nishikawa and M. Wakatani. Plasma physics. *Springer-Verlag, Berlin*, 2000.
- ¹⁷⁶ R. G. Hemker. Particle-In-Cell Modeling of Plasma-Based Accelerators in Two and Three Dimensions. *Thesis, University of California, Los Angeles*, 2000.
- ¹⁷⁷ D. Haberberger, S. Tochitsky, and C. Joshi. Fifteen terawatt picosecond CO₂ laser system. *Optics Express*, 18(17):17865, 2010.
- ¹⁷⁸ Sergei Tochitsky, Frederico Fiuza, and Chan Joshi. Prospects and directions of CO₂ laser-driven accelerators. *AIP Conference Proceedings*, 1777(2016), 2016.

- ¹⁷⁹ A. Bruce Langdon, Jonathan Arons, and Claire E. Max. Structure of relativistic magnetosonic shocks in electron-positron plasmas. *Phys. Rev. Lett.*, 61:779–782, Aug 1988.
- ¹⁸⁰ D. A. Tidman and N. A. Krall. Shock waves in collisionless plasmas. *Wiley, New York*,, pages 29–54, 1971.
- ¹⁸¹ David Alsop and Jonathan Arons. Relativistic magnetosonic solitons with reflected particles in electron-positron plasmas. *The Physics of Fluids*, 31(4):839–847, 1988.
- ¹⁸² Tzihong Chiueh. Relativistic solitons and shocks in magnetized $e^- - e^+ - p^+$ fluids. *Phys. Rev. Lett.*, 63:113–116, Jul 1989.
- ¹⁸³ M. C. Begelman and J. G. Kirk. Shock-drift particle acceleration in superluminal shocks - A model for hot spots in extragalactic radio sources. *apj*, 353:66–80, April 1990.
- ¹⁸⁴ K. Stasiewicz. Theory and observations of slow-mode solitons in space plasmas. *Phys. Rev. Lett.*, 93:125004, Sep 2004.
- ¹⁸⁵ Roald Z. Sagdeev and Charles F. Kennel. Collisionless shock waves. *Scientific American*, 264(4):106–115, 1991.
- ¹⁸⁶ Y. Sentoku, T. Zh. Esirkepov, K. Mima, K. Nishihara, F. Califano, F. Pegoraro, H. Sakagami, Y. Kitagawa, N. M. Naumova, and S. V. Bulanov. Bursts of superreflected laser light from inhomogeneous plasmas due to the generation of relativistic solitary waves. *Phys. Rev. Lett.*, 83:3434–3437, Oct 1999.
- ¹⁸⁷ M. Borghesi, S. Bulanov, D. H. Campbell, R. J. Clarke, T. Zh. Esirkepov, M. Galimberti, L. A. Gizzi, A. J. MacKinnon, N. M. Naumova, F. Pegoraro, H. Ruhl, A. Schiavi, and O. Willi. Macroscopic evidence of soliton formation in multiterawatt laser-plasma interaction. *Phys. Rev. Lett.*, 88:135002, Mar 2002.
- ¹⁸⁸ L. Romagnani, S. V. Bulanov, M. Borghesi, P. Audebert, J. C. Gauthier, K. Löwenbrück, A. J. Mackinnon, P. Patel, G. Pretzler, T. Toncian, and O. Willi. Observation of collisionless shocks in laser-plasma experiments. *Phys. Rev. Lett.*, 101:025004, Jul 2008.

- ¹⁸⁹ R. Z. Sagdeev. Cooperative Phenomena and Shock Waves in Collisionless Plasmas. *Reviews of Plasma Physics*, 4:23, 1966.
- ¹⁹⁰ D. Biskamp. Collisionless shock waves in plasmas. *Nuclear Fusion*, 13(5):719, 1973.
- ¹⁹¹ R. A. Treumann. Fundamentals of collisionless shocks for astrophysical application, 1. non-relativistic shocks. *The Astronomy and Astrophysics Review*, 17(4):409–535, Dec 2009.
- ¹⁹² Roger Blandford and David Eichler. Particle acceleration at astrophysical shocks: A theory of cosmic ray origin. *Physics Reports*, 154(1):1 – 75, 1987.
- ¹⁹³ Yukiharu Ohsawa. Ultrarelativistic particle acceleration in collisionless shock waves. *Physics Reports*, 536(4):147 – 254, 2014. Ultrarelativistic particle acceleration in collisionless shock waves.
- ¹⁹⁴ A Marcowith, A Bret, A Bykov, M E Dieckman, L Ošč Drury, B Lembège, M Lemoine, G Morlino, G Murphy, G Pelletier, I Plotnikov, B Reville, M Riquelme, L Sironi, and A Stockem Novo. The microphysics of collisionless shock waves. *Reports on Progress in Physics*, 79(4):046901, 2016.
- ¹⁹⁵ Yukiharu Ohsawa. Solitary wave of a relativistic magnetosonic wave propagating perpendicularly to a magnetic field. *The Physics of Fluids*, 29(8):2474–2478, 1986.
- ¹⁹⁶ Renaud Gueroult, Yukiharu Ohsawa, and Nathaniel J. Fisch. Role of magnetosonic solitons in perpendicular collisionless shock reformation. *Phys. Rev. Lett.*, 118:125101, Mar 2017.
- ¹⁹⁷ Renaud Gueroult, Amnon Fruchtman, and Nathaniel J. Fisch. Cumulative displacement induced by a magnetosonic soliton bouncing in a bounded plasma slab. *Physics of Plasmas*, 25(6):062118, 2018.
- ¹⁹⁸ K. Stasiewicz, P. K. Shukla, G. Gustafsson, S. Buchert, B. Lavraud, B. Thidé, and Z. Klos. Slow magnetosonic solitons detected by the cluster spacecraft. *Phys. Rev. Lett.*, 90:085002, Feb 2003.

-
- ¹⁹⁹ C. F. Kennel and R. Pellat. Relativistic nonlinear plasma waves in a magnetic field. *Journal of Plasma Physics*, 15(3):335–355, 1976.
- ²⁰⁰ Stanford E. Woosley. *High energy transients in astrophysics (University of California at Santa Cruz, CA)*. Proceedings of a Conference on High Energy Transients in Astrophysics, edited by S. E. Woosley, AIP Conf. Proc. No. 115. (AIP, New York, 1983).
- ²⁰¹ N. J. Zabusky and M. D. Kruskal. Interaction of "solitons" in a collisionless plasma and the recurrence of initial states. *Phys. Rev. Lett.*, 15:240–243, 1965.
- ²⁰² A. C. Scott. A Nonlinear Klein-Gordon Equation. *American Journal of Physics*, 37:52–61, January 1969.
- ²⁰³ P. K. Kaw, A. Sen, and T. Katsouleas. Nonlinear 1d laser pulse solitons in a plasma. *Phys. Rev. Lett.*, 68:3172–3175, 1992.
- ²⁰⁴ Deepa Verma, Ratan Kumar Bera, Atul Kumar, Bhavesh Patel, and Amita Das. Observation of 1-D time dependent non-propagating laser plasma structures using fluid and PIC codes. 123111, 2017.
- ²⁰⁵ Renaud Gueroult, Amnon Fruchtman, and Nathaniel J. Fisch. Cumulative displacement induced by a magnetosonic soliton bouncing in a bounded plasma slab. *Physics of Plasmas*, 25(6):062118, 2018.
- ²⁰⁶ Marco Brambilla. Slow-wave launching at the lower hybrid frequency using a phased waveguide array. *Nuclear Fusion*, 16(1):47–54, 1976.
- ²⁰⁷ T.H. Stix. Absorption of Plasma Waves. *Phys. Fluids*, 3:19–32, 1960.
- ²⁰⁸ Thomas H. Stix. Radiation and absorption via mode conversion in an inhomogeneous collision-free plasma. *Physical Review Letters*, 15(23):878–882, 1965.
- ²⁰⁹ K. Poder, M. Tamburini, G. Sarri, A. Di Piazza, S. Kuschel, C. D. Baird, K. Behm, S. Bohlen, J. M. Cole, D. J. Corvan, M. Duff, E. Gerstmayr, C. H. Keitel, K. Krushelnick, S. P.D. Mangles, P. McKenna, C. D. Murphy, Z. Najmudin, C. P. Ridgers, G. M. Samarin, D. R. Symes, A. G.R. Thomas, J. Warwick, and

- M. Zepf. Experimental Signatures of the Quantum Nature of Radiation Reaction in the Field of an Ultraintense Laser. *Physical Review X*, 8(3):31004, 2018.
- ²¹⁰ J. M. Cole, K. T. Behm, E. Gerstmayr, T. G. Blackburn, J. C. Wood, C. D. Baird, M. J. Duff, C. Harvey, A. Ilderton, A. S. Joglekar, K. Krushelnick, S. Kuschel, M. Marklund, P. McKenna, C. D. Murphy, K. Poder, C. P. Ridgers, G. M. Samarin, G. Sarri, D. R. Symes, A. G.R. Thomas, J. Warwick, M. Zepf, Z. Najmudin, and S. P.D. Mangles. Experimental Evidence of Radiation Reaction in the Collision of a High-Intensity Laser Pulse with a Laser-Wakefield Accelerated Electron Beam. *Physical Review X*, 8(1):11020, 2018.
- ²¹¹ M. Bailly-Grandvaux, J. J. Santos, C. Bellei, P. Forestier-Colleoni, S. Fujioka, L. Giuffrida, J. J. Honrubia, D. Batani, R. Bouillaud, M. Chevrot, J. E. Cross, R. Crowston, S. Dorard, J. L. Dubois, M. Ehret, G. Gregori, S. Hulin, S. Kojima, E. Loyez, J. R. Marques, A. Morace, Ph. Nicolai, M. Roth, S. Sakata, G. Schauermann, F. Serres, J. Servel, V. T. Tikhonchuk, N. Woolsey, and Z. Zhang. Guiding of relativistic electron beams in dense matter by longitudinally imposed strong magnetic fields. *Nature Communications*, (2018):1–8, 2018.
- ²¹² W. B. Mori, C. D. Decker, D. E. Hinkel, and T. Katsouleas. Raman forward scattering of short-pulse high-intensity lasers. *Physical Review Letters*, 72(10):1482–1485, 1994.
- ²¹³ C. Joshi, T. Tajima, J. M. Dawson, H. A. Baldis, and N. A. Ebrahim. Forward Raman Instability and Electron Acceleration. *Physical Review Letters*, 47(18):1285–1288, 1981.
- ²¹⁴ W. Rozmus, R. P. Sharma, J. C. Samson, and W. Tighe. Nonlinear evolution of stimulated Raman scattering in homogeneous plasmas. *Physics of Fluids*, 30(7):2181, 1987.
- ²¹⁵ Donna Strickland and Gerard Mourou. Compression of amplified chirped optical pulses. *Optics Communications*, 56(3):219–221, 1985.

-
- ²¹⁶ A. J. Kemp, F. Fiuza, A. Debayle, T. Johzaki, W. B. Mori, P. K. Patel, Y. Sentoku, and L. O. Silva. Laser-plasma interactions for fast ignition. *Nuclear Fusion*, 54(5), 2014.
- ²¹⁷ A Flacco, J Vieira, A Lifschitz, F Sylla, S Kahaly, M Veltcheva, L O Silva, and V Malka. Persistence of magnetic field driven by relativistic electrons in a plasma. *Nature Physics*, 11:409, apr 2015.
- ²¹⁸ Chandrasekhar Shukla, Atul Kumar, Amita Das, and Bhavesh Patel. Merger and reconnection of Weibel separated relativistic electron beam. 1302(2000):1–15, 2017.
- ²¹⁹ Masaaki Yamada. Progress in understanding magnetic reconnection in laboratory and space astrophysical plasmas. *Physics of Plasmas*, 14(5):058102, 2007.
- ²²⁰ I. T. Chapman, R. Scannell, W. A. Cooper, J. P. Graves, R. J. Hastie, G. Naylor, and A. Zocco. Magnetic reconnection triggering magnetohydrodynamic instabilities during a sawtooth crash in a tokamak plasma. *Phys. Rev. Lett.*, 105:255002, Dec 2010.
- ²²¹ Longqing Yi, Baifei Shen, Alexander Pukhov, and Tünde Fülöp. Relativistic magnetic reconnection driven by a laser interacting with a micro-scale plasma slab. *Nature Communications*, (2018):1–7, 2017.
- ²²² F Porcelli, D Borgogno, F Califano, D Grasso, M Ottaviani, and F Pegoraro. Recent advances in collisionless magnetic reconnection. *Plasma Physics and Controlled Fusion*, 44(12B):B389, 2002.
- ²²³ Masaaki Yamada, Russell Kulsrud, and Hantao Ji. Magnetic reconnection. *Rev. Mod. Phys.*, 82:603–664, Mar 2010.
- ²²⁴ H. E. Petschek. Magnetic Field Annihilation. *NASA Special Publication*, 50:425, 1964.
- ²²⁵ P. A. Sweet. The Neutral Point Theory of Solar Flares. In B. Lehnert, editor, *Electromagnetic Phenomena in Cosmical Physics*, volume 6 of *IAU Symposium*, page 123, 1958.

- ²²⁶ E. N. Parker. Sweet's Mechanism for Merging Magnetic Fields in Conducting Fluids. *Journal of Geophysical Research*, 62:509–520, December 1957.
- ²²⁷ J. W. Strutt and B. Reyleigh. Theory of Sound. *Macmillan and Co.*, 1, feb 1877.
- ²²⁸ I. B. Bernstein, E. A. Frieman, M. D. Kruskal, and R. M. Kulsrud. An Energy Principle for Hydromagnetic Stability Problems. *Proceedings of the Royal Society A: Mathematical, Physical and Engineering Sciences*, 244(1236):17–40, 1958.
- ²²⁹ S. Lundquist. On the stability of magneto-hydrostatic fields. *Phys. Rev.*, 83:307–311, Jul 1951.
- ²³⁰ Zsolt Lécz and Alexander Andreev. Laser-induced extreme magnetic field in nanorod targets. *New Journal of Physics*, 20(3), 2018.
- ²³¹ Atul Kumar, Predhiman Kaw, and Amita Das. Energy principle for 2D electromagnetic, relativistic, interpenetrating, counter streaming plasma flows. 2017.
- ²³² Oleg Polomarov, Igor Kaganovich, and Gennady Shvets. Merging of superalfvénic current filaments during collisionless weibel instability of relativistic electron beams. *Phys. Rev. Lett.*, 101:175001, Oct 2008.
- ²³³ C. Shukla, A. Das, and K. Patel. Effect of finite beam width on current separation in beam plasma system: Particle-in-cell simulations. *arXiv:1508.07701 [physics.plasm-ph]*, *arXiv.org*, 2015.
- ²³⁴ John Clyne, Pablo Mininni, Alan Norton, and Mark Rast. Interactive desktop analysis of high resolution simulations: application to turbulent plume dynamics and current sheet formation. *New Journal of Physics*, 9(8):301, 2007.
- ²³⁵ John Clyne and Mark Rast. A prototype discovery environment for analyzing and visualizing terascale turbulent fluid flow simulations. In *Electronic Imaging 2005*, pages 284–294. International Society for Optics and Photonics, 2005.
- ²³⁶ F Pegoraro, S V Bulanov, F Califano, and M Lontano. Nonlinear development of the weibel instability and magnetic field generation in collisionless plasmas. *Physica Scripta*, 1996(T63):262, 1996.

- ²³⁷ D Biskamp, E Schwarz, and JF Drake. Two-dimensional electron magnetohydrodynamic turbulence. *Physical review letters*, 76(8):1264–1267, 1996.
- ²³⁸ Akira Hasegawa. Theory of longitudinal plasma instabilities. *Phys. Rev.*, 169:204–214, May 1968.
- ²³⁹ F. Brunel. Anomalous absorption of high intensity subpicosecond laser pulses. *The Physics of Fluids*, 31(9):2714–2719, 1988.
- ²⁴⁰ Amita Das, Atul Kumar, Chandrasekhar Shukla, Ratan Kumar Bera, Deepa Verma, Bhavesh Patel, Y. Hayashi, K. A. Tanaka, Amit Lad, G. R. Kumar, and Predhiman Kaw. Evidence of new finite beam plasma instability for magnetic field generation. *arXiv:1712.03099v1[physics.plasm-ph]*, *arXiv.org*, pages 0–9, 2017.
- ²⁴¹ A Upadhyay, K Patel, B S Rao, P A Naik, and P D Gupta. Three-dimensional simulation of laser-plasma based electron acceleration. *Pramana - J Phys*, 78(613), 2012.
- ²⁴² Max Tabak, James Hammer, Michael E. Glinsky, William L. Kruer, Scott C. Wilks, John Woodworth, E. Michael Campbell, Michael D. Perry, and Rodney J. Mason. Ignition and high gain with ultrapowerful lasers*. *Physics of Plasmas*, 1(1626), 1994.
- ²⁴³ R Kodama, P A Norreys, K. Mima, A. E. Dangor, R. G. Evans, H. Fujita, Y. Kitagawa, K. Krushelnick, T. Miyakoshi, N. Miyanaga, T. Norimatsu, S. J. Rose, T. Shozaki, K. Shigemori, A. Sunahara, M. Tampo, K. A. Tanaka, Y. Toyama, Y. Yamanaka, and M. Zepf. Fast heating of ultrahigh-density plasma as a step towards laser fusion ignition. *Nature*, 412(798-802), 2001.
- ²⁴⁴ Sy-Bor Wen, Mao, Xianglei, Greif, Ralph, Russo, and Richard E. Laser ablation induced vapor plume expansion into a background gas. ii. experimental analysis. *Journal of Applied Physics*, 101(023115), 2007.
- ²⁴⁵ T. Tajima and J. M. Dawson. Laser electron accelerator. *Phys. Rev. Lett.*, 43(267), Jul 1979.

- ²⁴⁶ C. Joshi, W. B. Mori, T. Katsouleas, J. M. Dawson, J. M. Kindel, and D. W. Forslund. Ultrahigh gradient particle acceleration by intense laser-driven plasma density waves. *Nature*, 311(525-529), 1984.
- ²⁴⁷ M. Litos, E. Adli, W. An, C. I. Clarke, C. E. Clayton, S. Corde, J. P. Delahaye, R. J. England, A. S. Fisher, J. Frederico, S. Gessner, S. Z. Green, M. J. Hogan, C. Joshi, W. Lu, K. A. Marsh, W. B. Mori, P. Muggli, N. Vafaei-Najafabadi, D. Walz, G. White, Z. Wu, V. Yakimenko, and G. Yocky. High-efficiency acceleration of an electron beam in a plasma wakefield accelerator. *Nature*, 515(92-95), 2014.
- ²⁴⁸ J. Fuchs, J. C. Adam, F. Amiranoff, S. D. Baton, P. Gallant, L. Gremillet, A. Héron, J. C. Kieffer, G. Laval, G. Malka, J. L. Miquel, P. Mora, H. Pépin, and C. Rousseaux. Transmission through highly overdense plasma slabs with a subpicosecond relativistic laser pulse. *Phys. Rev. Lett.*, 80(2326), Mar 1998.
- ²⁴⁹ F. Califano, N. Attico, F. Pegoraro, G. Bertin, and S. V. Bulanov. Fast formation of magnetic islands in a plasma in the presence of counterstreaming electrons. *Phys. Rev. Lett.*, 86(5293), Jun 2001.
- ²⁵⁰ P. M. Nilson, L. Willingale, M. C. Kaluza, C. Kamperidis, S. Minardi, M. S. Wei, P. Fernandes, M. Notley, S. Bandyopadhyay, M. Sherlock, R. J. Kingham, M. Tatarakis, Z. Najmudin, W. Rozmus, R. G. Evans, M. G. Haines, A. E. Dangor, and K. Krushelnick. Magnetic reconnection and plasma dynamics in two-beam laser-solid interactions. *Phys. Rev. Lett.*, 97(255001), Dec 2006.
- ²⁵¹ Jiayong Zhong, Yutong Li, Xiaogang Wang, Jiaqi Wang, Quanli Dong, Chijie Xiao, Shoujun Wang, Xun Liu, Lei Zhang, Lin An, Feilu Wang, Jianqiang Zhu, Yuan Gu, Xiantu He, Gang Zhao, and Jie Zhang. Modelling loop-top x-ray source and reconnection outflows in solar flares with intense lasers. *Nature*, 6(984–987), 2010.
- ²⁵² Bruce A. Remington, David Arnett, R. Paul, Drake, and Hideaki Takabe. Modeling astrophysical phenomena in the laboratory with intense lasers. *Science*, 284(5419):1488–1493, 1999.

-
- ²⁵³ P. Gibbon. *Short Pulse Laser Interactions with Matter*. Imperial College Press, London, 2005.
- ²⁵⁴ M. H. Key, M. D. Cable, T. E. Cowan, K. G. Estabrook, B. A. Hammel, S. P. Hatchett, E. A. Henry, D. E. Hinkel, J. D. Kilkenny, J. A. Koch, W. L. Kruer, A. B. Langdon, B. F. Lasinski, R. W. Lee, B. J. MacGowan, A. MacKinnon, J. D. Moody, M. J. Moran, A. A. Offenberger, D. M. Pennington, M. D. Perry, T. J. Phillips, T. C. Sangster, M. S. Singh, M. A. Stoyer, M. Tabak, G. L. Tietbohl, M. Tsukamoto, K. Wharton, and S. C. Wilks. Hot electron production and heating by hot electrons in fast ignitor research. *Physics of Plasmas*, 5(1966), 1998.
- ²⁵⁵ L. Gremillet, F. Amiranoff, S. D. Baton, J.-C. Gauthier, M. Koenig, E. Martignoli, F. Pisani, G. Bonnaud, C. Lebourg, C. Rousseaux, C. Toupin, A. Antonucci, D. Batani, A. Bernardinello, T. Hall, D. Scott, P. Norreys, H. Bandulet, and H. Pépin. Time-resolved observation of ultrahigh intensity laser-produced electron jets propagating through transparent solid targets. *Phys. Rev. Lett.*, 83(5015), Dec 1999.
- ²⁵⁶ D. Bohm and E. P. Gross. Theory of plasma oscillations. a. origin of medium-like behavior. *Phys. Rev.*, 75(1851), Jun 1949.
- ²⁵⁷ Jeremy Martin Hill, Michael H. Key, Stephen P. Hatchett, and Richard R. Freeman. Beam-weibel filamentation instability in near-term and fast-ignition experiments. *Physics of Plasmas (1994-present)*, 12(082304), 2005.
- ²⁵⁸ F. Califano, R. Prandi, F. Pegoraro, and S. V. Bulanov. Nonlinear filamentation instability driven by an inhomogeneous current in a collisionless plasma. *Phys. Rev. E*, 58(7837), Dec 1998.
- ²⁵⁹ A. P. L. Robinson, M. Sherlock, and P. A. Norreys. Artificial collimation of fast-electron beams with two laser pulses. *Phys. Rev. Lett.*, 100(025002), Jan 2008.
- ²⁶⁰ Amita Das, Neeraj Jain, Predhiman Kaw, and Sudip Sengupta. Sausage instabilities in the electron current layer and its role in the concept of fast ignition. *Nuclear Fusion*, 44(1):98, 2004.

- ²⁶¹ Neeraj Jain, Amita Das, Predhiman Kaw, and Sudip Sengupta. Role of current shear driven turbulence in anomalous stopping of energetic electrons. *Physics Letters A*, 363:125 – 129, 2007.
- ²⁶² Neeraj Jain, Amita Das, and Predhiman Kaw. Kink instability in electron magnetohydrodynamics. *Physics of Plasmas*, 11(4390), 2004.
- ²⁶³ Sita Sundar and Amita Das. Electron velocity shear driven instability in relativistic regime. *Physics of Plasmas*, 17(022101), 2010.
- ²⁶⁴ Shao-ping Zhu Chun-yang Zheng Li-hua Cao Hong-bo Cai, Wei Yu, Z. Y. Chen Bin Li, and A. Bogerts. Short-pulse laser absorption in very steep plasma density gradients.
- ²⁶⁵ J. Tonge-W. B. Mori-F. S. Tsung-M. Fiore R. A. Fonseca L. O. Silva J.-C. Adam C. Ren, M. Tzoufras and A. Héron. A global simulation for laser-driven mev electrons in 50 um -diameter fast ignition targetsa).
- ²⁶⁶ S. Kar, A. P. L. Robinson, D. C Carroll, O Lundh, K. Markey, P. McKenna, P. Norreys, and M. Zepf. Guiding of relativistic electron beams in solid targets by resistively controlled magnetic fields. *Phys. Rev. Lett.*, 102(055001), Feb 2009.
- ²⁶⁷ J. Fuchs, P. Antici, E. DHumires, E. Lefebvre, M. Borghesi, E. Brambrink, C. A. Cecchetti, M. Kaluza, V. Malka, M. Manclossi, S. Meyroneinc, P. Mora, J. Schreiber, T. Toncian, and H. Ppin. Laser-driven proton scaling laws and new paths towards energy increase. *Nature Physics*, 2(48–54), 2006.
- ²⁶⁸ Antoine Rouse, Christian Rischel, and Jean-Claude Gauthier. Femtosecond x-ray crystallography. *Rev. Mod. Phys.*, 73(17–31), Jan 2001.
- ²⁶⁹ K.-H. Hong, B. Hou, J. A. Nees, E. Power, and G. A. Mourou. Generation and measurement of $>10^8$ intensity contrast ratio in a relativistic khz chirped-pulse amplified laser. *Applied Physics B*, 81(4), 2005.
- ²⁷⁰ J. D. Kmetec, C. L. Gordon, J. J. Macklin, B. E. Lemoff, G. S. Brown, and S. E. Harris. Mev x-ray generation with a femtosecond laser. *Phys. Rev. Lett.*, 68(1527), Mar 1992.

-
- ²⁷¹ J. E. Crow, P. L. Auer, and J. E. Allen. The expansion of a plasma into a vacuum. *Journal of Plasma Physics*, 14(65–76), 8 1975.
- ²⁷² L. V. Pariiskaya A. V. Gurevich and L. P. Pitaevskii. Self-similar motion of rarefied plasma. *JETP*, 22(449), 1966.
- ²⁷³ M. P. Kalashnikov, E. Risse, H. Schönagel, and W. Sandner. Double chirped-pulse-amplification laser: a way to clean pulses temporally. *Opt. Lett.*, 30(8), Apr 2005.
- ²⁷⁴ Hiromitsu Kiriyama, Norihiro Inoue, Yutaka Akahane, and Koichi Yamakawa. Prepulse-free, multi-terawatt, sub-30-fs laser system. *Opt. Express*, 14(1), Jan 2006.
- ²⁷⁵ Sharad Kumar Yadav. *ELECTRON MAGNETOHYDRODYNAMIC (EMHD) STUDIES ON ELECTRON TRANSPORT IN AN INHOMOGENEOUS PLASMA MEDIUM*. PhD thesis, Institute for Plasma Research, HBNI, 2011.
- ²⁷⁶ S. K. Yadav, A. Das, and P. Kaw. Propagation of electron magnetohydrodynamic structures in a two-dimensional inhomogeneous plasma. *Physics of Plasmas*, 15(062308), 2008.
- ²⁷⁷ S. Kar, A. P. L. Robinson, D. C Carroll, O Lundh, K. Markey, P. McKenna, P. Norreys, and M. Zepf. Guiding of relativistic electron beams in solid targets by resistively controlled magnetic fields. *Phys. Rev. Lett.*, 102(055001), FEBRUARY 2009.
- ²⁷⁸ G. Malka and J. L. Miquel. Experimental confirmation of ponderomotive-force electrons produced by an ultrarelativistic laser pulse on a solid target. *Phys. Rev. Lett.*, 77(75), Jul 1996.
- ²⁷⁹ Marian Karlický. Electron beam-plasma interaction and the return-current formation. *The Astrophysical Journal*, 690(1), 2009.
- ²⁸⁰ A. Bret, L. Gremillet, and M. E. Dieckmann. Multidimensional electron beam-plasma instabilities in the relativistic regime. *Physics of Plasmas*, 17(120501), 2010.

- ²⁸¹ A. R. Bell and R. J. Kingham. Resistive collimation of electron beams in laser-produced plasmas. *Phys. Rev. Lett.*, 91(035003), Jul 2003.
- ²⁸² A. P. L. Robinson, M. Sherlock, and P. A. Norreys. Artificial collimation of fast-electron beams with two laser pulses. *Phys. Rev. Lett.*, 100(025002), Jan 2008.
- ²⁸³ B. Ramakrishna, S. Kar, A. P. L. Robinson, D. J. Adams, K. Markey, M. N. Quinn, X. H. Yuan, P. McKenna, K. L. Lancaster, J. S. Green, R. H. H. Scott, P. A. Norreys, J. Schreiber, and M. Zepf. Laser-driven fast electron collimation in targets with resistivity boundary. *Phys. Rev. Lett.*, 105(135001), Sep 2010.
- ²⁸⁴ P. McKenna, A. P. L. Robinson, D. Neely, M. P. Desjarlais, D. C. Carroll, M. N. Quinn, X. H. Yuan, C. M. Brenner, M. Burza, M. Coury, P. Gallegos, R. J. Gray, K. L. Lancaster, Y. T. Li, X. X. Lin, O. Tresca, and C.-G. Wahlström. Effect of lattice structure on energetic electron transport in solids irradiated by ultraintense laser pulses. *Phys. Rev. Lett.*, 106(185004), May 2011.
- ²⁸⁵ J.R. Cary, Lester E. Thode, Don S. Lemons, Michael E. Jones, and Michael A. Mostrom. Simple criteria for the absence of the beam–weibel instability. *Physics of Fluids (1958-1988)*, 24(10), 1981.
- ²⁸⁶ Han S. Uhm and Martin Lampe. Return–current–driven instabilities of propagating electron beams. *Physics of Fluids (1958-1988)*, 25(8), 1982.
- ²⁸⁷ Gourab Chatterjee, Prashant Kumar Singh, Saima Ahmed, A. P. L. Robinson, Amit D. Lad, Sudipta Mondal, V. Narayanan, Iti Srivastava, Nikhil Koratkar, John Pasley, A. K. Sood, and G. Ravindra Kumar. Macroscopic transport of mega-ampere electron currents in aligned carbon-nanotube arrays. *Phys. Rev. Lett.*, 108(235005), Jun 2012.
- ²⁸⁸ Roswell Lee and Martin Lampe. Electromagnetic instabilities, filamentation, and focusing of relativistic electron beams. *Phys. Rev. Lett.*, 31(1390), Dec 1973.
- ²⁸⁹ M. Tatarakis, F. N. Beg, E. L. Clark, A. E. Dangor, R. D. Edwards, R. G. Evans, T. J. Goldsack, K. W. D. Ledingham, P. A. Norreys, M. A. Sinclair, M-

- S. Wei, M. Zepf, and K. Krushelnick. Propagation instabilities of high-intensity laser-produced electron beams. *Phys. Rev. Lett.*, 90(175001), Apr 2003.
- ²⁹⁰ Luís O. Silva, Ricardo A. Fonseca, John W. Tonge, Warren B. Mori, and John M. Dawson. On the role of the purely transverse weibel instability in fast ignitor scenarios. *Physics of Plasmas (1994-present)*, 9(2458), 2002.
- ²⁹¹ F. Califano, N. Attico, F. Pegoraro, G. Bertin, and S. V. Bulanov. Fast formation of magnetic islands in a plasma in the presence of counterstreaming electrons. *Phys. Rev. Lett.*, 86(5293), Jun 2001.
- ²⁹² A. Bret and C. Deutsch. Hierarchy of beam plasma instabilities up to high beam densities for fast ignition scenario. *Physics of Plasmas (1994-present)*, 12(082704), 2005.
- ²⁹³ A. J. Mackinnon, Y. Sentoku, P. K. Patel, D. W. Price, S. Hatchett, M. H. Key, C. Andersen, R. Snavely, and R. R. Freeman. Enhancement of proton acceleration by hot-electron recirculation in thin foils irradiated by ultraintense laser pulses. *Phys. Rev. Lett.*, 88(215006), May 2002.
- ²⁹⁴ G. Malka and J. L. Miquel. Experimental confirmation of ponderomotive-force electrons produced by an ultrarelativistic laser pulse on a solid target. *Phys. Rev. Lett.*, 77(75), Jul 1996.
- ²⁹⁵ H.-S. Park, D. M. Chambers, H.-K. Chung, R. J. Clarke, R. Eagleton, E. Giraldez, T. Goldsack, R. Heathcote, N. Izumi, M. H. Key, J. A. King, J. A. Koch, O. L. Landen, A. Nikroo, P. K. Patel, D. F. Price, B. A. Remington, H. F. Robey, R. A. Snavely, D. A. Steinman, R. B. Stephens, C. Stoeckl, M. Storm, M. Tabak, W. Theobald, R. P. J. Town, J. E. Wickersham, and B. B. Zhang. High-energy k α radiography using high-intensity, short-pulse lasers. *Physics of Plasmas (1994-present)*, 13(056309), 2006.
- ²⁹⁶ A. Bret, M.-C. Firpo, and C. Deutsch. Collective electromagnetic modes for beam-plasma interaction in the whole k space. *Phys. Rev. E*, 70(046401), Oct 2004.

- ²⁹⁷ Jacob Trier Frederiksen and Mark Eric Dieckmann. Electromagnetic turbulence driven by the mixed mode instability. *Physics of Plasmas (1994-present)*, 15(094503), 2008.
- ²⁹⁸ M. E. Dieckmann, J. T. Frederiksen, A. Bret, and P. K. Shukla. Evolution of the fastest-growing relativistic mixed mode instability driven by a tenuous plasma beam in one and two dimensions. *Physics of Plasmas (1994-present)*, 13(112110), 2006.
- ²⁹⁹ J.H. Nuckolls, L.Wood, A.Thiessen, and G.B.Zimmerman. Laser compression of matter to super-high densities: Thermonuclear (ctr) applications. *Nature*, 239(139), 1972.
- ³⁰⁰ Yosuke Mizuno, Philip E. Hardee, and Ken-Ichi Nishikawa. Spatial growth of the current-driven instability in relativistic jets. *APJ*, 784(167), 2014.
- ³⁰¹ K.-I. Nishikawa, Hardee P., Zhang B., Dutan I., Medvedev M., Choi E. J., Min K. W., Niemiec J., Mizuno Y., Nordlund A., Frederiksen J. T., Sol H., and and D. H. Hartmann Pohl M. Magnetic field generation in a jet-sheath plasma via the kinetic kelvin-helmholtz instability. *Annales Geophysicae*, 31(9):1535–1541, 2013.
- ³⁰² R.A. Chevalier, J. M. Blondin, and R. T. Emmering. Hydrodynamic instabilities in supernova remnants: self-similar driven waves. *Astrophysical Journal*, 392:118–130, 1992.
- ³⁰³ S. V. Bulanov, F. Pegoraro, and A. S. Sakharov. Magnetic reconnection in electron magnetohydrodynamics. *Physics of Fluids B*, 4(8), 1992.
- ³⁰⁴ Amita Das. Nonlinear aspects of two-dimensional electron magnetohydrodynamics. *Plasma Physics and Controlled Fusion*, 41(A531), 1999.
- ³⁰⁵ D. Jovanović and F. Pegoraro. Two-dimensional electron-magnetohydrodynamic nonlinear structures. *Physics of Plasmas*, 7(889), 2000.
- ³⁰⁶ G. Bodo, A. Mignone, and R. Rosner. Kelvin-helmholtz instability for relativistic fluids. *Phys. Rev. E*, 70(036304), Sep 2004.

-
- ³⁰⁷ P. G. Drazin and W. H. Rnumber. *Hydrodynamic Stability*. Cambridge University Press, Cambridge, 1982.
- ³⁰⁸ P. L. Pritchett and F. V. Coroniti. The collisionless macroscopic kelvin-helmholtz instability: 1. transverse electrostatic mode. *Journal of Geophysical Research: Space Physics*, 89(A1), 1984.
- ³⁰⁹ H. Matsumoto and Y. Omura. *Computer Space Plasma Physics: Simulation Techniques and Software:KEMPO1*. Terra Scientific Publishing Company (TERRAPUB), Tokyo, 1993.
- ³¹⁰ William H. Press, Saul A. Teukolsky, William T. Vetterling, and Brian P. Flannery. *Numerical Recipes in C*. Cambridge University Press, 1992.
- ³¹¹ Charles K. Birdsall and A. Bruce Langdon. *Plasma physics via computer simulation*. Series in plasma physics. Taylor & Francis, New York, 1985. Originally published: New York ; London : McGraw-Hill, 1985.
- ³¹² Roger W. Hockney and James W. Eastwood. *Computer simulation using particles*. Adam Hilger, Bristol, 1988. Includes indexes.
- ³¹³ T. Umeda, Y. Omura, T. Tominaga, and H. Matsumoto. A new charge conservation method in electromagnetic particle-in-cell simulations. *Computer Physics Communications*, 156(73-85), December 2003.
- ³¹⁴ Amita Das and Predhiman Kaw. Nonlocal sausage-like instability of current channels in electron magnetohydrodynamics. *Physics of Plasmas*, 8(4518), 2001.
- ³¹⁵ Chandrasekhar Shukla, Amita Das, and Kartik Patel. 1d3v pic simulation of propagation of relativistic electron beam in an inhomogeneous plasma. *Phys. Scr.*, 90(085605(10p)), 2015.
- ³¹⁶ Chandrasekhar Shukla, Amita Das, and Kartik Patel. Two-dimensional studies of relativistic electron beam plasma instabilities in an inhomogeneous plasma. *Physics of Plasmas*, 22(112118), 2015.